UNIVERSIDADE D
COIMBRA

Rita Maria Mendes Silveira de Almeida Martins

DEVELOPMENT AND CHARACTERIZATION OF SILICA NANOPARTICLES TO MEDIATE AN ANTITUMORAL STRATEGY INVOLVING DRUG AND RECOMBINANT PROTEIN

Dissertação no âmbito do Mestrado em Bioquímica orientada pelo Professor Doutor Henrique Manuel dos Santos Faneca e pela Professora Doutora Paula Cristina Veríssimo Pires e apresentada ao Departamento de Ciências da Vida da Universidade de Coimbra.

Outubro de 2020

FACULDADE DE CIÊNCIAS E TECNOLOGIA
UNIVERSIDADE D COIMBRA

DEVELOPMENT AND CHARACTERIZATION OF SILICA NANOPARTICLES TO MEDIATE AN ANTITUMORAL STRATEGY INVOLVING DRUG AND RECOMBINANT PROTEIN

Rita Maria Mendes Silveira de Almeida Martins

Professor Doutor Henrique Manuel dos Santos Faneca

Professora Doutora Paula Cristina Veríssimo Pires

Coimbra,

October 2020

This work was performed at the Nanosystems and targeted antitumor strategies and the Biotechnology groups, at the Center for Neuroscience and Cell Biology of University of Coimbra, Portugal, under the supervision of Prof. Dr. Henrique Faneca (DCV-UC) and Prof. Drª. Paula Veríssimo (DCV-UC).

Agradecimentos

Inicio esta dissertação com uma nota de agradecimento a todos aqueles que durante este último ano contribuíram para a minha aproximação à investigação científica, a qual acredito que irá enriquecer a minha vida profissional e pessoal.

Expresso a minha profunda gratidão ao Professor Doutor Henrique Faneca e à Professora Doutora Paula Veríssimo, pela disponibilidade, apoio e orientação do meu projeto de mestrado. O inesgotável conhecimento que partilham, contribuiu de forma marcante para a aprendizagem que traduzo nesta dissertação.

À Drª. Rosemeyre Cordeiro, pelo acompanhamento permanente, pela atitude dedicada e preocupada que possibilitou a minha aprendizagem das bases do trabalho laboratorial, pela forma como me integrou no grupo e pela amizade que sempre demonstrou.

À Drª Rosário Faro pelas palavras de incentivo e pela incessante ajuda no laboratório de Biotecnologia.

À Daniela, ao Alexandro, à Flávia e à Dina pelo espírito de equipa e pelo companheirismo que sempre demonstraram.

Aos meus pais, pelos valores e ensinamentos que me transmitiram, por todo o apoio nos momentos de maior pressão e carinho constantes e aos meus avós e tios que têm sempre todo o amor do mundo para dar.

À Rute, a minha companheira de curso e grande amiga, com quem pude partilhar momentos de alegria, mas também de desespero e sempre esteve lá para me ajudar a superá-los.

À Margarido, que também me acompanhou em parte desta jornada e com quem pude discutir temas diversos, construindo assim uma amizade que vai para além do curso.

Aos meus amigos da BUCHA e grupo dos cafés, Anita, Guiga, Bigó, Gabi, Bea, Kika, Kikas, Riquito, João, Rafa, Raquel, Mariana, Gonçalo, Maria Ana, Babi, Pedro, Chicória, Rita, Alex, André, Érica, Diogo, Reis, Rúben, Pedro C., Rui A., sem vocês a minha vida não faria sentido, estou extremamente grata por existirem e mantermos amizades de longa data, por vezes com milhares de km's de distância, mas que prevalecem em qualquer circunstância.

À Ana Isabel, que me conheceu antes de nascer e com a qual partilho uma relação de amizade inigualável.

Ao meu namorado Rui, que sempre se interessou por debater ciência comigo e me apoiou nos momentos mais difíceis.
Ao Agrupamento 109 - Santo António dos Olivais e aos meus grandes amigos escuteiros, por darem mais cor e felicidade à minha vida e me ensinarem a deixar o mundo sempre um pouco melhor do que o encontramos.

Um obrigado sincero,
Que venha a próxima etapa!

Resumo

Com o passar dos anos, as doenças cancerígenas tornaram-se um dos maiores e mais letais problemas de saúde em todo o mundo. No entanto, os tratamentos convencionais contra o cancro têm vindo a ser caracterizados como muito invasivos e prejudiciais para os pacientes, devido aos efeitos secundários indesejáveis e à alta toxicidade, uma vez que não apresentam especificidade para células tumorais. Numa tentativa de superar essas limitações, a nano e a biotecnologia surgiram como ferramentas inteligentes para transportar e entregar agentes terapêuticos no tratamento do cancro e torná-los mais eficientes.

As nanopartículas mesoporosas de sílica (MSN) são um nanossistema de entrega promissor com propriedades físico-químicas notáveis, que podem oferecer uma abordagem interessante para a atual investigação no tratamento do cancro e para a prática clínica. Assim, este trabalho tem como objetivo desenvolver e caracterizar um novo sistema de entrega, baseado em MSN, para uma potencial terapia combinada contra Carcinoma Hepatocelular (CHC), utilizando um Interferon α-2b humano recombinante (IFNα-2b) e Epirrubicina (Epi) como agentes terapêuticos.

Durante este projeto, as MSN foram sintetizadas e modificadas com (3-Aminopropil) trietoxisilano (APTES) para serem funcionalizados com ácido hialurónico (HA), o que permite que as partículas se liguem especificamente às células tumorais. As nanopartículas obtidas (MSN-HA) apresentaram uma superfície carregada negativamente e um diâmetro hidrodinâmico médio de 467 nm, determinado pelas leituras de LDV e DLS.

O IFNα-2b recombinante foi produzido e purificado com sucesso, resultando num grande stock de proteína para ensaios de carregamento e citotoxicidade. Ambos os agentes terapêuticos foram carregados nas MSN-HA, apresentando resultados de alta eficiência e capacidade de carregamento, quando comparados com estudos anteriores. Finalmente, a biocompatibilidade das nanopartículas e o potencial terapêutico do nanossistema carregado foram avaliados em células HepG2. O resultado final foi bastante promissor, uma vez que o MSN-HA provou ser biocompatível quando descarregado, e as nanopartículas carregadas com Epi e IFNα-2b mostraram um efeito antitumoral sinergístico.

Palavras-chave: cancro, carcinoma hepatocelular, nanopartículas mesoporosas de sílica, terapia combinada, ácido hialurónico, interferon humano α-2b recombinante, epirrubicina, efeito antitumoral sinergístico.

Abstract

Over the years, cancer diseases have become one of the biggest and most lethal health problems worldwide. However, conventional cancer treatments have shown to be too invasive and harmful for patients, due to undesirable side effects and high toxicity since they don't present specificity for tumour cells. In order to try to overcome these limitations nano and biotechnology emerged as smart tools to transport and deliver therapeutic agents in cancer treatment and making them more efficient.

Accordingly to that, mesoporous silica nanoparticles (MSN) are a promising delivery nanosystem with remarkable physicochemical properties that can offer an interesting approach for the current cancer treatment research and clinical practice. Thus, this work aims to develop and characterize a new delivery system, based on MSN's, to a potential combination therapy against Hepatocellular Carcinoma (HCC), using a recombinant human Interferon α-2b (IFNα-2b) and Epirubicin (Epi) as therapeutic agents.

During this project, MSN were synthesized and modified with (3-Aminopropyl) triethoxysilane (APTES) to be functionalized with hyaluronic acid (HA), which allowed them to specifically bind to tumour cells. The obtained nanoparticles (MSN-HA) presented a negatively charged surface and an average hydrodynamic diameter of 467 nm, determined by Laser Doppler Velocimetry (LDV) and Dynamic Light Scattering (DLS) readings.

Recombinant IFNα-2b was successfully produced and purified resulting in a great protein stock for loading and cytotoxicity assays. Both therapeutic agents were loaded in MSN-HA presenting high loading efficiency and capacity results when compared with previous studies.

Finally, nanoparticles' biocompatibility and the therapeutic potential of the loaded nanosystem were evaluated in HepG2 cells. The outcome was very promising, since MSN-HA were proven to be biocompatible when unloaded, and the loaded nanoparticles with Epi and IFNα-2b have shown a synergistic antitumour effect.

Keywords: cancer, hepatocellular carcinoma, mesoporous silica nanoparticles, combination therapy, hyaluronic acid, recombinant human interferon α-2b, epirubicin, synergistic antitumour effect

List of Acronyms and Abbreviations

(3-Aminopropyl)triethoxysilane	APTES
Aldehyde-functionalized dendritic mesoporous silica nanoparticles	DMSNs-CHO
Ammonium hydroxide	NH_4OH
Arbitrary units	a.u.
Bis [propyl 3- (triethoxysilane)] tetrasulfide]	BTESPT
Bovine serum albumin	BSA
Cancer stem cells	CSC
Catenin beta 1	CTNNB1
Centro Hospitalar da Universidade de Coimbra	CHUC
Cetyltrimethylammonium bromide	CTAB
Cetyltrimethylammonium chloride	CTAC
Commercial IFNα-2b	IFN-C
Cytochrome c	CytC
Deoxyribonucleic acid	DNA
Diethanolamine	DEA
Dithiothreitol	DTT
Dynamic Light Scattering	DLS
Enhanced Permeability and Retention	EPR
Epirubicin	Epi
Escherichia coli	*E. coli*
Ethanol	EtOH
Ethylene diamine tetraacetic acid	EDTA
Extrahepatic cholangiocarcinoma	EHC
Fourier Transform Infrared Spectroscopy	FTIR
Generally Recognized as Safe	GRAS
Glutathione	GSH
HA receptor for endocytosis	HARE
Hepatitis B Virus	HBV
Hepatitis C Virus	HCV
Hepatocellular carcinoma	HCC
High molecular weight	HMW

Hollow mesoporous silica capsules	HMSC
Hyaluronic acid	HA
Hydrochloric acid	HCl
Immobilized Metal Affinity Chromatography	IMAC
Immunoglobulin G	IgG
Interferon Alpha/beta Receptor	IFNAR
Interferon Stimulated Genes	ISG
Interferon Stimulated Response Element	ISRE
Interferon α-2b	IFNα-2b
Intrahepatic cholangiocarcinoma	ICC
Isopropyl β-D-1-thiogalactopyranoside	IPTG
Janus Kinase	JAK
Janus Kinase – Signal Transducers and Activators of Transcription	JAK-STAT
Laser Doppler Velocimetry	LDV
Loading Capacity	LC
Loading Efficiency	LE
Low molecular weight	LMW
Luria Broth	LB
Lymphatic vessel endothelial HA receptor-1	LYVE-1
Mesoporous Silica Nanoparticles	MSN
Mobil Crystalline Materials	MCM-41
Molecular weight	Mw
Mononuclear phagocyte system	MPS
N-(3-Dimethylaminopropyl)-N′-ethylcarbodiimide hydrochloride	EDC
N-Hydroxysulfosuccinimide	NHS
National Center for Biotechnology Information	NCBI
Non-Alcoholic Fatty Liver Disease	NAFLD
Non-Alcoholic Steatohepatitis	NASH
Optical Density	O.D.
Orthoclone	OKT-3
Phosphate-Buffered Saline	PBS
Polydispersity Index	PDI
Programmed cell death ligand 1	PDL-1
Receptor for hyaluronate-mediated mobility	RHAMM

Recombinant IFNα-2b	IFN-R
Reticuloendothelial system	RES
Ribonucleic acid	RNA
Scanning electron microscopy	SEM
Signal Transducers and Activators of transcription	STAT
Small Ubiquitin-related Modifier	SUMO
Sodium dodecyl sulfate – polyacrylamide gel electrophoresis	SDS-PAGE
Sodium hydroxide	NaOH
Sodium oxide	Na_2O
Sodium silicate	Na_2SiO_3
Standard Deviation	SD
Sulforhodamine B	SRB
Telomerase reverse transcriptase	TERT
Tetraethyl orthosilicate;	TEOS
Tetrakis(2-hydroxyethyl) orthosilicate	THEOS
Tetramethoxy silane	TMOS
Tetrapropoxy silane	TPOS
Therapeutic Peptides and Proteins database	THPdb
Toll-like receptors	TLR
Transmission electron microscopy	TEM
Triethanolamine	TEA
Triisopropylbenzene	TIPB
Trimethoxyvinylsilane	TMVS
Trisodium acid	$Na_3C_6H_5O_7$
Tumour protein 53	TP53
Tyrosine Kinase 2	TYK-2
U.S. Food and Drug Administration	FDA
Water	H_2O

List of Figures

List of Tables

Table of contents

Chapter 1
Introduction

1. Use of nanotechnology in cancer treatment

1.1. Cancer disease

During the last decades, cancer became the leading cause of premature death all over the world (Mahjub, Jatana, Lee et al., 2018). In fact, cancer is the biggest barrier to increasing life's average expectancy (Bray, Ferlay, Soerjomataram, et al., 2018), and clearly an issue worth exploring.

Even though oncology research has shown signs of progress, the number of new cancer cases increases every year, particularly cancer types with poor prognostic, such as liver cancer, being the most frequent cause of cancer-related death worldwide (Limeres, Moretton, Bernabeu, Chiappetta, & Cuestas, 2019; Madduru, Ijaq, Dhar, Sarkar, Poondla, Das, & Suravajhala, 2019; Yang, Hainaut, Gores, Amadou, Plymoth, & Roberts, 2019). For instance, in 2018 18.1 million new cases and 9.6 million cancer deaths were estimated (Bray et al., 2018). The poor prognostic cancers are very frequently diagnosed only at an advanced stage of the disease, making it more difficult to succeed on their treatment (Yang et al., 2019; Ye, Zhao, El-Sayed, Muhammed, & Hassan, 2018). For most of these patients, more aggressive approaches are needed, including higher drug doses, which can easily lead to lethal secondary effects. In fact, the survival of cancer patients is chiefly dependent on the early detection of cancer, on targeted therapies to cancer cells and tissues, and finally on personalized medicine based on the individual genetic profile (Ye et al., 2018).

Nanotechnology has emerged as a tool to design smarter solutions to fight cancer. Both for transporting therapeutic agents specifically to the affected zone and for providing more accurate techniques to diagnose the disease at an early stage and to monitor the treatment effectiveness. Some nanodevices have the ability to improve the pharmacokinetics, biodistribution and to accumulate cytotoxic agents in tumour site (Perry et al., 2017), overcoming the unfavourable side effects of systemic administration of chemotherapeutic drugs. Moreover, they can act as bioimaging agents, using fluorescent dyes, quantum dots, magnetic or upconverting nanoparticles, to detect cancer cells (Jafari et al., 2019; Poonia, Lather, & Pandita, 2018).

Nanosystems research has been increasingly focused on finding the best way to target cancer cells from each type of cancer-based on cell genesis, to decrease side effects from conventional strategies, and to allow the development and implementation on new antitumor strategies based on different therapeutic molecules.

1.2. Hepatocellular carcinoma

Hepatocellular carcinoma (HCC) is a leading cause of cancer-related death worldwide, which incidence has been increasing in the last years (Forner, Reig, & Bruix, 2018).
It was estimated by the Global Cancer Observatory, a World Health Organization project, that 841 080 new cases of liver cancer emerged in 2018 worldwide and 781 631 people dyed due to this type of cancer (Figure 1), making HCC the sixth cancer with the highest incidence rate and the fourth most deadly cancer all over the world. The statistics for liver cancer in Portugal are equally overwhelming, having been reported 1386 new cases and 1372 deaths also in 2018 (Global Cancer Observatory).

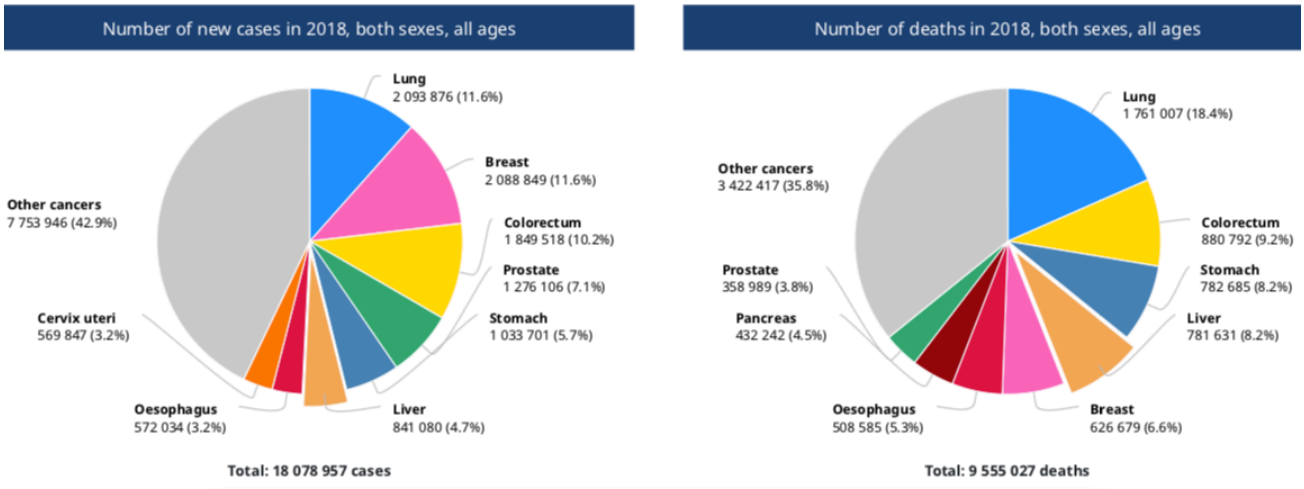

Figure 1: Incidence and death rate of cancer types worldwide (adapted from Global Cancer Observatory).

HCC is the most common form of primary liver cancer, representing approximately 90% of the cases and is derived from the malignant transformation of the liver parenchyma (Khemlina, Ikeda, & Kurzrock, 2017). HCC is also closely related to the development of chronic liver disease and chronic hepatitis B and C infections (Forner et al., 2018; Gbolahan et al., 2017). Primary liver cancer also comprises Intrahepatic

cholangiocarcinoma (ICC), which tend to metastasize early and to distant organs (Seehawer et al., 2018).

Besides HCC and ICC, there are other invasive carcinomas in the hepatobiliary cancers spectrum such as extrahepatic cholangiocarcinoma (EHC) and the gallbladder carcinoma (Mondaca, Yarmohammadi, & Kemeny, 2019).

HCC may rise in two different ways, mature hepatocytes degenerate into cancer cells after undergoing sequential genomic insults or by dedifferentiation into precursor cells that can later be transformed in cancer cells (Craig, von Felden, Garcia-Lezana, Sarcognato, & Villanueva, 2019; Seehawer et al., 2018). Six different subgroups of HCC that are related to specific genetic and clinical characteristics were identified (Table 1) (Calderaro et al., 2017; Yang et al., 2019).

Table 1: Subclasses of Hepatocellular Carcinoma.

HCC subclasses	Characterization	Range of proliferation
G1, G2, G3	Chromosomal instability	Proliferative
G1, G2, G3	Cell cycle activation	Proliferative
G2, G3	TP53 mutations	Proliferative
G1, G2	HBV infection	Proliferative
G4, G5, G6	Chromosomal stability	Less proliferative
G5, G6	Wnt/β-catenin pathway activation	Less proliferative

The most common genetic alterations are the mutations in the Telomerase reverse transcriptase (TERT) promoter, responsible for regulating transcription of the catalytic subunit in telomerase; CTNNB1 which encodes for β-catenin, a proto-oncogene in the WNT signalling pathway; and TP53, that is in charge of regulating cell division by keeping cells from growing and dividing too fast or in an uncontrolled way (Calderaro et al., 2017). Some mutations are related to specific aetiologies, such as the genetic alterations in the TERT promotor or the TP53 gene that are related to Hepatitis B Virus (HBV)-associated HCC, whereas CTNNB1 mutations are more associated to alcohol-related HCC (Yang et al., 2019). Particularly, genetic alterations in the TP53 are frequently associated with reduced patient survival (Ally et al., 2017; Yang et al., 2019).

Chronic HBV infection is considered the dominant risk factor for HCC, which is usually acquired by maternal-child transmission (El-Serag & Rudolph, 2007). In addition to chronic HBV infection, regular HBV and Hepatitis C Virus (HCV) infections are also common risk factors for HCC. Alcohol consumption, exposure to aflatoxins and metabolic disorders like diabetes, obesity, and hemochromatosis, and liver associated diseases like Non-Alcoholic Fatty Liver Disease (NAFLD), Non-Alcoholic Steatohepatitis

(NASH) also contribute to the development of liver cancer (Madduru et al., 2019). HCC shows an unfavourable growing trend in non-developed countries where people are more exposed and predisposed to these risk factors (Chew, Moscato, George, Azimi, & Danti, 2019).

1.2.1. Therapeutic strategies

Increasing survival while maintaining the best quality of life is the principal aim of cancer treatments. Among the therapeutic methods currently used, liver transplant is the gold standard treatment for patients who have a single tumour mass, since it might cure cancer and the underlying cirrhosis (Forner et al., 2018). Besides that, surgical resection and ablation, are the most definitive therapies to HCC patients in early stages of the tumour and without cirrhosis (Gbolahan et al., 2017).

Systemic therapies, as conventional chemotherapy, immunotherapy and hormone therapy are not very effective due to the side effects that they can create and to multidrug resistance (Limeres et al., 2019). In fact, there are few cases where these types of treatments improve patients survival (Avila, Berasain, Sangro, & Prieto, 2006). Chemotherapy is usually applied to patients with an advanced progression of HCC and metastasis. On the other hand, immune-based therapies are used when tumour cells express on their surface membrane the programmed cell death ligand 1 (PDL-1), which makes the immune system unable to perform its function against tumour cells (Chew et al., 2019). Furthermore, hormone therapies aim to prevent production of hormones or impeding hormone activities (H. Yang, 2016). It is also known that several stimulating hormone receptors are overexpressed in some tumour cells, being the main target of this type of therapy (Bonci et al., 2017).

For patients with unresectable HCC, Radiation therapy and chemoembolization, are also possible treatments for different tumour stages and purposes (Chew et al., 2019). Radiation therapy takes advantage of radiation to kill or damage tumour cells preventing them to grow, multiply or spread, whereas in chemoembolization there are injected chemotherapeutic drugs and embolization particles in the artery that supplies blood for the tumour (Yang et al., 2019). Actually the combination of these treatments have presented interesting results as a first-line treatment for HCC (Kim et al., 2019).

Other approaches can be can be followed like gene and protein therapies, which are treatments that involve introducing genetic material (RNA or DNA) into a person's cells or deliver a therapeutic protein to the cell's surroundings or inside them, respectively (Chew et al., 2019; Leader, Baca, & Golan, 2008)

Currently, chemotherapy is the only treatment that can be provided to hopefully prolong the overall survival of patients with advanced progression of HCC and metastasis (Chew et al., 2019). Sorafenib is the first-line systemic treatment drug for HCC patients and was also the first one to be approved to that aim (Yang et al., 2019). Due to the innumerous side effects that systemic administration of chemotherapeutic drugs might cause, it is important to consider other drugs less harmful for the patient's organism, as well as other ways to administrate, transport and deliver them to the tumour site.

Nanotechnology is a recent field in biomedicine that has been developed to create novel nanoscale devices and new therapeutic platforms to improve clinical outcome (Limeres et al., 2019).

According to the strategy developed in this work, chemo and protein therapy can be conjugated in order to achieve more effective results, taking advantage of nanodevices to transport the therapeutic agents to the tumour site.

Protein therapy takes advantage of cytotoxic proteins to induce apoptosis on mutated cells or to interfere with their cell cycle, as Interferon α-2b (IFNα-2b). Proapoptotic proteins are promoters of apoptotic cell death, usually with a human origin, preventing the immunotoxicity related to heterologous protein drugs (Serna et al., 2018).

2. Transport and delivery vectors in biomedicine

2.1. Types of nanosystems

Nanotechnology applies nanostructures at various fields of science, overcoming biological and physical barriers (Patra et al., 2018). Their application in biomedicine and pharmaceutical science relies on nanoscale delivery systems as intermediaries for a wide range of therapies, such as chemo, immuno, gene or protein therapies (Villiers, Aramwit, & Kwon, 2019), with a wide focus on cancer treatment. Thus, nanosystems are characterized for being delivery and transport vectors, around 1 to 300 nm able to encapsulate or attach drugs, proteins or genetic material (Jeevanandam, Chan, & Danquah, 2016; J. Li, Qiao, & Wu, 2017).

Nanosystem formulations are able to overcome the limitations associated to free therapeutic agents in the human body verified in conventional cancer therapies (Dipak, Kosloski, & Balu-Iyer, 2010; Jeevanandam et al., 2016). These limitations might include high molecular weight, low solubility, low absorption properties, lack of targeting properties, inability to cross lipid membranes of most drugs and low circulation times,

instability and vulnerability to denaturation, hydrolysis, oxidation or proteolysis of proteins (Jeevanandam, Chan, & Danquah, 2016), which lead to severe secondary effects.

Taking advantage of the Enhanced Permeability and Retention (EPR) effect, nanoparticles can accumulate into tumour site more easily due to leaky vasculature and poor lymphatic drainage of tumour tissues, which enable them to extravasate from the tumour vasculature and keep inside the tumour mass (Nicolas W. Cortes-Penfield, Barbara W. Trautner, 2017; Perry et al., 2017).

The use of nanotechnology in the health field is very promising due to its capacity to improve certain molecule characteristics such as drug solubility, release profile, diffusivity, bioavailability and immunogenicity (Patra et al., 2018).

The smallest units of nanosystems are known as nanoparticles, which are mostly used for biomedical applications as image agents to diagnose and detect cancer cells or other types of abnormalities and as drug or gene delivery agents to different therapeutic approaches (Xiaoming Li, Wang, Fan, Feng, & Cui, 2012).

The formulation of new nanosystems depends on the pretended application and function within the body. For that effect, they can be designed taking into consideration different proprieties resumed in Table 2.

Table 2: Properties of nanosystems.

Categories	Description	Reference
Enhancing permeability and solubility in drug delivery	Entrapping more than one compound on the same nanosystem, leading to a combined material delivery	(Meng et al., 2016)
Targeted delivery	Nanostructures are functionalized with specific ligands of receptors or antibodies of molecules overexpressed on interest spots, decreasing toxicity and increasing efficacy, which is known by active targeting. Passive targeting can also occur when the nanoparticles circulate through the bloodstream and are driven by affinity to the target point, by properties like pH, temperature, molecular shape and size.	(Banerjee & Chen, 2010; Patra et al., 2018)
Achieve intracellular	Coating nanosystems with molecules that trigger their cellular internalization or avoid their ablation	(Ganta, Singh,

delivery and prevent nanosystems to be captured by immune cells	by the immune system and extending their blood circulation time	Coleman, Williams, & Amiji, 2014)
Response to specific microenvironments	Adding molecular switches that respond to pH variation, temperature or redox levels to obtain a controlled drug released.	Albanese, Tang, & Chan, 2012)

A nanosystem formulation may include all these types of properties, in order to increase the delivery vector efficacy.

Regarding nanoparticles composition, they can be composed by an interfacial layer which consists of organic molecules such as surface and capping ligands, stabilizers or passivating agents, surrounding the core (Batista, Larson, & Kotov, 2015), and in some cases by an inorganic moiety, which can have many mineral sources, such as gold, iron oxide, carbon nanotubes, quantum dots or even silicates (Rawal & Patel, 2019).

On the other hand, some nanoparticles may also be exclusively made of inorganic or organic material, like liposomes, polymer micelles, dendrimers, proteins or poly (lactic-co-glycolic acid) (Patra et al., 2018). The diversity of materials used in nanoparticles leads to a growing world of possible nanodevice's formulations, as shown in Figure 2, each one with specific properties and advantages.

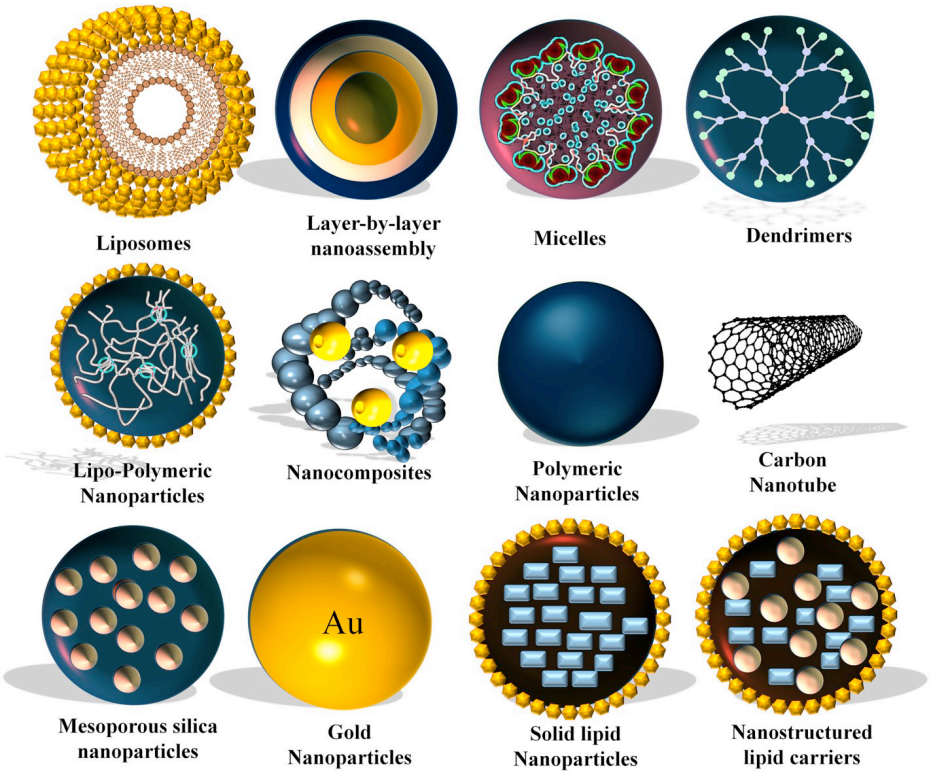

Figure 2: Representative illustration of different types of nanoparticles (reproduced from Rawal & Patel, 2019).

Nanoparticles applications have been substantially expanded in biomedicine, specifically in cancer treatments, being possible to distinguish at least 4 types of applications: 1) delivery of different types of anticancer drugs to tumour site and concentrate them in the tumour microenvironment; 2) delivery of immunotherapy agents such as cancer antigens to immune cells or proteins that stimulate the immune system; 3) promotion of the abscopal effect, a phenomenon characterized by the systemic regression of metastatic lesions driven by local tumour treatment; 4) using nanoparticles imaging and magnetic features to diagnose tumours and metastasis in the human body (Cheng, Castro, Liu, & Lau, 2019; Xiaoming Li et al., 2012; F. Liu et al., 2019; Lopez-Campos, Candini, Carrasco, & Berenguer Francés, 2019; Min et al., 2017).

In the last 5 years, different formulations have been tested and optimized, differing in the material used, size, shape, charge and molecular covers which are adapted to each type of final goal, exemplified in table 3.

Table 3: Different types of formulations.

Nanosystem	Effectiveness	Therapy	Reference
Hypoxia-responsive copper metal-organic frameworks	Nanoparticles accumulated in the tumour and released the therapeutic agents in response to hypoxia, exhibiting photo-acoustic imaging capability.	Multimodel cancer therapy	(K. Zhang, Meng, Yang, Dong, & Zhang, 2020)
Albumin-MnO_2 gated hollow mesoporous silica particles	The fabricated nanoplatform demonstrated to have a highly effective synergistic antitumour efficacy and to be a strong candidate for controlled delivery of therapeutic agents.	Chemo and Photodynamic therapy	(Fang et al., 2019)
Polysaccharides-based supramolecular nanosystem (HES@PGEA)	This supramolecular nucleic acid delivery system enhanced cellular internalization and improved gene transfection, exhibiting great antitumour effects.	Gene therapy	(Xu et al., 2020)
Lysine-embedded cellulose-based nanosystem	The synthesized nanosystem have better clearance time compared with other formulations and was able to successfully induce apoptosis in cancer cells, achieving efficient multi-drug delivery.	Chemo therapy	(Moghaddam et al., 2020)
Hollow mesoporous organosilica-based nanosystem	The biodegradable nanosystem showed high biocompatibility and high synergistic treatment efficacy against tumour cells and in tumour growth inhibition.	Chemo and photothermal therapy	(J. Chen et al., 2020)
PAMAM dendrimers	Polyamidoamine dendrimers overcome	Gene and Chemo therapy	(Ghaffari et al., 2020)

	the limitations of the clinical use of the chosen therapeutic agents, inducing apoptosis in cancer cells.		
Cationic tri-block copolymer-based nanoparticles (PDMAEMA-b-PβAE-b-PDMAEMA)	This nanosystem presented a better biocompatibility and a higher transfection efficiency compared to previous data.	Gene therapy	(Cordeiro et al., 2017)
Molybdenum selenide nanoparticles (MoSe2 NPs)	Nanoparticles with good biocompatibility, light stability and targeting ability, achieved a healing, anti-migration and anti-proliferative effects.	Photothermal and photodynamic therapy	(Y. Liu et al., 2020)
Poly[(2-dimethylamino) ethyl methacrylate] (PDMAEMA)- and poly(β-amino ester) (PβAE)-based homopolymer nanosystems	The polyplexes generated present a higher transfection efficiency and high biological activity in several types of human cells.	Gene therapy	(Santo et al., 2017)
Asialofetuin-Lipoplex nanosystem	The nontoxic cationic lipid-based nanosystem presents a high biological activity, having the ability to specifically and efficiently deliver genetic material to HCC cells.	Gene therapy	(Farinha, Pedroso De Lima, & Faneca, 2014)
Folate-targeted lipid-based nanosystem	These liposomes exhibit a high cellular uptake through folate-receptor mediated endocytosis and present a high anticancer efficiency owing to combination therapy.	Chemo and imaging therapy	(Karpuz et al., 2020)

2.2. Nanoparticles clearance and biodistribution

Nanoparticle-based therapeutics are usually administrated by intravenous injection, having the ability to directly enter the circulatory system since they bypass the barriers in the epithelial absorption process. Mononuclear phagocyte system (MPS), the renal and immune system are responsible for immediately control the nanoparticle clearance (Sun et al., 2014). MPS involves spleen, liver and bone marrow, which are rich organs in phagocytic cells, like macrophages, Kupffer cells and monocytes. Since phagocytic cells are responsible for digest and engulf nanoparticles, MPS is considered the principal system responsible for clearance of majority nanoparticles larger than 10nm (Longmire, Choyke, & Kobayashi, 2008).

Once the nanosystems enter in circulation, their properties affect the performance within the human organism, regarding targeting and clearance (Petros & Desimone, 2010). Given that, nanoparticle's size, shape, dispersity, charge, and hydrophobicity can be controlled, as well as surface modifications, to improve their biocompatibility and toxicity profiles (F. Chen, Hableel, Zhao, & Jokerst, 2018; Xiaoming Li et al., 2012).

Nanoparticle's size is determinant to their fate in the different clearance systems. The kidneys are responsible to filter and clear out most of the particles smaller than 6 nm. Particles between 10 and 150 nm are cleared by the liver due to phagocytic uptake and hepatic filtration. Additionally, the spleen is responsible for the rapid clearance of particles larger than 200 nm (Sun et al., 2014).

As a matter of fact, charge also plays an important role in the destination of nanoparticles. Negatively charged nanosystems have a longer circulation time, altering their binding affinity and consequently their reactivity with other proteins and molecules present in the blood (F. Chen et al., 2018). Differing from positive nanoparticles, which are taken up at a faster rate due to favourable electrostatic interactions with the negatively charged membrane, and lead to a higher systemic toxicity, since they can promote hemolysis or platelet aggregation, as it is mentioned by Tianmeng Sun and his coworkers (Sun et al., 2014).

At the same time, nanoparticles rounding 30 to 200 nm can be easily accumulated in cancer tissues because of the EPR effect. This response occurs due to the large fenestrations that tumours possess between the endothelial cells of blood vessels produced by angiogenesis, retaining particles located in the blood because of the leaky vasculature and the lack of lymphatic drainage (Albanese, Tang, & Chan, 2012; Limeres et al., 2019; Watermann & Brieger, 2017). Passive targeting is achieved by this ability of nanoparticles be conducted to the tumour site. Figure 3 describes the clearance behaviour of nanosystems according to their characteristics.

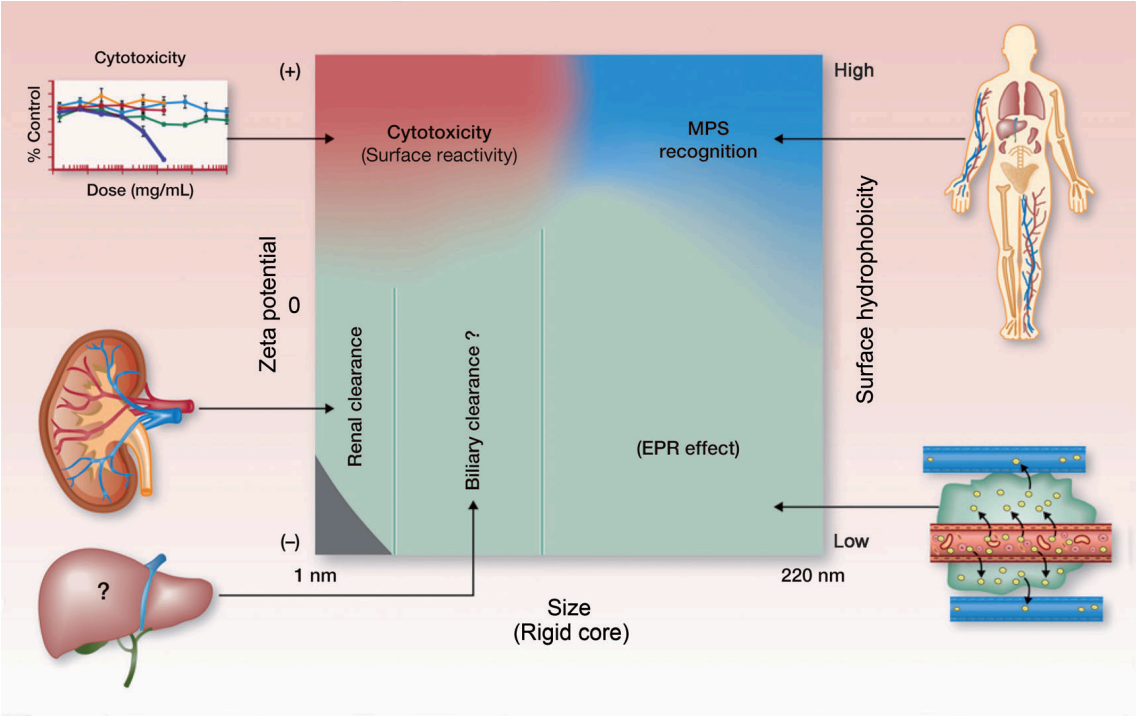

Figure 3: Cytotoxic and clearance profiles of nanosystems with different characteristics (reproduced from Sun et al., 2014)

2.3. Mesoporous Silica Nanoparticles – based nanosystems

2.3.1. Mesoporous silica materials

One of the most attractive nanosystems up to date are the ones well dispersed and with porous components (Farjadian, Roointan, Mohammadi-Samani, & Hosseini, 2019), giving focus to the Mesoporous Silica Nanoparticles (MSN) due to the large surface area and high structural order nanodevices, as a result of the use of surfactants as structure-directing agents. Indeed, silica is considered a Generally Recognized as Safe (GRAS) material by US FDA, since it is an abundant element in cartilage and bone, is used as an excipient in tablet-form drug formulations, and is also taken as a dietary supplement (Rosenholm, Mamaeva, Sahlgren, & Lindén, 2012).

Preliminary studies of mesoporous silica materials date back to 1992 where Mobil Research and Development Cooperation synthesized mesoporous silicates from aluminosilicate gels using a liquid-crystal template mechanism (Narayan, Nayak, Raichur, & Garg, 2018). Their product became known as Mobil Crystalline Materials or Mobil Composition of Matter, MCM-41, being characterized for having a hexagonal

shape, wherein cationic surfactants were used as templates to form porous structures with a diameter of 2.6 to 6 nm (Beck et al., 1992).

Apart from this many other materials have been explored, varying in their structural arrangement or pore size. Table 4 summarizes information about the first nanoparticles types synthesized by different companies and research teams, that support many of nowadays nanoformulations. These include nanoparticles with a complex hierarchical structure, such as hollow mesoporous spheres, core-in-(hollow porous shell) spheres, hollow spheres with multiple porous shells and hierarchically porous spheres (Du & He, 2011).

Table 4: List of mesoporous silica nanoparticles types and their characteristics.

MSN type	Composition	Mesoscopic structure	Pore size (nm)	References
MCM-41	CTAB H_2O NH_4OH TEOS	Hexagonal	1.5 – 8	(D. Kumar, Schumacher, Du Fresne von Hohenesche, Grün, & Unger, 2001)
MCM-48	CTAB H_2O Na_2O TEOS	Cubic	2 - 5	(D. Kumar et al., 2001)
MCM-50	C16TMABr H_2O NaOH TEOS	Lamellar	2 – 5	(S. Wang & Li, 2006)
SBA-11	$C_{16}H_{33}(OCH_2CH_2)_{10}OH$ H_2O HCl TEOS	Cubic	2.1 – 3.6	(Ukmar & Planinšek, 2010)
SBA-12	$C_{38}H_{78}O_{11}$ H_2O HCl Na_2SiO_3	Hexagonal	3.1	(Ge et al., 2018)
SBA-15	Pluronic P123 H_2O HCl TEOS	Hexagonal	6	(Galarneau et al., 2003)
KIT-5	EO_{106}- $PO_{70}EO_{106}$ H_2O	Cubic	9.3	(Kleitz et al., 2003)

	HCl TEOS			
COK-12	$EO_{20}PO_{70}EO_{20}$ H_2O Citric acid $Na_3C_6H_5O_7$ Na_2SiO_3	Hexagonal	5.8	(Jammaer, Aerts, D'Haen, Seo, & Martens, 2009)

CTAB - n-cetyltrimethylammonium bromide; H_2O – water; NH_4OH – ammonium hydroxide; TEOS – tetraethyl orthosilicate; Na_2O – sodium oxide, C16TMABr - cetyltrimethylammonium bromide; NaOH - sodium hydroxide; $C_{16}H_{33}(OCH_2CH_2)_{10}OH$ - polyoxyethylene (10) cetyl ether; HCl – Hydrochloric acid; Na_2SiO_3 – sodium silicate; $C_{38}H_{78}O_{11}$ - Polyoxyethylene 10 stearyl ether; EO_{106}- $PO_{70}EO_{106}$ – (EO – ethylene oxide, PO – propylene oxide); $Na_3C_6H_5O_7$ – trisodium acid

2.3.1.1. Synthesis methods

Up to date, MSN's synthesis methods depend on surfactants as structure-directing agents. A variety of methods can be used, as sol-gel, microwave synthesis, hydrothermal synthesis, template synthesis, modified aerogel methods, soft and hard templating methods and fast self-assembly (Farjadian, Roointan, Mohammadi-Samani, & Hosseini, 2019).

The modified Stöber's method is the most frequently used technique, in which the pioneers of monodispersed silica nanospheres were Werner Stöber and Arthur Fink whom by hydrolysis and condensation of alkyl silicates in alcohols and aqueous ammonia media prepared spherical silica particles for the first time (Stöber & Fink, 1968). In their research work, has been demonstrated the possibility to control particles size by varying parameters such as chain size and source of alkyl silicates, type of alcohols and ammonia concentration (Stöber & Fink, 1968).

Afterwards, the idea of using soft templates as surfactants or copolymers at low concentrations guaranteed the synthesis of mesoporous silica nanoparticles (Galarneau et al., 1998), giving rise to the modified Stöber method. This technique is also identified as a Sol-gel process, in which a network is formed around a template when silicone alkoxide precursors are present. In this process, hydrolysis and condensation of alkoxide monomers into a colloidal solution (sol) take place almost simultaneously and co-dependently, acting as a precursor to form an ordered network (gel), originating the particles (Narayan et al., 2018).

There are three main mandatory intervenients to MSN synthesis, a silica precursor, a surfactant as a template or structure-directing agent and a catalyst. The above

mentioned elements can have different sources, that along with changes of pH, temperature, and the ratio between the reagents themselves, alter the characteristics of the particles (Narayan et al., 2018). The most commonly used reagents are summarized in table 5.

Table 5: List of commonly used reagents in MSN synthesis (adapted from Narayan et al., 2018)

Chemical constituents	Function
Tetraethyl orthosilicate (TEOS)	Inorganic silica source
Tetramethoxy silane (TMOS)	Inorganic silica source
Tetrakis(2-hydroxyethyl) orthosilicate (THEOS)	Inorganic silica source
Trimethoxyvinylsilane (TMVS)	Inorganic silica source
Sodium silicate	Inorganic silica source
(3-Aminopropyl)triethoxysilane (APTES)	Silica precursor
Ethanol	Cosolvent to solubilize TEOS
Sodium hydroxide (NaOH)	Base catalyst
Ammonium hydroxide (NH_4OH)	Base catalyst
Triethanolamine (TEA)	Base catalyst, complexing agent and growth inhibitor
Diethanolamine (DEA)	Base catalyst
Cetyltrimethylammonium bromide (CTAB)	Structure directing agent/template/surfactant
Cetyltrimethylammonium chloride (CTAC)	Structure directing agent/template/surfactant
Triton X-100	Surfactant
Tween 20, 40, 60, 80	Surfactant
Disodium hydrogen phosphate-sodium dihydrogen phosphate buffer solution	Reaction medium
Triisopropylbenzene (TIPB)	Pore-expanding agent
Tetrapropoxysilane (TPOS)	Pore-expanding agent
Pluronic polymer P103	Pore-expanding agent

For many years, scientists suggested two models to explain monodispersed silica particles, which involve monomer addition and controlled aggregation. The first one, demonstrate that first there is a burst of nucleation, and then the addition of other hydrolyzed monomers to nuclei's surface result in their growth (T. Matsoukas & Gulari, 1988). The second mechanism suggests that the nucleation phase occurs along all the process, forming primary particles that became aggregated originating larger ones (Bogush & Zukoski IV, 1991).

More recently, Zhifeng Yi and his team, proposed for the first time a swelling-shrinking model, to interpret more accurately MSN's growth and organization, represented in Figure 4. This model suggests that owing to the solubilization of TEOS in CTAB hydrocarbon cores and to the adsorption of silica monomers onto CTAB micelles electrostatically, CTAB micelles size is expanded and the micellar shape changes. Then silica monomers are gradually released from the micelles' core and create a silica shell around them. Throughout this process micelles' size keeps reducing until all the silica monomers form the shell, and aggregation of silica shells with a micelle core occurs. At the end of this step, monodispersed mesoporous silica nanoparticles are achieved (Yi et al., 2015).

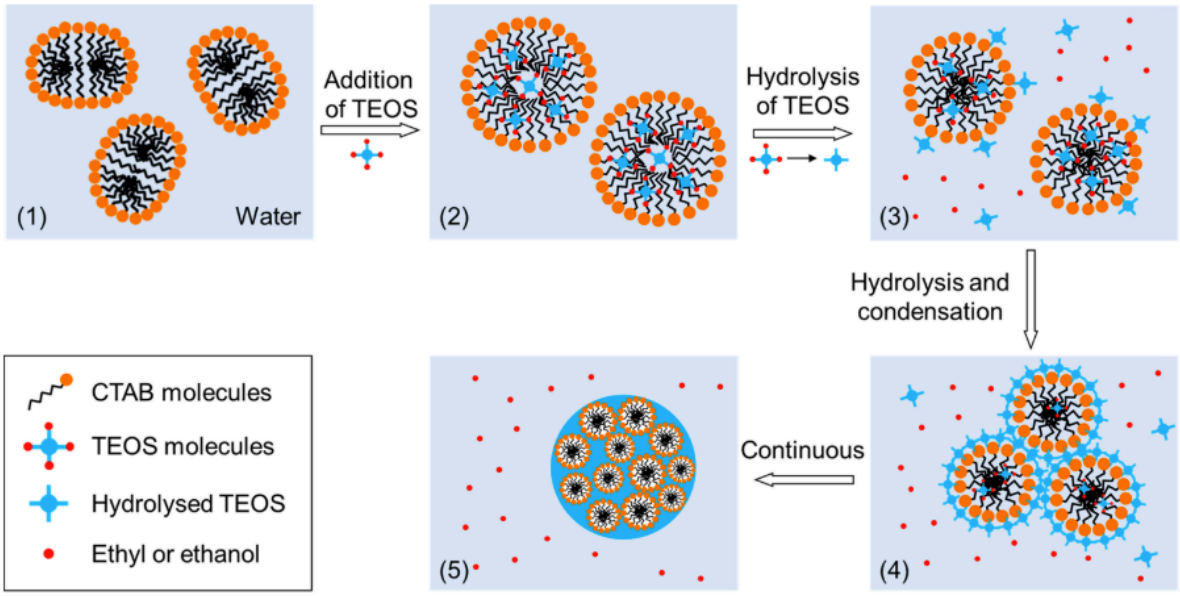

Figure 4: Schematic representation of the swelling-shrinking model (reproduced from Yi et al., 2015)

2.3.2. Properties and characteristics

Mesoporous silica nanoparticles have unique structural and biomedical characteristics that turn them into one of the most promising nanodevices to drug delivery for cancer therapy (Sábio, Meneguin, Ribeiro, Silva, & Chorilli, 2019).

The ordered porous structure and the tunable pore size allows them to store drugs and peptides and other therapeutic agents much more efficiently than other nanosystems, preventing their premature release, degradation and deactivation (Rawal & Patel, 2019; Sábio et al., 2019; Zhou et al., 2018). The large pore volume and surface area show their high potential for molecules loading and dissolution enhancement (Zhou et al., 2018), also their two functionalized surfaces can be selectively functionalized (Xu Li et al., 2013) giving them more control on the loading and release of the therapeutic agents.

Furthermore, these nanosystems can be tailored synthesized in order to achieve specific and efficient biological interactions, sufficient systemic bioavailability, targeted cellular uptake and immune-surveillance (Barkat et al., 2019).

Concerning MSN's safety, they have already been proven to have good biocompatibility and to be biodegradable (Bhakta et al., 2011; Chung et al., 2007; Farjadian et al., 2019; Shahbazi, Herranz, & Santos, 2012; J. Wang et al., 2014), due to their ability to deliver therapeutic agents without damaging healthy cells, tissues or even organs (Sábio et al., 2019), and also because they present an efficient clearance within the organism since they degrade themselves into nontoxic silicic acid *in vivo* (F. Chen et al., 2018). In addition, hybrid nanoparticles such as MSNs coated with a biopolymer, can have an advantage in the biocompatibility, showing a significant improvement in terms of toxicity, when compared with simple inorganic silica particles (Barkat et al., 2019; Hu et al., 2013).

Besides the biocompatibility properties, MSN's own structure allow them to be degraded in the intracellular environment, mainly in tumour cells. Disulfide bonds present in the base structure of some silica nanoparticles are easily broken, triggered by a red-ox reaction, due to high concentrations of glutathione (GSH), which are much higher in tumour cells (Hadipour Moghaddam, Yazdimamaghani, & Ghandehari, 2018; Saito, Swanson, & Lee, 2003). This characteristic promotes a sustained released of the therapeutic agents and contributes to the biodegradability of the nanosystem within the intracellular environment.

2.3.3. Surface modification and capping strategies

Due to the ability of the MSN to be easily functionalized, a wide diversity of chemical groups and molecules can be attached to the nanoparticles, such as antibodies and peptides for active targeting as schematized in Figure 5, fluorophores and magnetic nanoparticles for imaging, gating molecules to control the therapeutic agent release, functional groups to tune surface charge, and therapeutic agents (F. Chen et al., 2018; Sábio et al., 2019; Watermann & Brieger, 2017), allowing them to connect with specific targets and perform their function.

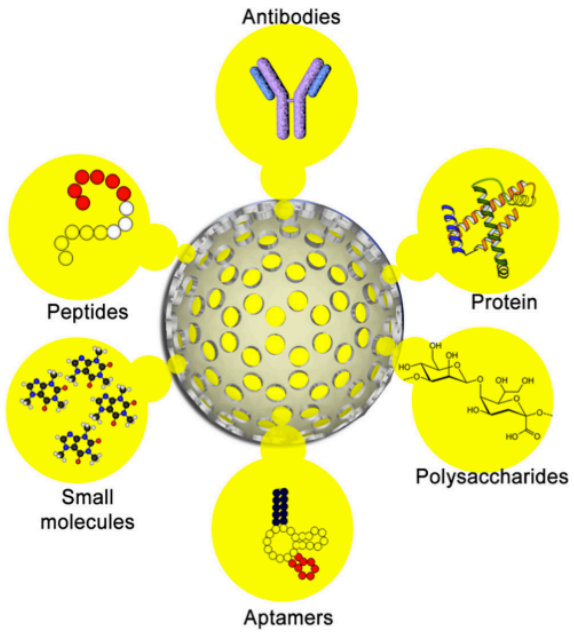

Figure 5: Ligands to functionalize MSN for active tumour targeting (reproduced from Sábio et al., 2019).

As an example, MSN can be modified with 3-aminopropyl-triethoxysilane (APETS) to cover their surface with amine groups and consequently providing them positive charge and the possibility to be functionalized with several molecules with specific functions, such as targeting (Zhou et al., 2018). For instance, to target cancer cells, the nanoparticles can be functionalized with hyaluronic acid (HA) under basic conditions (Hermanson, 2008). The connection between HA and the anime groups present on the nanoparticles' surface is activated by the carbodiimide method using N-(3-Dimethylaminopropyl)-N′-ethylcarbodiimide hydrochloride (EDC) and n-Hydroxysulfosuccinimide (NHS) (Hermanson, 2008). The reaction catalyzed by carbodimiides, of hyaluronic acid with monofunctional amines leads to the formation of

an amide linkage, resulting in functionalized MSNs with the ability to target cancer cells (Kuo, Swarm, & Prestwich, 1991).

These nanodevices can also be stimuli-responsive systems, in which MSNs can be functionalized with gatekeepers molecules, resulting on the manipulation of the carried agents release, avoiding the premature drug release, according to different stimuli characteristic of each tissue environment or external induced stimuli (Mekaru, Lu, & Fuyuhiko, 2017). Overall, this strategy enhances the release of the therapeutic agents in the tumour tissue and reduces the side effects (T. Li et al., 2019). Figure 6 shows the variety of gatekeeper molecules that can be added to the surface of mesoporous silica nanoparticles. Each molecule responds to a specific stimulus such as pH, light, magnetism and variations in their reduction or oxidation (Watermann & Brieger, 2017).

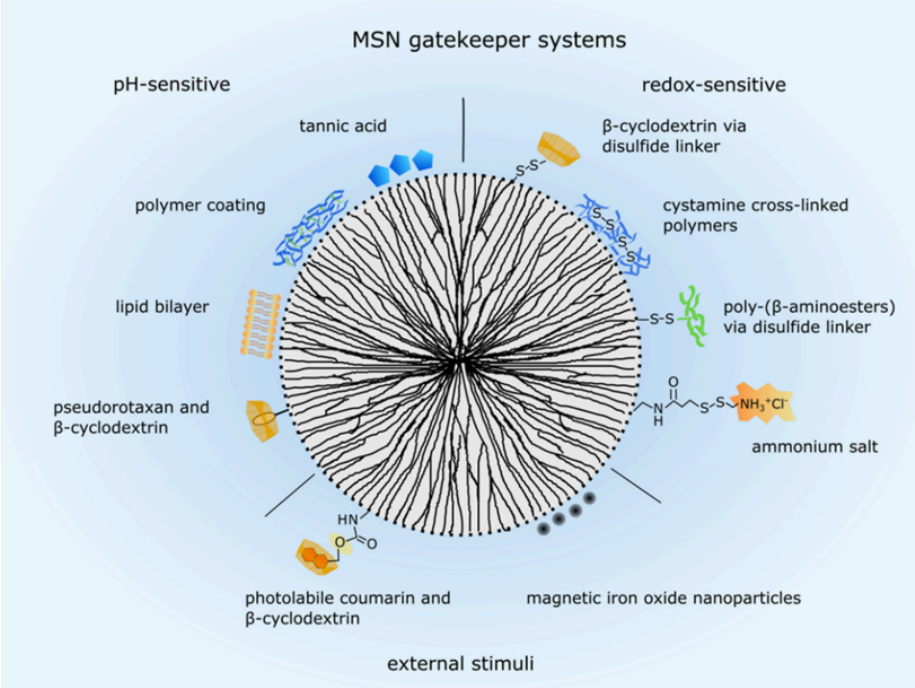

Figure 6: MSN gatekeeper systems to control drug release (reproduced from Watermann & Brieger, 2017).

2.3.4. Hyaluronic acid and it's specificity to cancer cells

The identification of cell-surface molecular targets in cancer is crucial for the development of targeted therapies. An interesting characteristic of cancer cells is the ability to express or overexpress on their surface specific types of molecules like membrane receptors or markers that can act as targets for anchorage and specific cell penetration through functionalization with ligands (Serna et al., 2018; Yao et al., 2016). Binding to these receptors promotes an endosomal uptake, leading to the internalization of nanodevices which present the specific ligands for the receptors (Unzueta et al., 2015).

These membrane markers or receptors usually are common to different types of tumours, being those from cancer stem cells (CSC), such as CD44, CD133, CD24, ESA, CXCR4, a2b1, MDR1 and ABCE2, ones of the most studied (Serna et al., 2018).

CD44, a transmembrane glycoprotein, which expression is upregulated in many cancer cells, specifically on HCC hepatocytes, is also associated with shorter survival rates in HCC patients (Dhar et al., 2018). Besides that, CD44 may be overexpressed on hepatocytes in cirrhosis and chronic hepatitis, since these are pre-neoplastic conditions (Endo & Terada, 2000).

Therefore, CD44 receptor is a promising target for nanosystem design to therapeutic strategies for HCC.

Hyaluronic acid (HA), also known as Hyaluronan, is an anionic non-sulfated glycosaminoglycan and also a mucopolysaccharide, contributing to cell propagation and migration, being able to modulate cell differentiation, adhesion, mobility, growth and inflammation (Frey, Schroeder, Manon-Jensen, Iozzo, & Schaefer, 2013; Kouvidi et al., 2011). HA structure consists of repetitions of disaccharide of glucuronic acid and N-acetylglucosamine, and it's synthesized on the plasma membrane of mammalian cells (Figure 7) (Itano & Koji, 2002).

This ligand has very appealing properties such as biocompatibility, biodegradability and non-immunogenic toxicity since it is one of the major constituents of the extracellular matrix and it's rapidly degraded by the lysosomal enzyme hyaluronidase-1 (Hyal-1), one of the most common enzymes in the tumour microenvironment (Z. Chen et al., 2013; Y. Wang et al., 2017; Zhao et al., 2015).

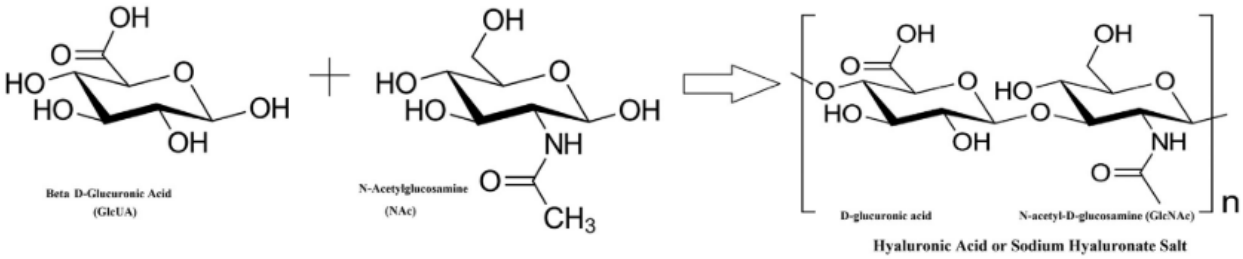

Figure 7: Chemical structure of Hyaluronic Acid.

Controversially to the aim of this work, HA can also have a pro-tumorigenic action. Hyaluronic acid not only binds to CD44 receptor but also to many other receptors, receptor for hyaluronate-mediated mobility (RHAMM), lymphatic vessel endothelial HA receptor-1 (LYVE-1), HA receptor for endocytosis (HARE), stabillin-2, toll-like receptors TLR2 and TLR4 (Figure 8), being HA's molecular weight the main responsible for the activated signalling pathway (Petrey & de la Motte, 2014; Prevo, Banerji, Ferguson, Clasper, & Jackson, 2001).

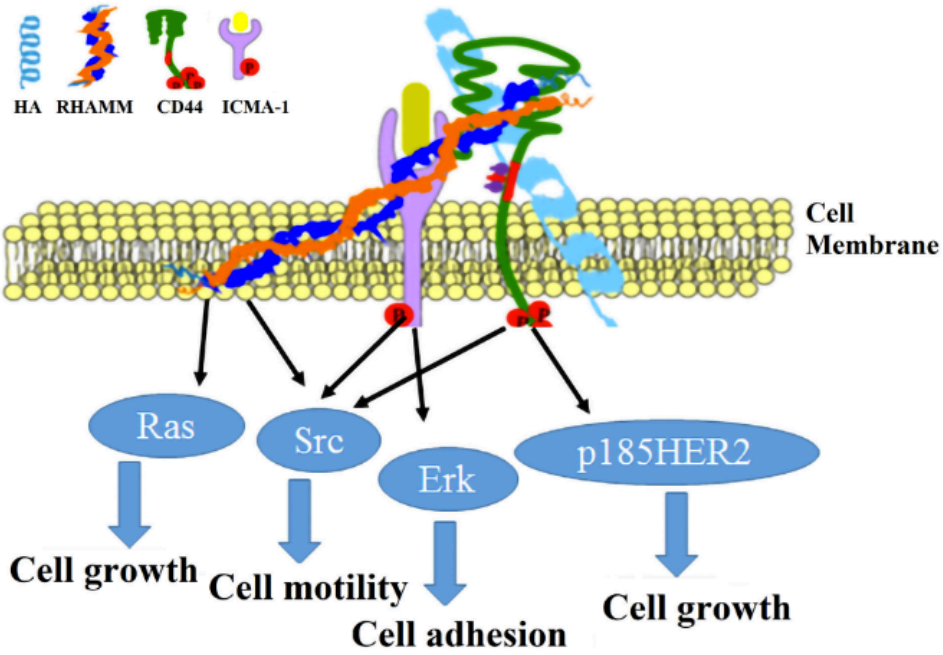

Figure 8: HA connection with its receptors and respective activation of cell mechanisms (reproduced from (Vasvani, Kulkarni, & Rawtani, 2019).

High molecular weight (HMW) HA molecules (>1000 kDa) have anti-angiogenic, anti-inflammatory and immunosuppressive characteristics, contrary of the ones presented by Low molecular weight (LMW) HA (10-250 kDa), which stimulates angiogenesis, inflammation, cell migration and proliferation. Surprisingly, HA molecules even smaller than LMW HA can induce tumour cell death (Monslow, Govindaraju, & Puré, 2015; Stern, Asari, & Sugahara, 2006; Toole & Slomiany, 2008).

Regardless this information, using HA as a target ligand to functionalize nanoparticles, is a gateway to their cellular uptake via the HA receptor-mediated endocytosis pathway, due to the affinity with the CD44, consequently ensuring the successful delivery of the therapeutic agents into cancer cells (Vasvani et al., 2019). In this case, HA's function as an activator for nanosystem internalization in cancer cells prevails over its possible pro-tumorigenic action. In fact, when HA is used as an un-loaded nanodevice ligand it doesn't exhibit toxicity to tumour cells. Only if nanoparticles are already loaded with the desired therapeutic agent, is possible to verify alterations in cell viability (Z. Chen et al., 2013; Lin et al., 2019; Wan et al., 2016; B. Zhang et al., 2019).
Even though the use of HA as a ligand for the application of nanomedicine in cancer therapies has emerged in the last years, its activity and toxicity in each nanodevice and tissue is still poorly understood, requiring further investigation on this topic (Vasvani et al., 2019).

2.3.5. Nanoparticles internalization

Regarding cellular uptake of MSN, different surface modifications lead to different internalization pathways (Farjadian et al., 2019). It has been demonstrated that nanoparticles cellular uptake not only depends on their dosage and time, but also on the cell type, particle size and shape and on their surface charge and chemistry (Shahbazi et al., 2012; Slowing, Trewyn, & Lin, 2006; Tao, Toms, Goodisman, & Asefa, 2009).
Nanoparticles can be uptake by cells via endocytosis through two main mechanisms: phagocytosis, performed by specialized cells shuch as macrophages, neutrophils, monocytes and dendritic cells, through membrane invaginations which form membrane-bound vesicles known as phagosomes; or pinocytosis, which is a process present in all types of cells can be accomplished by clathrin-dependent or independent pathways (Sahay, Alakhova, & Kabanov, 2010). Generally, endocytosis involves a first step where cargo is engulfed in membrane invaginations forming membrane-bound vesicles, endosomes. Next, endosomes deliver the cargo to specialized vesicular structures that

lead it to different destinations. Finally, cargo is transported to different cell compartments where it is recycled to the extracellular matrix or transported to secondary endosomes which fuse with lysosomes (Sahay et al., 2010; Shahbazi et al., 2012).
Several studies using specific inhibitors of cellular entrance MSN's routes, showed that mesoporous silica nanoparticles are mainly internalized by clathrin-coated vesicles (Chung et al., 2007; Farjadian et al., 2019; Huang et al., 2005).

3. Protein/peptide therapy

3.1. Therapeutic approaches using proteins and peptides

In the last decades, the use of proteins and peptides as therapeutic agents has gained great interest from the scientific community. In fact, treating health problems with something naturally produced by the human body was a revolutionary idea (Dipak et al., 2010). In the late 1980s, there were commercialized the first three recombinant proteins, orthoclone (OKT-3), human insulin and tissue plasminogen activator (Manning, et al, 2010), and since then new treatments based on recombinant proteins or peptides have become increasingly studied. Currently, for the treatment of human pathologies, more than 130 therapeutic proteins have already been approved by the FDA (Shi et al., 2019), some examples are shown in Table 6.
Proteins and peptides differ from conventional drugs because they present specific mechanisms of action and are highly potent. However there are still some limitations such as denaturation, aggregation, precipitation, adsorption, instability, immunogenicity and short circulation time in our organism (Shi et al., 2019; Dipak et al., 2010). To enhance stability and improve cellular uptake, a delivery system is frequently necessary (Shi et al., 2019). Moreover, there was created a "second and third generation" of protein therapeutics to try to overcome these issues, in which the protein or peptide can suffer mutations, or covalent attachment of other material moieties, or a change in their formulation (Dipak et al., 2010).

Table 6: Examples of recombinant therapeutic proteins and peptides approved by FDA (data obtained from the Therapeutic Peptides and Proteins database (THPdb)).

Therapeutic protein/peptide commercial name	Type of disorder
Ranibizumab	Hematological/Eye Disorder
Botulinum Toxin Type B	Neurological Disorder

Peginterferon beta-1a	Neurological Disorder
Becaplermin	Cardiac Disorder
Insulin Regular	Genetic/Hormonal Disorder
Human Serum Albumin	Hematological/Metabolic/genetic Disorder
Salmon Calcitonin	Osteological Disorder
Elotuzumab	Cancer
Interferon alfa – 2b	Cancer

3.2. Recombinant protein design and technology

At the beginning of the use of proteins as therapeutic agents, they were purified from animal and human sources, but now they are synthesized by a revolutionary technique, the recombinant DNA technology (Kimchi-Sarfaty et al., 2013). This strategy is known for the insertion of a gene into a DNA vector (often a plasmid) to form a new DNA molecule or genetic combination that can be perpetuated in a host cell and useful for the science, medicine, agriculture and industry (Glick, Pasternak, & Patten, 2008).
The protein engineering involves three main strategies: binding the therapeutic protein to another protein or polymer, introducing mutations or deletions in the primary sequence of the protein, or modifying the genetic sequence of the recombinant protein for codon optimization (Kimchi-Sarfaty et al., 2013). Thus, it is possible to give better features to the desired protein and avoid some of the typical limitations associated to the use of therapeutic proteins.

3.3. Protein transport and delivery by nanosystems

Encapsulating therapeutic proteins or peptides within a nanosystem can be an interesting solution to expand the circulation time of the therapeutic agents, to protect them from denaturation and aggregation and to promote their efficient and specific intracellular delivery (Shi et al., 2019).

In this regard, mesoporous silica nanoparticles are very promising nanosystems, since they present good biocompatibility, an easy functionable surface and an enhanced loading capacity due to its pores, as already been mentioned in section 2.3.3.

Intriguingly, in the literature there aren't many reports of MSN's carrying therapeutic proteins. However, researchers have started to evaluate the ability of these nanocarriers to be loaded with model proteins, as illustrated in Table 7.

Table 7: Different types of mesoporous silica particles loaded with model proteins.

Type of nanoparticle	Protein	Loading Efficiency (%)	Loading ratio	References
DMSNs-CHO	BSA	13.6	1:1	(Tian, Xu, & Zhu, 2017)
MSN	CytC	3.2	1:4	(Gu et al., 2013)
HMSC	BSA	9	0.26:1	(Lim, Lee, Choi, & Hwang, 2012)
HMSC	IgG	10	0.126:1	(Lim et al., 2012)

DMSNs-CHO - aldehyde-functionalized dendritic mesoporous silica nanoparticles; BSA - bovine serum albumin, MSN - mesoporous silica nanoparticles; CytC – cytochrome c; HMSC - hollow mesoporous silica capsules; IgG – immunoglobulin G.

3.4. Interferon alpha 2 b

The immune system is mainly regulated by Cytokines, which are proteins that enable the communication between immune cells, working as molecular messengers (Conlon, Miljkovic, & Waldmann, 2019). Many different types of cytokines are involved in those functions, each one with its affinity to certain receptors, specific cells and several final purposes, as schematized on Figure 9.

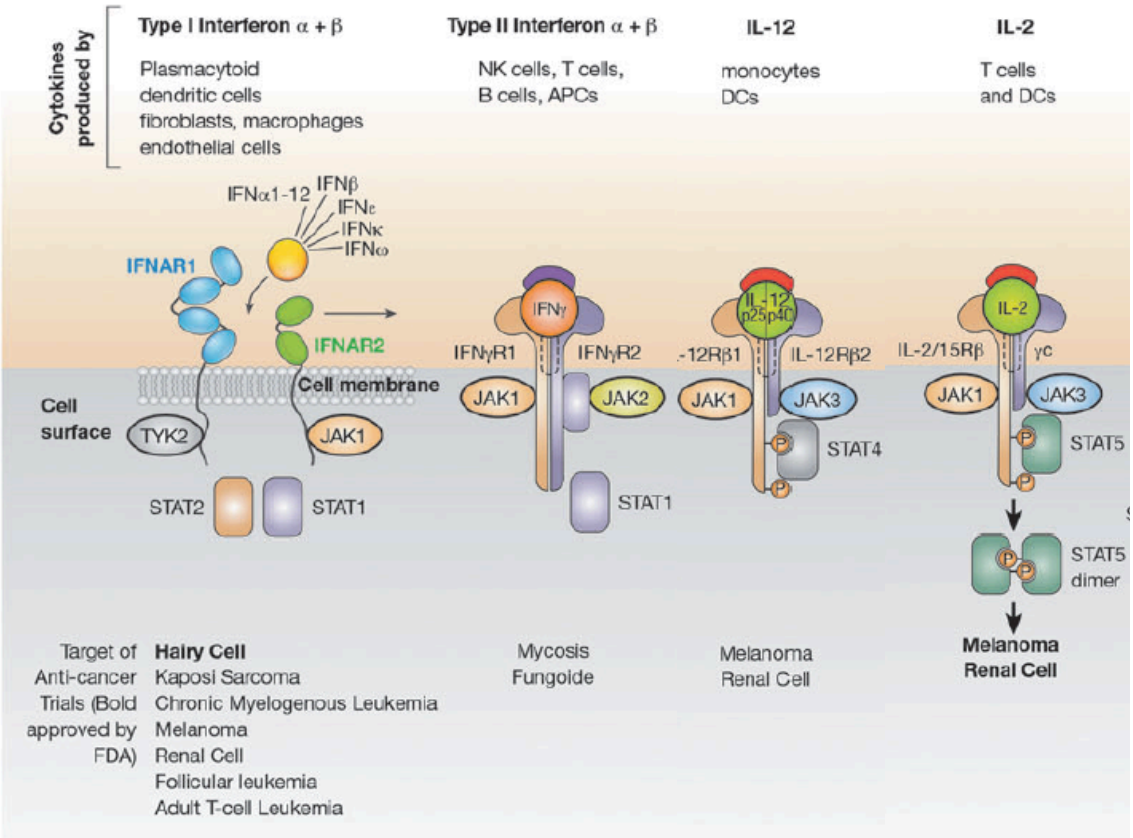

Figure 9: Representation of IFN type I and II, IL-2 and IL-12 and their receptors (adapted from (Conlon et al., 2019).

Interferon (IFN) is a multifunctional protein from the cytokine's family with varied forms, and depending on their affinity to receptors in the cell membrane, they can be divided in type I, II and III interferons. Type I interferons recognize the Interferon Alpha/beta Receptor formed by two subunits IFNAR-1 and IFNAR-2, englobing IFN α, IFN β, IFN ω and IFN τ; while type II includes IFN γ; and type III IFN λ (Asmana Ningrum, 2014; Gao, Wang, Lafdil, & Feng, 2012).

IFN-α2b, the anticancer agent chosen for this study, is a glycoprotein with 166 amino acids known for its antiproliferative, immunomodulating and antiviral properties. The cell cycle arrest and apoptotic activity promoted by IFNα-2b (Figure 10), turn it into a very appealing candidate to prevention and treatment of carcinomas, such as HCC (Damdinsuren, Nagano, Wada, Noda, et al., 2007).

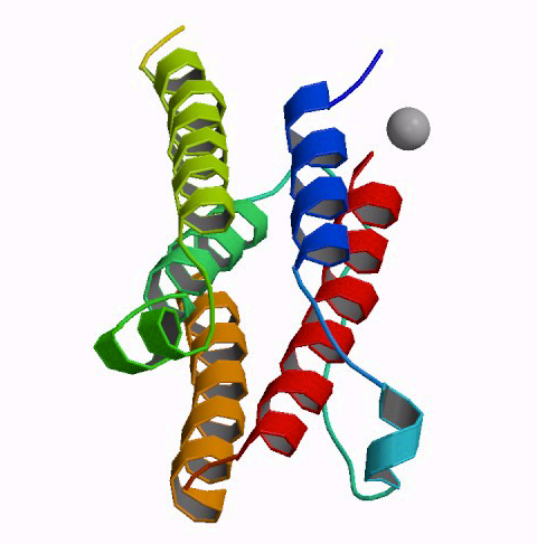

Figure 10: Molecular structure of IFNα-2b.

In fact, recombinant human IFNα-2b was the first therapeutic protein approved by the United States Food and Drug Administration (FDA) in 1986, used to treat viral infections, Hepatitis B and C, and some neoplastic diseases (Asmana Ningrum, 2014; Shimomura & Nishiguchi, 2012). Moreover, this protein is used as monotherapy or in combination with other drugs for hepatitis and cancers (Samarin et al., 2018).
Nowadays, the challenge is to find the best way to administrate it, in order to reduce the dose-dependent side effects, which include flu-like symptoms, dizziness, tiredness, weight loss, nausea and weakness (Bekisz, Baron, Balinsky, Morrow, & Zoon, 2010).

Considering the apoptotic effect induced by IFNα-2b, it is mediated by an increase in the reactive oxygen species, depending in the deregulation of Bcl-2 family consequently leading to the increase of Bax levels in mitochondria and overexpression of the gene p53 (de Luján Alvarez et al., 2002).
When IFNα-2b binds to cell membrane receptors IFNAR-1 and IFNAR-2, a signal transduction and transcription activation of Janus Kinase – Signal Transducers and Activators of transcription (JAK-STAT) occurs in HCC cells (Asmana Ningrum, 2014; Damdinsuren, Nagano, Wada, Noda, et al., 2007).
JAK 1 and Tyrosine Kinase 2 (TYK-2) are tyrosine kinase enzymes, from the Janus Kinase (JAK) protein family, that phosphorylate both IFNAR-1 and IFNAR-2 subunits, consequently causing the phosphorylation of Signal Transducers and Activators of transcription ,STAT 1 and STAT 2. Monomers STAT 1 and STAT 2 are released into the cells cytosol forming heterodimers by Interferon regulatory factor 9/p48 protein, to form an active transcription factor complex known as IFN-stimulated gene factor 3. This complex shits to the nucleus, binding to Interferon Stimulated Response Element (ISRE)

and activating the transcription of Interferon Stimulated Genes (ISG), namely ISG12a (Bekisz et al., 2010; Gao, Hong, & Radaeva, 2004; Jonasch & Haluska, 2001). The signalling cascade activated by IFN α is summarized in Figure 11.

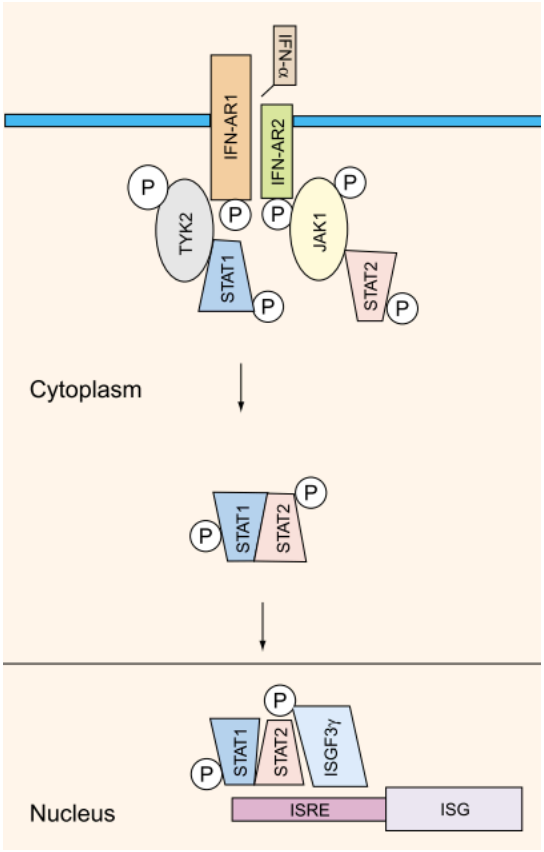

Figure 11: IFN intracellular signalling pathway (Reproduced from Jonasch & Haluska, 2001)

ISG12a is a small hydrophobic protein, encoded from the FAM14 ISG, that interferes with the mitochondrial function decreasing cell viability and enhancing sensitivity to DNA-damage-induced apoptosis (Rosebeck & Leaman, 2008). This gene leads to cytochrome c release, Bax activation and loss of mitochondrial membrane potential, showing a clear activation of the intrinsic mitochondrial-dependent cell death pathway in most cancer cells (Kotredes & Gamero, 2013).

The activation of PI3K/AKT signalling pathway by IFNα-2b also promotes the ERK 1/2 and JNK pathway activation, involving the activation of Bcl-2 family protein members Bax, Bak and Bid, causing an apoptotic effect in cancer cells (Kotredes & Gamero, 2013; Nalaskowski et al., 2003).

Nevertheless, there certainly are other unknown signalling pathways involved in the apoptotic effect and cell cycle arrest of HCC cell lines promoted by IFN-α2b, which require further research and investigation, but till now there is a significant use of type I interferon in cancer therapy research, conjugated, or not, with other therapeutic agents or nanosystems, as resumed in Table 8.

Table 8: Type I interferon use in cancer therapy.

IFN type	Dosage	Cell lines	Therapeutic outcome	References
IFN-β compared to IFN-α	2.5 ng/ml of IFN- α or IFN-β	HuH7, PLC/ PRF/5 and HLE human HCC cell lines	IFN- β exhibit a stronger antitumour effect	(Damdinsuren, Nagano, Wada, Kondo, et al., 2007)
Interferon-alpha	0, 1, 10 and 100 ng/ml IFNα For 72 hours	SCC4, Cal27, HN4, HN6 and HN30. SCC4 and Cal27	IFN-α induce PDL1 and PD1 expression as a new immunosuppression mechanism, inhibiting the killing of immune cells	(Ma et al., 2019)
Novel recombinant type I interferon	1 μg/mL or 50 μg/mL interferon for four days	Human amnion epithelium WISH cells, human (A549, HeLa, HT-29, SMMC-7721) and murine (MC38, LLC, B16F10) cancer cell lines	This interferon presents an enhanced ligand binding affinity to their receptors as well as an enhanced antiproliferative activity *in vitro*.	(K.-J. Zhang et al., 2017)
Mutant interferon alpha 2	Added at serial dilutions to the growth medium for 72 hours	WISH and MDA-MB-231 cells	Mutant interferon demonstrates a high antiproliferative activity related to an induction of apoptosis.	(Kalie, Jaitin, Abramovich, & Schreiber, 2007)
Interferon-α subtypes	(1–1024 IU/mL) of each IFNα subtypes	KYN-2, 22 KYN-3, 23 HAK-1A, 24 HAK-1B, 24 HAK-2, 25, HAK-3 and two combined hepatocellular and cholangiocarcinoma cell lines (KMCH-1 26 and KMCH-2)	The antiproliferative effect of each IFN-α subtype varies according to the cell line, conferred by apoptosis and S-phase arrest.	(Yano, Yanai, et al., 2006)
Interferon-α	5000 units/ml of IFN-α For 24 or 48 hours	Multiple myeloma cell line U266 (26) and the SV40-transformed	IFN-α induces apoptosis in cancer cells, however an intact PI3K/mTOR pathway is	(Thyrell et al., 2004)

		keratinocyte cell line Rhek-1	mandatory to this event to happen.	
IFN-aCon1	0.004, 0.016, 0.064, 0.256 or 1.024 ng/mL for 96 hours	KYN-3, HAK-1A, HAK-1B, HAK-2, HAK-3, HAK-4, HAK-5, and HAK-6, and 2 human combined hepatocellular and cholangiocarcinoma (CHC) cell lines (KMCH-1 and KMCH-2	IFN-aCon1 expressed a dose-dependent growth inhibitory effect.	(Hisaka et al., 2004)
Interferon-α	IFN-α (500 IU/mL) for 8 days	HuH7, PLC/PRF/5, HLE, HLF, HepG2 and Hep3B	IFN-α show a higher growth-inhibition activity for PLC/PRF/5 cell line	(Damdinsuren, Nagano, Wada, Noda, et al., 2007)
Recombinant IFN-α2b	rIFN- α2b (100, 500, 1000, 2000 IU/ml) During 72 hours	Human epidermoid carcinoma KB cell line	There is a dose and time-dependent growth inhibitory effect mediated by rIFN- α2b and a cell cycle perturbation.	(Quesada et al., 2003)
IFNα-2b	IFNα-2b (102, 103, 104, 105 U/mL) For 48 hours	MCF-7 cells	IFNα-2b inhibit the proliferation and migration ability of cancer cells.	(Herheliuk, Perepelytsina, Ugnivenko, Ostapchenko, & Sydorenko, 2019)
IFN-α and 5-Fluorouracil	IFN- α alone were 50 to 25,000 units/mL and those of 5- FU were 0.05 to 10 μg/mL (The medium and drugs were changed every 48 hours for ten days)	HuH7, PLC/PRF/5, HLE, and HLF, cell lines	The combination of IFN-α and 5-FU strongly induce cell growth inhibition	(Kondo et al., 2005)
Smac mimetic BV6 and interferon-α	0 to 50 ng/mL IFN, for 72 hours	RCC cell lines	This combination therapy reduces cell viability and induce apoptosis in cancer cell lines.	(Reiter, Eckhardt, Haferkamp, & Fulda, 2016)
Interferon α-2b, interleukin-2 and peripheral blood mononuclear cells (PBMC)	IFNα-2b (0–2500 U/ml) During 3 and 5 days	NIH:OVCAR-3 (CAR-3) and SKOV-3	IFNα-2b has a synergistic effect with IL-2 and PBMC increasing the cytotoxicity by 20%.	(Ingersoll et al., 2009)

IL-4, IFN-α and IFN-γ	200, 40, 8, 1.6 ng/mL for three days	OVCAR5 and A2780 cells	The combination of IL-4, IFN-α and IFN-γ present an increased ovarian cell death, being this synergistic atitumour effect dependent on interferon signalling.	(Green et al., 2019)
Pegylated IFNα-2b	PEG-IFN-a2b (16, 64, 256, 1024, or 4096 IU/ml). (cultured for 24, 48 and 72h	KIM-1, KYN- 1, KYN-2, KYN-3, HAK-1A, HAK-1B, HAK-2, HAK-3, HAK-4, HAK-5, and HAK-6; HCC cell lines	Continuous contact with PEG-IFNα-2b induces strong antitumor effects and the down-regulation of IFNAR-2 in HCC cells	(Yano, Ogasawara, et al., 2006)
Sorafenib and pegylated IFN-α2b	PEG-IFN-α2b (0, 2,000, 4,000, 8,000 IU/ ml) (constant-ratio combination) Cultured for 72 h	KIM-1 and HAK-1B cell lines	Sorafenib and pegylated IFN-α2b present a synergistic antiproliferative effect.	(Kusano, Ogasawara, et al., 2013)
Pegylated interferon α2b	PEG-IFN-a2b ($1x10^3$, $1x10^4$,$1x10^5$ IU/mL) For 24 hours	MH134 cells (HCC)	This nanosystem has remarkable anti-metastatic effects via inhibition of angiogenesis and cell adhesions.	(Arakawa et al., 2012)
Cyclic chimeric interferon-α2b	1 mg/ml IFN-α2b or 20 mg/ml of cyclic derivative in a total volume of 0.2 ml of the corresponding culture medium for 72 hours	WISH and HeLa cells	IFN-α2b cyclic peptide did not modify cell cycle phases and behave as a potent inducer of apoptosis.	(Blank, Peña, & Roguin, 2007)
Chitosan Nanoparticles for Oral Administration of Interferon-α	Chitosan nanoparticles containing 24 µg of IFN	MDBK (kidney cell line) and patients' cells	The encapsulated IFN-α conserved its activity and the particles enhanced the oral absorption of IFN-α.	(Cánepa et al., 2017)
Pegylated interferon-α	3.6–3600 ng/mL for 48 hours in serum free medium	HepG2	The antiproliferative effects of pegylated IFN-α occur due to the downregulation of miR-155.	(Ying Zhang et al., 2019)

Pegylated interferon-α2a	PEG-IFN-α2a (0.016 to 4,194 ng/mL). For 96 hours	(KYN-3, HAK-1A, HAK-1B, HAK-2, HAK-3, HAK-4, HAK-5, and HAK-6) and 2 human combined hepatocellular and cholangiocarcinoma (CHC) cell lines (KMCH-1 and KMCH-2)	PEG-IFN-α2a induces a stronger antitumour effect *in vivo* that *in vitro*.	(Kusano, Akiba, et al., 2013)

Direct administration of Interferons is presented in Table 8 with a light blue background, this strategy besides presenting a significant antitumour activity is not specific for targeted cells. To enhance the efficiency of this cytokine two approaches can be chosen, either IFN can be combined with another therapeutic agent, as is exemplified in Table 8 with a white background, or it can be encapsulated or loaded in a nanosystem (Table 8 – green background). Combination therapies have usually more positive outcomes because they can lead to synergistic or additive effects, and therefore a lower dosage of each therapeutic agent is required (Mokhtari et al., 2017). When delivered through a nanosystem or nanoplatform, therapeutic agents can specifically reach the target cells, since nanostructures can be functionalized with specific ligands of receptors or antibodies of molecules overexpressed on interest spots (Banerjee & Chen, 2010; Patra et al., 2018). Nanosystems can also overcome the limitations associated to free therapeutic agents (Jeevanandam et al., 2016) as is has already been mentioned in section 2.1.

After all, there are many reported studies about IFN and its therapeutic efficiency with promising results, but combination therapies using nanosystems to deliver the therapeutic agents are the most chosen approach of the current research works and clinical studies.

4. Chemotherapy

4.1. Types of drugs used for Hepatocellular Carcinoma

HCC is one of the cancers which exhibits the poorest response to chemotherapeutic treatments, presenting high resistance to certain drugs (Di-Wen et al., 2016). Anthracycline class of drugs, which is one of the most efficient for tumours with this type of characteristics, are cytotoxic anticancer agents that lead to cell death through several

mechanisms, which will be discussed further bellow (Bardal et al., 2011). Common drugs from this family are doxorubicin (the prototype), epirubicin, daunorubicin, idarubicin, aclarubicin and mitoxantrone (Rayner & Cutts, 2014; Šimůnek et al., 2009), which chemical structures are represented in Figure 12.

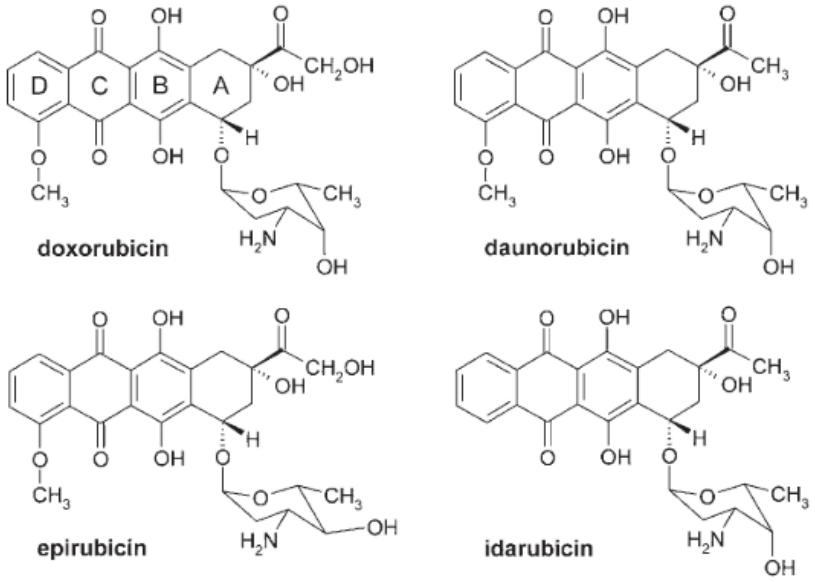

Figure 12: Chemical structures of four main anthracyclines (Reproduced from Šimůnek et al., 2009)

Considering the drug used in this study, epirubicin, the mechanism of action occurs through the intercalation of the DNA Topoisomerase II complex, inhibiting it's action and leading to a high number of DNA fragments, consequently increasing the levels of p53 and caspases, promoting the apoptosis of cancer cells, as illustrated in Figure 13 (Bardal et al., 2011; Chang, Wu, Tsai, Yu, & Tsai, 2009; Mays et al., 2010).

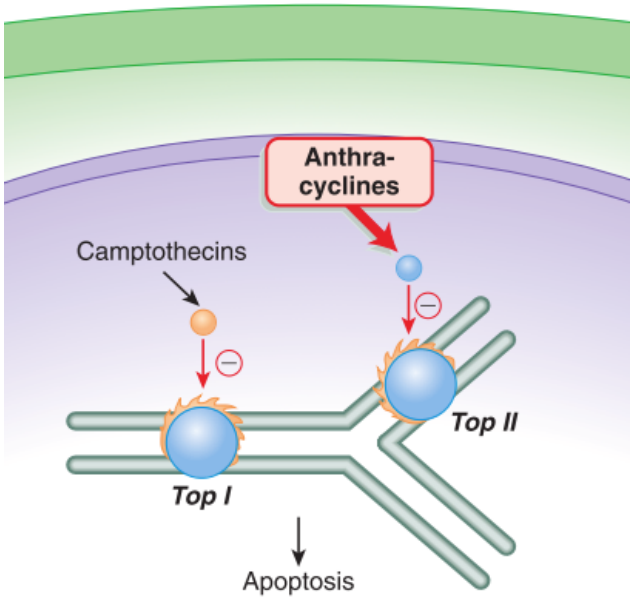

Figure 13: Anthracyclines mechanism of action (Reproduced from Bardal et al., 2011)

Besides this mechanism, anthracyclines also induce the release of reactive oxygen species which damage the cell membrane, lipids and proteins, and since they are characterized as intercalators, insert themselves into the DNA chain, also inhibiting the transcription and replication (Bardal et al., 2011; Mays et al., 2010).
Unfortunately, the anticancer effects of these drugs are accompanied by several side effects. Nausea and vomiting, alopecia (hair loss), mucositis or stomatitis, soft tissue necrosis, cardiotoxicity and myelosuppression are the most frequent side effects due to the administration of anthracyclines (Di-Wen et al., 2016). Additionally, this type of drugs is usually quickly cleared by the reticuloendothelial system (RES), weakening drug efficacy by reducing the probabilities of the drug reaching the tumour site (Šimůnek et al., 2009).

Therefore, is urgent to design delivery systems with the ability to overcome the epirubicin side effects. Nanotechnology broke this border, by developing nanosystems to avoid the drug toxicity, becoming the most efficient strategy to transport epirubicin, particularly MSN as a biodegradable and highly functionalized nanodevice.

5. Motivations and purpose of the present work

Nowadays, cancer is one of the most common causes of death worldwide, being HCC the fourth deadliest type of cancer. Since the conventional treatments are either too invasive or too harmful for the patients, with regard to the side effects, it is urgent to develop new strategies to fight this disease. Nanotechnology offers a whole new world of different approaches to combat cancer which are worth being investigated. A silica-based nanosystem was the nanocarrier chosen for this work, in view of its loading with a combination of two therapeutic agents to develop a new and more efficient strategy for cancer treatment.

The main purpose of this project, was to develop a functionalized mesoporous silica nanoparticle formulation with hyaluronic acid, to mediate an antitumor strategy to HCC, by accomplishing all the functionalization steps, as represented in Figure 14, and by proceeding with the nanosystem characterization and evaluation.

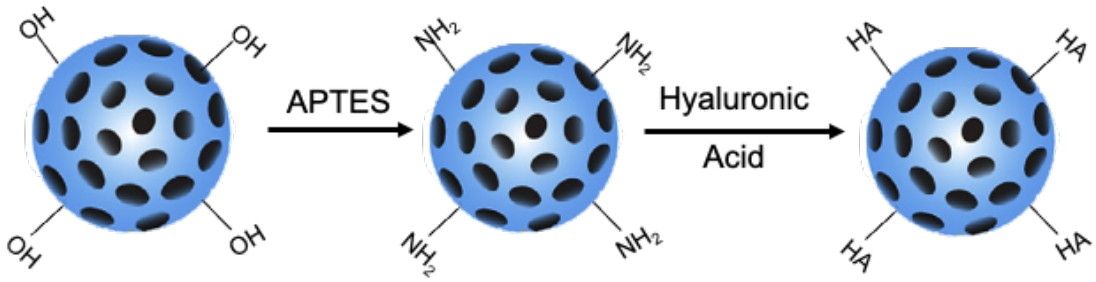

Figure 14: Schematic representation of the nanosystems functionalization steps.

The nanosystem designed for this project should be able to efficiently load and deliver two therapeutic agents to combat HCC (Figure 15), the recombinant IFNα-2b, as a pro-apoptotic and cell cycle arrest inducer protein, and epirubicin also as a programmed cell death promoter.

In order to accomplish the main goal of this study several objectives must be achieved:

- Synthesis and functionalization of the nanosystem
- Characterization of MSN's

- Protein production and characterization
- Loading of both therapeutic agents
- Evaluation of the therapeutic strategy
- Analysis of the cytotoxicity results, compared with the conventional approach

After completing these objectives, is possible to characterize this nanosystem as a promising combination therapeutic strategy to combat HCC and hopefully proceed with more studies to better characterize it and evaluate its efficiency in more detail.

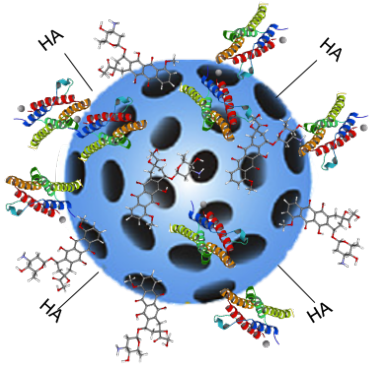

Figure 15: Schematic representation of MSN-HA loaded with both therapeutic agents.

Chapter 2
Materials and Methods

1 MSN synthesis

The synthesis method of tetrasulfide-containing mesoporous silica nanoparticles is described by Hadipour Moghaddam and co-authors (Hadipour Moghaddam, Saikia, Yazdimamaghani, & Ghandehari, 2017), and some adaptations were made from a procedure described in the literature (Cui, Li, Zhang, Zhang, & Duan, 2014; Nairi et al., 2018) to modify and functionalize the particles with Hyaluronic Acid, as referred below.

The following compounds were received from Sigma-Aldrich sodium hydroxide (NaOH ≥ 97.0%), tetraethyl orthosilicate (TEOS ≥ 99.0%), bis [propyl 3- (triethoxysilane)] tetrasulfide] (BTESPT ≥ 90.0%), 3-aminopropyltriethoxysilane (APTS ≥ 99.0%), hyaluronic acid sodium salt (HA), N-(3-Dimethylaminopropyl)-N′-ethylcarbodiimide hydrochloride (EDC ≥ 98.0 %), N-Hydroxysulfosuccinimide (NHS ≥ 97.0 %), resazurin sodium salt and sulforhodamine B monosodium salt (SRB = 75.0 %).
Hydrochloric acid (HCl ≥ 37%), absolute ethanol (EtOH), tris-base (≥ 99.0%), triethylamine (TEA) and glacial acetic acid (≥ 99.7%) were purchased from Thermo Fisher Scientific. Hexadecyltrimethylammonium bromide (CTAB, ≥ 98.0%) was obtained from Merck. Ultrapure water (H2O) was obtained using the Milli-Q® ultrapure water system (Millipore).

1.1. MSN-OH

For synthesizing tetrasulfide-containing MSN's, 110 mL of ultra-pure water, 10 mL of ethanol, 220 mg of CTAB and 900 µL of an aqueous solution of NaOH (2M) were mixed in a 250 mL round-bottomed flask at 80 ºC, with a stirring rate of 500 rpm, under reflux for 30 min. Then, a mixture of TEOS (1.24 mL) and BTESPT (0.42 mL) was added dropwise with a molar ratio of 6.6:1, simultaneously the stirring rate was increased to 1,400 rpm and the reaction occurred for 6 h.

When the previous reaction ended, the nanoparticles were precipitated and washed two times with ethanol, using centrifugation (Avanti J-20 Centrifuge – Beckman Coulter) at 14,000 rpm, 4 ºC, for 10 min.
With two sessions of 2 min in an ultrasound probe (50 W, 20 kHz, sonication amplitude 60%), the possible aggregates of nanoparticles formed were undone.
To remove the CTAB and induce the pore formation, the nanoparticles were suspended in acidic ethanol, using 1 mL of HCl 36.5% and 30 mL of EtOH 100%, and kept under reflux for 6 h at 500 rpm.
Then, nanoparticles were once again precipitated and washed two times with ethanol and ultra-pure water, using centrifugation at 14,000 rpm, 4 ºC, for 10 min. In the end, the nanoparticles were frozen to be stored before being freeze-dried.
To obtain dry and disaggregated MSN the nanoparticles were freeze-dried (CoolSafe Freeze Dryers – ScanVac, Labogene) and stored at room temperature.

1.2. MSN-NH_2

To modify the MSN-OH, a suspension of 50 mg of MSN-OH in 25 mL of ultra-pure water was prepared in a round-bottomed flask. This mixture was taken to the ultrasounds probe, in two sessions of 2 min, to be homogenized. Then 50 µL of APTES were added, and the mixture was left under stirring at 500 rpm, 50 ºC, for 24 hours.
Then the nanoparticles were submitted to centrifugation to separate them from the reagents that didn't react, at 14,000 rpm, 20 ºC, for 10 minutes, and the supernatant was discarded. MSN-NH_2 were also washed with water by two centrifugation cycles at 14,000 rpm, 20 ºC, for 10 minutes, to be then freeze-dried overnight and stored.

1.3. MSN-HA

To functionalize the nanoparticles, 60 mg of HA were added to 30 mL of ultra-pure water to be totally dissolved and remained in agitation (500 rpm) in a separate beaker for approximately 1 hour. An aqueous solution of EDC (33.9 mg) and NHS (55.8 mg) was prepared in 30 mL of ultra-pure water. After that, both the solutions previously made were mixed and homogenized. In order to mix the reagents with the silica nanoparticles, 50 mg of MSN-NH_2 were dispersed and homogenized in 50 mL of ultra-pure water in a round-bottomed flask using ultrasounds, and then the EDC/NHS mixture and the HA solution were poured into the MSN-NH_2 dispersion. The pH of the final mixture was

adjusted to 9, through the addition of a very diluted solution of TEA and was left reacting overnight in a 38 ºC bath at 500 rpm.
To obtain pure functionalized nanoparticles, a centrifugation was performed, at 14,000 rpm, 20 ºC, for 10 minutes, to separate them from the unreacted HA and possible leftovers of the remaining reagents. Then they were washed two times with water, by centrifugation at 14,000 rpm, 20 ºC, for 10 minutes, and freeze-dried overnight to finally be stored.

2. MSN characterization

In order to monitor the nanoparticles size and surface charge, in each step of the made successive modifications, measurements using Dynamic Light Scattering (DLS) and Laser Doppler Velocimetry (LDV) were performed.
In the first place, aqueous suspensions of MSN-OH, MSN-NH2 and MSN-HA were prepared with ultra-pure water (pH=7) at a final concentration of 100 µg/mL and submitted to two cycles of two minutes of ultrasounds to avoid particles aggregates. Next, the suspensions were transferred to a disposable folded capillary cell DTS1070 (ZetaSizer Nanoseries, Malvern) and introduced in the Zetasizer Nano ZS (Malvern Instruments Ltd., UK).
The Hydrodynamic Diameter and the respective Polydispersity Index of each type of particle were firstly determined by DLS measurements at 25 ºC, with a detection angle of 173º (backscatter detection). Then, the zeta potential measurements were performed using LDV to every nanoparticles type, applying the Smoluchowski Model. With this method is possible to access the electrokinetic potential between the dispersion medium and the stationary layer of fluid attached to the dispersed particle, giving an idea about the charge of the last layer present in nanoparticles (Barba et al., 2019).

3. Protein production and purification

The following described transformation and cloning procedures were adapted from the literature (Sambrook & Russel, 2001), and the methodology used in the protein expression was adapted from the NZYTech® protocol for the BL21(DE3) Competent Cells.

Within the materials used, LB Broth powder, Agar, Kanamycin (monosulphate), Isopropyl β-D-1-thiogalactopyranoside (IPTG), Imidazole, TEMED, AMPS and SDS were obtained from NZYTech.

3.1. Expression vector details

The expression vector used to produce the recombinant protein was synthesized and modified by *GeneCust*, a biotechnology company, and consisted in a high copy Kanamicyn resistant plasmid (pSMART® HCKan plasmid) (Figure 16) with an optimized sequence of IFNα-2b, for a more efficient and accurate expression in a prokaryotic system. In 2017, Kang-Jian Zhan and his team have proven the enhanced antitumorigenic effect of the optimized recombinant IFNα-2b (Zhang et al., 2017), which sequence was inserted into the plasmid used in this work.

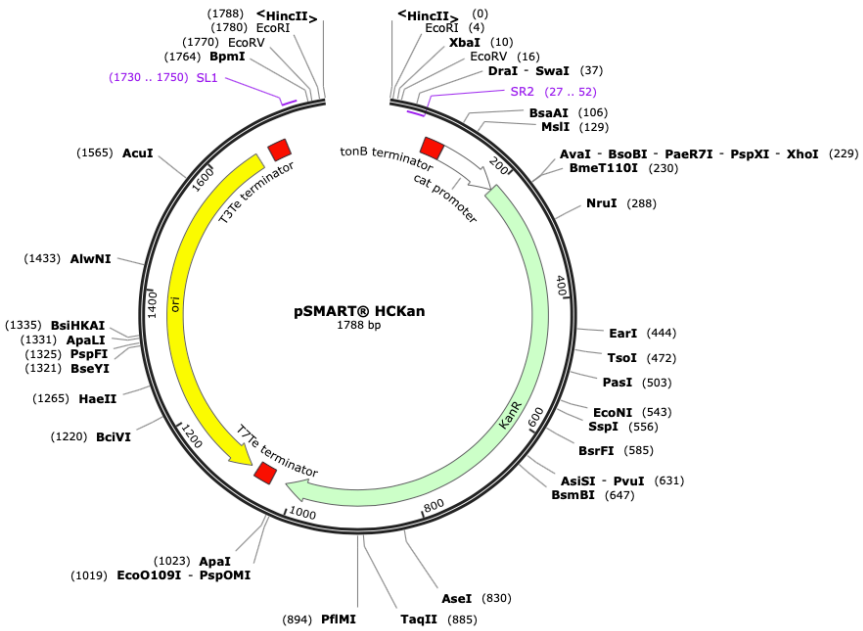

Figure 16: Schematic representation of the High Copy Kanamycin-resistant pSMART ® vector. (https://www.snapgene.com/resources/plasmid-files/?set=basic_cloning_vectors&plasmid=pSMART_HCKan_(linearized))

3.2. LB Medium and LB medium plates with agar preparation

In order to prepare 500 mL of Luria Broth (LB) medium, 12.5 g of LB powder were dissolved in 500 mL of ultra-pure water and subjected to an autoclave sterilization period. In the case of the medium destined for the plates, 12.5 g of LB powder were also dissolved in 500 mL of ultra-pure water and 7.5 g of agar were added, this flask was also subject to autoclave sterilization. After a cooldown period, a volume of 0.5 mL of Kanamycin (30 mg/mL) was added to each flask under sterile conditions. The flask containing agar was gently shaken and approximately 10 mL of medium were transferred to sterile Petri dishes. Upon medium solidification, Petri dishes were stored at 4 ºC.

3.3. Transformation and cloning of *E. coli* competent cells

A sample of the original dried stock of plasmid sent by the company was resuspended in 10 µL of ultra-pure water. To measure the plasmid concentration, NanoDrop™ 2000 Spectrophotometer (Thermo-Fisher) was used, by which was possible to verify that the plasmid presented a concentration of 320.5 ng/µL. Another dilution of 1:10 was made to the plasmid sample ending up with 10 µL of 32.05 ng/ µL of DNA.

Next 1.5 µL of the plasmid suspension (32.05 ng/µL) was added to 50 µL of two *E. coli* competent strains, BL 21 *star* and BL 21 c *plus*, which were left on ice for incubation for 30 minutes. Cells were then transferred into a bath at 42 ºC for 40 seconds, in which the heat chock took place, followed by 2 minutes on ice once again.

Then 900 µL of sterile LB medium at 37 ºC was added to the cells tube and during 1-hour cells were left to recover from the heat chock under a rotation of 225 rpm at 37 ºC. After the recovering period, cells were centrifuged (Sigma 1-15) for 1 minute at 12,000 rpm at room temperature and around 700 µL of the supernatant were discarded and pellets were resuspended in 200 µL of LB medium.

Lastly, the remaining 200 µL of the cell suspensions were resuspended and spread in prewarmed LB - Kanamicyn plates at 37 ºC. The plates were left incubating over-night in an inverted position. On the next day, plates containing a substantial colony growth were sealed with parafilm and stored at 4 ºC.

3.4. Glycerol cell stocks preparation

Isolated colonies from the plates were picked to a falcon tube with 5 mL of LB medium with Kanamycin (30 mg/mL) and were left grown overnight at 37 ºC with a stirring rate of 200 rpm.
On the next day, 250 µL of the cell culture suspension were added to 250 µL of sterile 87% glycerol (1:1) and stored at -80 ºC, resulting in several glycerol cell stocks than can be further used to do pre-inoculates.

3.5. Pre-inoculate

To prepare the pre-inoculate, 200 µL of glycerol cell stock containing BL21 Star cells, previously transformed with the plasmid, were suspended in 10 mL of LB medium with 30 µL of Kanamicyne. The cell culture was left to grow overnight at 37 ºC with constant stirring in a shaking incubator.

3.6. IFNα-2b expression

The cell culture of the pre-inoculate, 10 mL, was added to 500 mL of the previously prepared LB medium, along with 0.5 mL of Kanamycin (30 mg/mL) in a ratio of 1:1000. Then, this cell culture was placed to grow on an incubator at 37º C with a stirring rate of 180 rpm, while the Optical Density (O.D.) at 600 nm was controlled by a spectrophotometer (LKB Biochrom 4050 Ultraspec), for approximately 2 hours and 30 min.
After this period, when the O.D. reached the 0.560 arbitrary units (a.u.) the temperature was lowered to 20º C for 20 minutes, in order to decrease the cell metabolism and proceed with the protein expression induction when the O.D. was between the 0.6 – 0.8 a.u.
Then, 0.2 mM IPTG were added for the IFNα-2b expression induction. The culture was grown overnight at 20º C with a stirring rate of 200 rpm (Novagen, 2003).

3.7. Cellular lysis

The cell culture was distributed for two flasks and *E. coli* cells were sedimented through centrifugation (Avanti J-20 Centrifuge – Beckman Coulter) at 6,000 rpm, 4º C, for 10 minutes. The supernatant was discarded, and the pellets were frozen at -20º C overnight. For the cell lysis, NZY Bacterial Cell Lysis Buffer from NZYTech was used. The cell pellet was resuspended at room temperature on 5 mL of Buffer per gram of sample. 2 µL of lysozyme and 2 µL of DNAse I were added per mL of Buffer. The cell suspension was incubated on a shaking platform for 10 to 20 minutes at room temperature. The protein was recovered by centrifugation at 15,000 g for 15 minutes at 4º C and the supernatant was collected, since it contained the protein on its soluble form.

3.8. Protein purification

The sample containing the supernatant was filtered through a sterile, endotoxin-free, hydrophilic, cellulose acetate membrane with 30 mm of diameter and 0.45 µm of pore diameter (Orange Scientific).

Then to proceed with the protein purification, an IMAC affinity chromatography was performed at medium pressure using the ÄKTA start protein purification system, with a 5 mL HisTrap HP histidinetagged protein purification column (GE Healthcare).

The column was equilibrated with 25 ml of PBS supplemented with 20 mM Imidazole at a flow rate of 2 ml per minute. Subsequently, it was loaded with 50 ml of soluble protein at a flow rate of 1 ml per minute. After loading, 10 to 15 ml of PBS with 20 mM imidazole were perfused through the column. Once absorbance levels stabilize and reach baseline levels, elution was performed sequentially with PBS solutions supplemented with 100mM and 500mM Imidazole.

During all the purification process, fractions of 2 to 7 ml were collected and stored at -4º C in falcon tubes. In an attempt to optimize the collection of fractions with a greater amount of protein and in a purer state, the volume collected to each falcon tube correspondent to the absorbance peaks was smaller, trying to never exceed the 5 mL for the most significant points.

3.9. Sodium dodecyl sulfate – polyacrylamide gel electrophoresis (SDS-PAGE)

The electrophoresis allows us to check whether the purest fractions of the chromatography actually contain the desired protein. The protocol involves three main steps: firstly, the polyacrylamide 12% gel preparation, then electrophoretic separation of the various protein fractions, and finally revealing the gels.

For the resolving gel 4.8 mL of ultra-pure water; 4.6 mL of Tris pH 8.8 (1.5 M); 4.4 mL of 40% acrylamid:bisacrylamide (29:1); 140 µL of 20% SDS; 140 µL of 10% AMPS and 20 µL of TEMED were mixed on a 50 mL falcon tube. Then this mixture was rapidly homogenized, transferred into the gel holder and covered with isopropanol to prevent the bubble formation and the correct gel polymerization. Next a stacking gel was prepared using 3.8 mL of ultra-pure water; 1.5 mL of Tris pH 6.8 (0,625 M); 600 µL of 40% acrylamide:bisacrylamide (29:1); 60 µL of 20% SDS; 60 µL of 10% AMPS and 15 µL of TEMED on a 50 mL falcon tube. The isopropanol was removed, the mixture was rapidly homogenized and transferred into the gel holder followed by the introduction of the comb.

Samples of the relevant protein fractions were denatured with a Denaturation Buffer (2 mg/ml protein with 1% SDS, 10% glycerol, 10 mM Tris-Cl, pH 6.8, 1 mM ethylene diamine tetraacetic acid (EDTA), 80 mM dithiothreitol (DTT) and bromophenol blue (~0.05 mg/ml)) (1:1) in an Eppendorf tube and incubated in a hot bath at 100 ºC in a thermoblock (Stuart Scientific) for 5 minutes. A protein ladder (Precision Plus Protein™ All Blue Protein Standards – Bio-Rad) was loaded into the polyacrylamide gel, which was already immersed in an electrophoresis recipient, as well as all the samples already denaturized. For the electrophoretic separation of the various protein fractions, the gels were submitted to a 130 V voltage for 15 minutes, which was then increased to 180 V during 45 minutes at room temperature. In order to reveal the gels, they were stained with a Coomassie Blue Staining Solution (0.1% Coomassie Blue dye in 50% methanol, 10% glacial acetic acid) for 15 min in a shaker and then destained overnight with Coomassie Blue Destaining Solution (50% methanol, 10% glacial acetic acid) at room temperature.

3.10. Protein dialysis

After analyzing the electrophoresis results, only three fractions were chosen to be dialyzed to remove the PBS and Imidazole salts.
The membrane with 24 Å of pore size (Medicell International Ltd.) was left in ultrapure water for 20 to 30 minutes to hydratate. Then the protein fractions were transferred for the membrane and stayed under constant stirring for 15 minutes at room temperature. The membrane was then left overnight at 4º C and the water was changed whenever possible. On the next day, before collecting the sample, the water was once again changed, and the membrane stayed in a constant stirring for 20 minutes. The protein soluble fraction was transferred for two falcon tubes and frozen at -80º C, being then freeze-dried for 24 hours.

4. Protein loading in MSN

To load the nanoparticles with the recombinant protein, a water-based suspension of nanoparticles was mixed with a solution of IFNα-2b, based on the solution-immersion method and adapted from previous protein loading studies (Shi et al., 2019; Vieira, 2019)

Specifically, 7 mg of MSN-NH_2 or 7 mg of MSN-HA were suspended in 1 mL of ultrapure water and homogenized with an ultrasonic probe in two cycles of 1 minute. For each suspension, a solution of 7 mg of IFNα-2b in 1 mL of water was used, and gently mixed for 10 seconds. Samples were centrifugated at 14,000 rpm for 5 min at room temperature (Eppendorf 5810R Centrifuge –Eppendorf) and washed with ultrapure water to remove the unloaded protein. The supernatants were collected to quantify the amount of unloaded protein and the pellets were frozen at -80º C and stored to be further freeze-dried. After that, the amount of protein present on each supernatant was quantified by the Bio-Rad protein assay, which is based on the bradford method.
In a 96-well plate there were added 160 µL of the supernatants and 40 µL of the dye reagent in each well, the absorbance was read at 595 nm using a spectrophotometer spectramax Plus 384 (Molecular Devices LLC). For the calibration curve, the absorbance of BSA solutions in ultrapure water with increasing concentrations (0 to 80 µg/mL) was measured at 595 nm, and used to assess the protein concentration in the supernatants.

The loading efficiency (LE) and loading capacity (LC) of nanosystems were then calculated with the following formulas:

$$LE(\%) = \frac{weight\ of\ the\ loaded\ protein}{weight\ of\ the\ initial\ protein} \times 100 \quad (1)$$

$$LC(\%) = \frac{weight\ of\ the\ loaded\ protein}{weight\ of\ the\ nanoparticles} \times 100 \quad (2)$$

5. Drug loading in MSN

Epirubicin Teva 2 mg/mL (Epi), hydrocloride solution for injection, was obtained from Centro Hospitalar da Universidade de Coimbra (CHUC), through the existing protocol with *Instituto de Biofísica da FMUC*, and kindly given by Prof. Dr. Ana Cristina Santos.

Epirubicin, an anticancer drug used in chemotherapy treatments, was loaded into mesoporous nanoparticles according to the procedure described by Yuanyuan Zhang *et al.* (Yuanyuan Zhang et al., 2015).

For that purpose, aliquots of 5 mg of MSN-HA were suspended in 1 mL of epirubicin solution (2 mg/mL), using an ultrasonic probe. Then the suspensions were left in the roller for 24 hours protected from light. On the next day, the samples were centrifugated (Eppendorf 5810R Centrifuge – Eppendorf), at room temperature and 14,000 rpm for 5 minutes, and washed twice with ultrapure water to remove the remaining drug that couldn't be loaded in the particles. The supernatants were collected for further quantification and the pellet with the loaded nanoparticles was frozen to be then freeze-dried.

To quantify the amount of drug present in the supernatants, the absorbance of the sample triplicates, previously diluted, was read at 480 nm using a spectrophotometer Spectramax Plus 384 (Molecular Devices LLC). Successive dilutions of epirubicin were made to obtain the calibration curve, from which was possible to determine the drug concentration of each supernatant.

Finally, the loading efficiency and loading capacity of the nanosystem were accessed using the same equations mentioned in section 4 of this chapter.

6. Loading of both therapeutic agents

In order to obtain a nanosystem loaded both with epirubicin and IFNα-2b, a sample of 5 mg of previously drug-loaded MSN-HA was suspended in 1 mL of a solution containing 5 mg of the recombinant protein, using the same procedure described in the above-mentioned section 4.

The sample was centrifugated at 14,000 rpm for 5 min at room temperature (Eppendorf 5810R Centrifuge – Eppendorf) and washed with ultrapure water to remove the unloaded protein. The supernatants were collected to quantify the amount of unloaded protein and the pellet was frozen at -80º C and stored to be further freeze-dried. The concentration of unloaded protein present in the supernatants was once again accessed using UV-Vis absorption spectroscopy (Spectramax Plus 384 - Molecular Devices LLC), based on the bradford method as mentioned in section 4.

Lastly, the loading efficiency and loading capacity of the drug-loaded nanosystem were evaluated considering equations 1 and 2 of the section 4.

7. Cytotoxicity assays

7.1. MSN-HA biocompatibility

The biocompatibility of mesoporous silica nanoparticles has already been proven by various studies (Bhakta et al., 2011; Chung et al., 2007; Farjadian et al., 2019; Shahbazi et al., 2012; J. Wang et al., 2014). Nevertheless, is mandatory to ensure that these MSN functionalized with Hyaluronic Acid didn't confer cytotoxicity by themselves. Thereby, a screening of different concentrations of unloaded MSN-HA was performed in HepG2 cells. This cell line was derived from the liver tissue of a 15-year-old Caucasian American male with well-differentiated HCC. The cells were maintained at 37 ºC, under 5% CO2 in DMEM-HG, supplemented with 10% (v/v) heat-inactivated FBS, penicillin (100 U/mL) and streptomycin (100 µg/mL).

Cells were seeded onto 48-well plates with a density of 80,000 cells per well and incubated to grow for 24 hours. The culture medium was then removed and substituted for fresh medium containing different concentrations of MSN-HA ranging from 72.2 to 617.3 µg/mL in a total volume of 0.5 mL per well. Fresh medium without particles was used for the positive control and all the samples were tested in triplicates. Cell viability was accessed using the Alamar Blue assay at 48, 72 and 144 hours after the cells have been incubated with the particles. Following each one of these times, the culture medium

was replaced for 300 µL of new medium containing 10% (v/v) of resazurin, prepared from a 0.1 mg/ml stock solution of resazurin, and the cells were incubated for further 2 hours. After this period the colouration should change from blue to pink due to the resazurin reduction to resorufin, caused by metabolic active cells. This assay measures the red-ox potential of cells. From each well, 180 µL of supernatant was collected and transferred to a 96-well plate in order to measure the absorbance at 570 and 600 nm in a spectrophotometer SpectraMax Plus 384 (Molecular Devices, USA).
Cell viability was calculated based on the absorbance results, considering the positive (C^+) and negative (C^-) controls, according to the following formula:

$$Cell\ viability\ (\%) = \frac{(A_{570} - A_{600}) - (C^-_{570} - C^-_{600})}{(C^+_{570} - C^+_{600}) - (C^-_{570} - C^-_{600})} \times 100 \quad (3)$$

7.2. Protein activity evaluation

For the assessment of the effect of IFNα-2b in the viability of HCC cell lines, several concentrations of the produced recombinant protein (IFN-R) and of one sample of IFNα-2b provided by the company responsible for the development of the recombinant plasmid, were incubated with HepG2 cells. The company protein sample is also a recombinant protein, produced from the same cloning vector and according to the company's protocols and equipments, from now on, it will be designated as commercial protein (IFN-C).
Cells were seeded onto 48-well plates with a density of 40,000 cells per well and incubated to grow for 24 hours. The culture medium was then removed and substituted for fresh media samples with IFN-R and IFN-C concentrations ranging from 0.5 to 25 µg/mL in a total volume of 0.5 mL per well. For the positive control group, fresh media without proteins was used. Samples were all tested in triplicates and incubated for 48 hours. After this period, the cell viability was evaluated using the Alamar Blue assay and cells were once again incubated with the same conditions for another period of 48 hours. At the end of the incubation time (96 hours), the cell viability was accessed again with the Alamar Blue assay and also with the Sulforhodamine B (SRB) assay.

For each condition, the percentage of living cells, according to the Alamar Blue assay was calculated as described in section 7.1.

The SRB assay is based on the measurement of cellular protein content, used for cell density and proliferation determination. To perform this assay, at the end of all incubations, each well of the plate was washed 3 times with PBS and then filled up with 200 µL of a solution composed by 1% of acetic acid in methanol, and the plates were placed at -20 ºC for at least 1 hour. Then, the solution in the wells was discarded and the plates were dried for 1h 30 min at 37º C.

Afterwards, 200 µL of a solution of 0.5% of SRB and 1% of acetic acid were used to stain the remaining cells and the plates were let to dry for 1 hour at 37 ºC. Then the wells were washed 3 times with a solution of 1% of acetic acid and dried for another 1h 30 minutes at 37 ºC.

Finally, the wells were filled up with 1 mL of a solution of Tris Base at 10 mM and pH=10 and the plates were left in an orbital spinning for 20 minutes.

At last, 200 µL of each well were transferred to a 96 well plate and the absorbances were read at 540 nm in a spectrophotometer SpectraMax Plus 384 (Molecular Devices, USA).

Cell viability according to the SRB assay was calculated using the following equation:

$$Cell\ viability\ (\%) = \frac{A_{540} - C_{540}^{-}}{C_{540}^{+} - C_{540}^{-}} \times 100 \quad (4)$$

7.3. Loaded nanoparticles cytotoxicity

For the evaluation of the cytotoxicity of nanoparticles loaded with both therapeutic agents, HepG2 cells were seeded onto 48-well plates at a density of 40000 cells per well and incubated to grow for 24 hours. Then the culture media was removed and replaced with fresh media containing functionalized nanoparticles loaded with the therapeutic agents or containing free drug and/or free protein. The tested conditions are resumed in Table 9.

Table 9: Experimental conditions of the cytotoxicity assay.

Accessed conditions	**Concentration depending on the therapeutic agent (µg/mL)**
Free Epi	0.13, 0.31, 3, 12.5
MSN-HA-Epi	0.13, 0.31, 3, 12.5
Free recombinant IFNα-2b	0.5, 1.25, 12, 50
MSN-HA-IFNα-2b	0.5, 1.25, 12, 50
Free Epi + IFNα-2b	(0.13+0.5), (0.31+1.25), (3+12), (12.5+50)
MSN-HA-Epi- IFNα-2b	(0.13+0.5), (0.31+1.25), (3+12), (12.5+50)

Fresh medium without particles or therapeutic agents was used as a positive control. After 48 hours of incubation with these experimental conditions, cell viability was accessed using the Alamar Blue assay described in section 7.1. Next, cells were incubated for an additional period of 48 hours with the conditions previously tested and at the end of this period cell viability and proliferation was evaluated with the Alamar Blue assay and SRB assay explained in section 7.2.

Chapter 3
Results and Discussion

This chapter contain the results obtained during this work as well as their respective discussion. During this project, several subjects were studied, so this chapter was dived in four main sections: synthesis and characterization of MSN; protein production; loading of the therapeutic agents; and evaluation of the anticancer potential of the designed formulation.

1. Mesoporous Silica Nanoparticles synthesis, pore induction and functionalization with Hyaluronic Acid

Synthesis of MSN was performed according to the modified Stöber method, where hydrolysis and condensation reactions of silica sources take place (Narayan et al., 2018). Firstly, the surfactant CTAB acts like a template and forms molecular clusters, micelles, when in contact with the aqueous solvent. Then, the silica precursors TEOS and BTESPT hydrolyze in silica species and ethanol, and their condensation lead to the formation of siloxane connections around the micelles (Figure 17), originating rounded nanoparticles with hydroxyl groups in their external surface, MSN-OH (Zhuravlev, 2000). It is important to notice that BTESPT contains tetrasulfide bonds, which are easily degraded when exposed to Glutathione (GSH) (Hadipour Moghaddam et al., 2017). Besides GSH concentration levels being significantly different in the extracellular fluids (10 μM) and intracellular medium (1 to 10 mM), the cytosolic concentration of GSH in most tumour cells is usually 3-folds higher than in normal cells (Saito et al., 2003). This can be advantageous for a partially controlled release of the therapeutic agents encapsulated within the MSN, which presents a tetrasulfide-containing silica matrix, once they are internalized by the tumour cells.

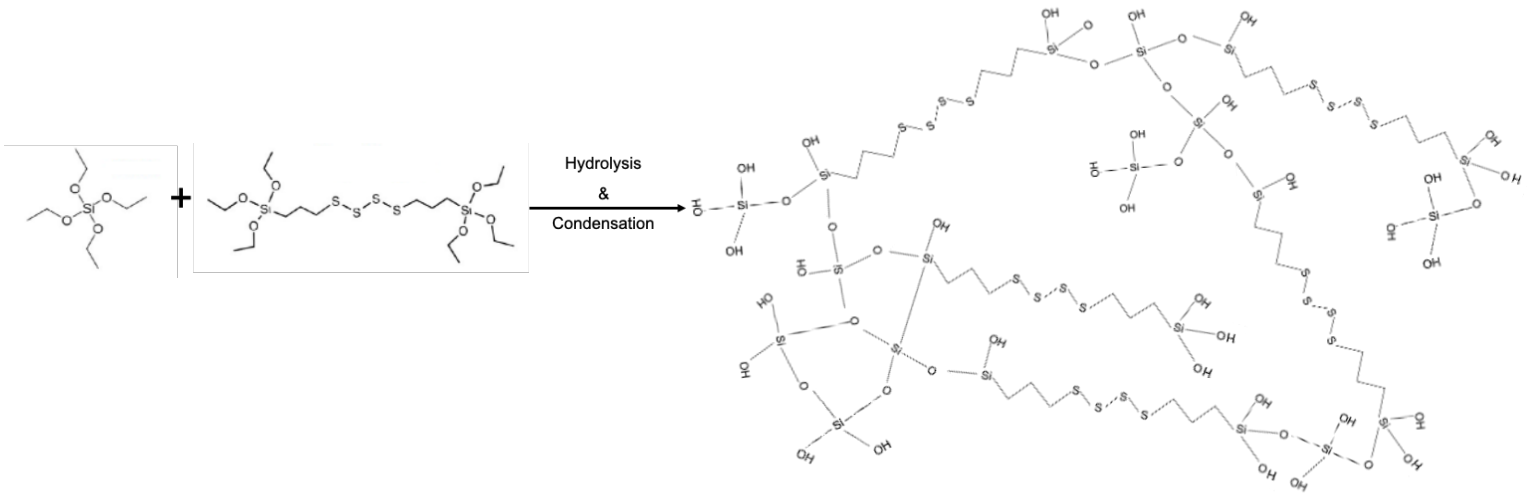

Figure 17: Brief representation of the silica matrix formation.

Nevertheless, the surfactant needs to be removed from the nanosystem to form the mesopores (in average rounding 5 to 20 nm of diameter (Hadipour Moghaddam et al., 2017)) and decrease the toxicity of the preparation. So, the nanoparticles were washed and precipitated in an acidic ethanol solution, resulting in the extraction of the surfactant with the solvent (Alvarez-Toral et al., 2017) (Figure 18).

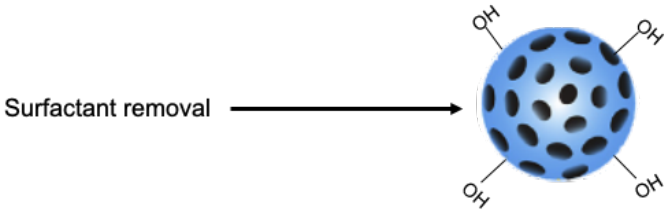

Figure 18: Representation of mesoporous silica particles after CTAB removal.

The nanoparticles modification with amine groups occurred through covalent binding of APTES to the hydroxyl groups, conferring positive charge to the MSN (Hadipour Moghaddam et al., 2017), denominated MSN-NH_2. In detail, firstly occurs the APTES hydrolysis, followed by a silanol condensation in which, APTES is covalent bonded to the hydroxyl groups on the surface of MSN-OH, as illustrated in Figure 19 (Hermanson, 2008).

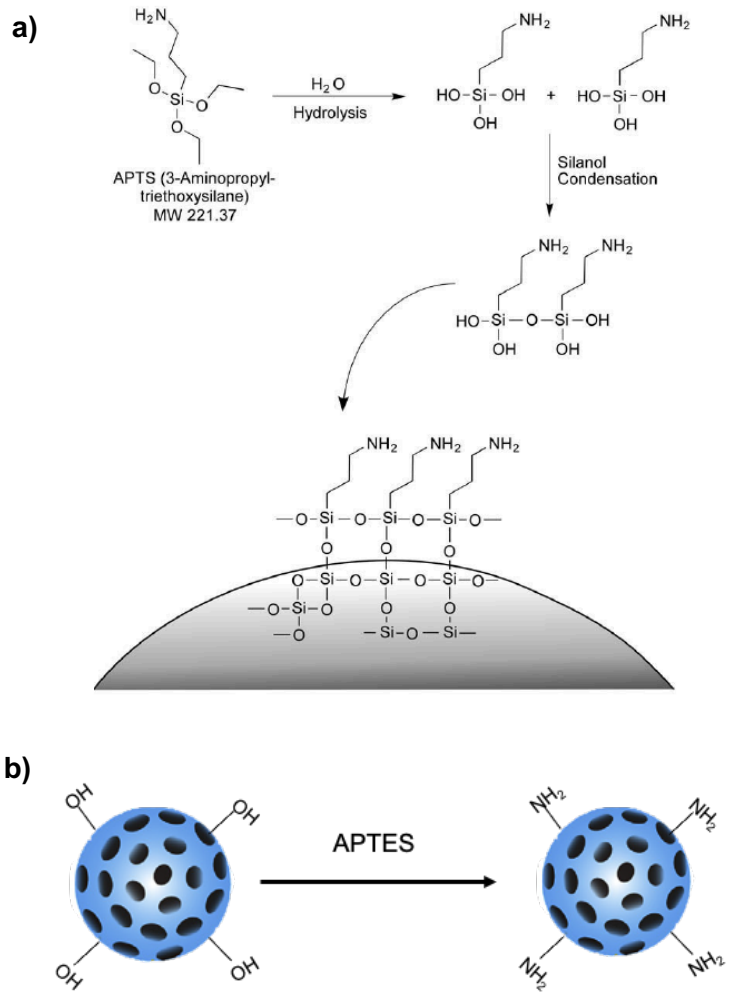

Figure 19: a) Formation of covalent coating containing primary amine groups, due to the deposition of APTES on a silica surface (adapted from (Hermanson, 2008)). **b)** Representation of MSN modification with APTES.

In order to coat MSN-NH_2 with the desired ligand, hyaluronic acid, amidation reactions took place mediated by the bio conjugative reagents EDC and NHS.

These bio conjugative reagents are carbodiimides which work as crosslink agents. They activate the HA carboxylic groups originating an active-ester intermediate, finally forming an amide bond in the presence of an amine nucleophile (Hermanson, 2008). In this way, nanoparticles got negative charge again conferred by the hydroxyl groups of the hyaluronic acid, MSN-HA (Figure 20).

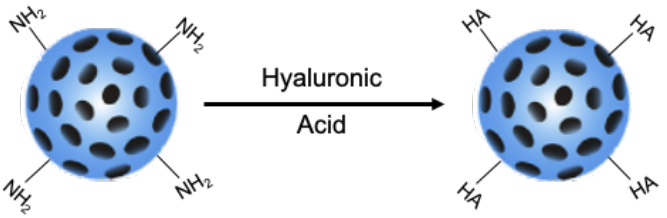

Figure 20: Schematic representation of the functionalization of the MSN-NH_2 with hyaluronic acid.

With the purpose of verifying if the nanoparticles have reached successfully each step of the synthesis and modification process, their surface zeta potential can be accessed. Using this type of measurement, it's possible to associate a negative particle charge to their hydroxyl groups present in MSN-OH and MSN-HA, and a positive charge to the amine groups from the surface of MSN-NH_2. To characterize the evolution of MSN size, the hydrodynamic diameter was also accessed.

To do so, nanosystem surface charge and hydrodynamic diameter were evaluated using Laser Doppler Velocimetry (LDV) and Dynamic Light Scattering (DLS) techniques. For each step of nanoparticle synthesis, the average diameter and zeta potential are resumed in Table 3. Before being submitted to these measurements, approximately 0.1 mg of nanoparticles were dispersed in 1 mL of ultrapure water (pH=7) and were disaggregated using an ultrasonic probe in two sessions of two minutes each. Nanoparticles mustn't present aggregates and should be well dispersed in the suspension, in order to obtain a good correlation and an accurate size determination.

Zeta potential measurements are used for determining the surface charge of nanoparticles. Because of nanosystems' charge, they attract ions, that cover the nanoparticles and create a layer around them. The electric potential at the surface of that layer is known as Zeta Potential, being its magnitude predictive of the colloidal stability of the suspension (A. Kumar & Dixit, 2017).

As expected, MSN-OH presented a negative surface charge of approximately -30 mV, indicating that the cationic surfactant was successfully removed and confirming the presence of silanol groups (Si-OH) that become deprotonated in the presence of ultrapure water. The zeta potential data obtained for the MSN-NH_2 and MSN-HA also indicate that the modification with APTES and the functionalization with HA occurred as expected, shifting from positive to negative values as shown in Figure 21 a). All the measurements were manifestly positive (30 mv) or negative (-30 mv) indicating that these nanoparticles have a reliable level of stability (A. Kumar & Dixit, 2017).

Considering the hydrodynamic diameter, this measurement represents the size of the apparently hydrated or solvated particle, calculated through the diffusional properties of

nanoparticles (Instruments, Malvern, 2011). The Polydispersity Index (PDI) characterizes the size distribution range of nanoparticles. With values varying between 0 and 1, PDI gives us an idea of the dispersion homogeneity, where the closer to 1, more heterogeneous is the nanoparticles population (A. Kumar & Dixit, 2017). Usually, values over 0.5 are not eligible for a good and accurate reading.

Table 10 and Figure 21 b) show the nanoparticles size in each stage of their synthesis. As expected, they increase in size after each modification, since a new component is being attached to their surface changing their size and volume. However, their exacerbated size can also indicate that occurred some agglomeration. Usually, the hydrodynamic diameter of MSN-OH is approximately 120 to 160 nm (Hadipour Moghaddam et al., 2017), for MSN-NH2 is 120 to 180 nm, and to MSN-HA is around 150 to 200 nm (Jin, Liu, Bai, Zhou, & Chen, 2018; Nairi et al., 2018; B. Zhang et al., 2019). Nevertheless, these values vary accordingly to the technique used for nanoparticle synthesis and with fluctuation of parameters like temperature, pH and stirring, that can easily compromise nanoparticles size.

Table 10: Average hydrodynamic diameter, Polydispersity Index and zeta potential from DLS and LDV readings.

MSN types	d (nm)	PDI	ZP (mV)
MSN-OH	342.48±50.26	0.27±0.08	-30.85±0.59
MSN-NH2	486.39±84.84	0.23±0.03	30.56±3.38
MSN-HA	467.67±118.51	0.35±0.07	-29.65±2.73

Data are expressed as mean ± SD of 3 replicates of MSN-OH, 8 of MSN-NH_2 and MSN-HA.

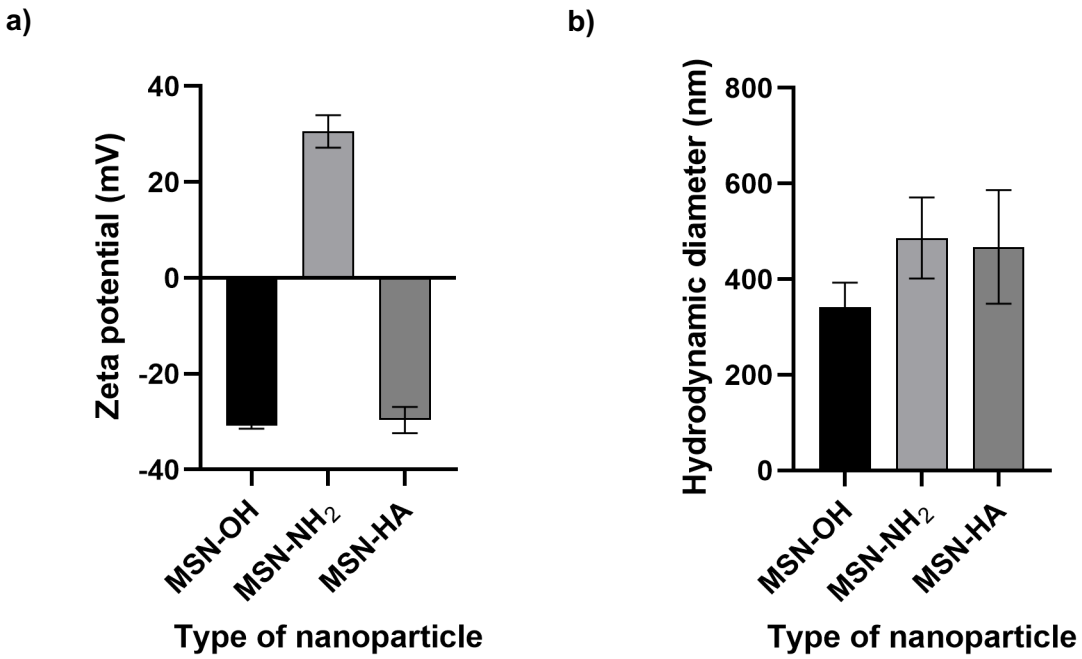

Figure 21: Zeta potential **(a)** and Hydrodynamic diameter **(b)** average results of MSN in the different synthesis stages. Results are presented as mean ± SD, n=3 for MSN-OH, and n=8 for MSN-NH_2 and MSN-HA

Although this type of nanoparticles can present aggregation issues (Shi et al., 2019), the conditions in which the ultrasound probe was used and the HA characteristics may have contributed to the sizes unconformity and to nanoparticles' oversize. HA is known for its mucoadhesive and hygroscopic properties (Vasvani et al., 2019), which when in a solution can lead to an excess of water molecules interacting with it, increasing the hydrodynamic diameter.

Other techniques can be used to determine the nanoparticles size, such as transmission electron microscopy (TEM), in which water molecules no longer interfere with the mean diameter measurement, because this technique provides the size of dehydrated particles (Tu et al., 2016). Additionally, this technique also gives detailed information about the nanoparticles structure and shape.

It is extremely important to invest in the size minimization of nanoparticles to prevent it from being an obstacle for their biodistribution and cellular internalization.

In what concerns the chemical characterization of the nanosystem, the Fourier Transform Infrared (FTIR) Spectroscopy is used to identify the functional groups present in each stage of the nanoparticles' synthesis. Previous work developed by João Vieira

et al., using the same synthesis processes, proved that every step of MSN formulation, modification and functionalization occurred as expected (Vieira, 2019). In Figure 22, it is possible to identify the transmittance peaks assigned to the characteristic groups of the unmodified (MSN-OH), modified (MSN-NH_2) and functionalized (MSN-HA) mesoporous silica nanoparticles, demonstrating the structural alterations in the MSN structure during all the synthesis process.

Based on this analysis, it is very likely that a similar FTIR Spectrum would be obtained for the nanoparticles synthesized in the current work, ensuring the correct modification and functionalization of the particles.

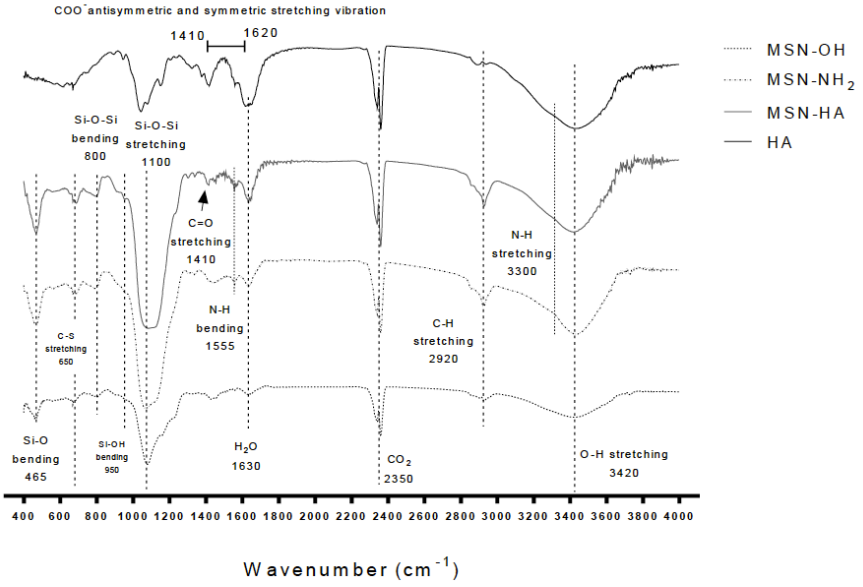

Figure 22: FTIR analysis of the functional groups present on unmodified (MSN-OH), modified (MSN-NH2) and functionalized (MSN-HA) mesoporous silica nanoparticles, (reproduced from (Vieira, 2019)).

2. Recombinant IFNα-2b production and purification

Specific bacterial strain, *E. coli* BL21 Star®, was transformed with a high copy number plasmid containing the information for IFNα-2b expression and a selection mark to Kanamycin resistance. The sequence for the protein expression was synthesized and modified to express a soluble and active version of IFNα-2b, which presents an enhanced ligand binding affinity to IFNAR1, that is known to trigger a more intense antiproliferative activity in cancer cells (K.-J. Zhang et al., 2017).

In a previous research study, João Vieira *et al* analyzed the protein sequence provided by the company that developed the recombinant plasmid and found that the protein had two different tags. In addition to the His-Tag and IFNα-2b sequences there was a second tag identified as the Small Ubiquitin-related Modifier (SUMO), which serves to modulate the protein interaction, activity and stability. SUMO is also recognized for increase the overexpression of the recombinant protein in the soluble form (Bis, Stauffer, Singh, Lavoie, & Mallela, 2014; Vieira, 2019).

So, the sequence present in the pSMART® HCKan plasmid has a total of 274 amino acids, as illustrated in Figure 23, which means more 86 amino acids than the original human IFNα-2b sequence, according to NCBI. The recombinant protein also presents a higher molecular weight of 31.8 KDa and a pI of 5.8 (Vieira, 2019).

MGHHHHHHMSDSEVNQEAKPEVKPEVKPETHINLKVSD
GSSEIFFKIKKTTPLRRLMEAFAKRQGKEMDSLRFLYDGI
RIQADQTPEDLDMEDNDIIEAHREQIGGQGSCDLPQTHS
LGSRRTLMLLAQMRKISLFSCLKDRHDFGFPQEEFGNQ
FQKAETIPVLHEMIQQIFNLFSTKDSSAAWDETLLDKFYT
ELYQQLNDLEACVIQGVGVTETPLMKEDSILAVRKYFQRI
TLYLKEKKYSPCAWEVVRAEIMRSFSLSTNLQESLRSKE

Figure 23: Amino acid sequence of the recombinant protein present in the pSMART® HCKan plasmid (Vieira, 2019).

Firstly, a pre-inoculum containing kanamycin was made, ensuring that only bacteria which have integrated the plasmid grew in the medium. In the next day, a bigger culture was made (the inoculum) and was incubated at 37 ºC, and the expression of the protein was induced by the addition of IPTG, due to the characteristics of the pET system. Approximately one hour before this step, the incubation temperature was wittingly decreased to 20 ºC to assure the best conditions for protein expression immediately after the IPTG addition. The colder induction has been shown to decrease the unwanted aggregation of improperly folded protein molecules (Tolia & Joshua-Tor, 2006). Besides that, enhances the soluble expression of recombinant proteins (Qing et al., 2004) and reduces the exacerbated growing of the bacterial culture. If the temperature was maintained at 37 ºC, the bacteria would take a long time until the protein starts to be expressed, and in these ideal conditions would keep investing in replicating themselves. Besides that,

Through the pET expression system, it is possible to control proteins expression. Specific bacterial strains, which have the λDE3 lysogen, that codifies for the T7 RNA

Polymerase, are the host for the vector. Under normal conditions, in the bacterial genome, the lac repressor would be bonded to the promoter before the T7 RNA Polymerase gene and its transcription wouldn't occur. However, the addition of IPTG to the system causes a dissociation of the lac repressor and then RNA polymerase is able to transcribe the T7 gene. Once T7 RNA Polymerase is expressed it will initiate the target gene transcription in the vector, in this case the IFN α-2b. This way, the target protein is only expressed when IPTG is present, otherwise, the lac repressor would remain bound to the promoter and the T7 gene would never be transcript (Cam, 2003).
Next, for the cell lyses, a commercial buffer was used, inducing the cell wall burst. Theoretically, the protein, which is on its soluble form, remains on the supernatant after the lysate centrifugation, which was collected and stored to be purified. Besides this approach, the cell culture can instead be frozen to be then subjected to the ultrasounds, in which the ice crystals formed, would start to break the cell wall and membrane due to their interaction with the vibration waves. Regardless of this methodology can result in a bigger recovery of soluble protein, takes much longer to be executed and ends up being a mechanical procedure, rather than an enzymatic, as it happens with the cell lysis buffer used. This technique using Tris-buffered formulation (pH 7.5) with lysozyme and DNase I, releases the recombinant protein without denaturation and allows a most efficient extraction.

To separate IFNα-2b from other soluble proteins that might be expressed by bacteria, a purification using affinity chromatography is necessary. In this technique, the soluble portion containing the protein, passes through a column with nickel beads that will bind to the His-Tag tail present in the protein structure, as represented in Figure 24. This is known for being the loading phase of the protein in the column represented in Figure 26. Then, to collect fractions containing IFNα-2b with a high purity degree, PBS supplemented with Imidazole was also passed through the column in different rising concentrations, 100 and 500 mM. This reagent will compete with the protein bounded to the nickel beads connecting itself to these column structures, since the Imidazole ring is part of the histidine structure, as observe in Figure 25 (Tagliavia & Nicosi, 2012). As the Imidazole connects with the nickel beads, the protein is eluted from the column and divided by fractions (T1 to T10) accordingly to the Imidazole concentration used and to the absorbance picks represented on the chromatogram. To optimize the process, smaller volumes for each fraction were collected, in an attempt to have more fractions with fewer impurities. Theoretically, a higher imidazole concentration leads to a higher amount of released protein. However, this process must be gradual in order to first discard other proteins and impurities that might have been connected to the column.

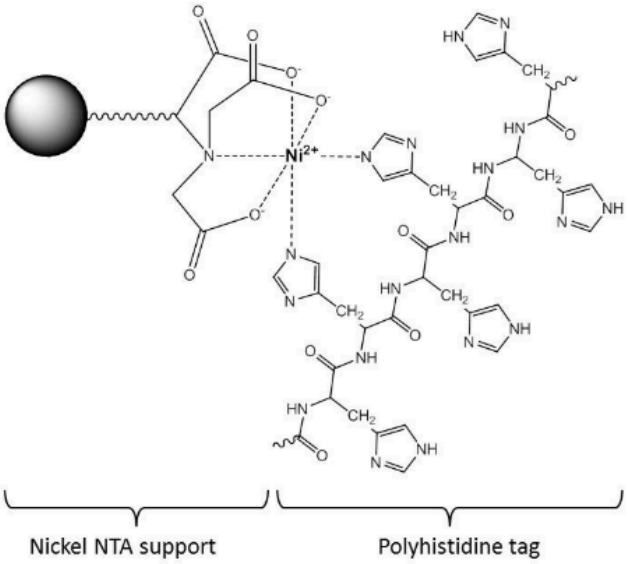

Figure 24: Binding of the histidine tag present in the protein structure to the nickel beads, reproduced from (Magdeldin & Moser, 2012).

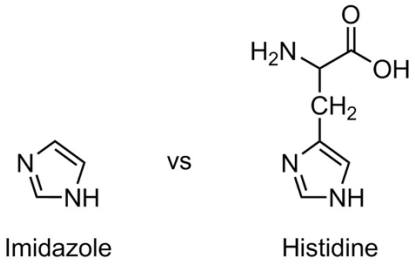

Figure 25: Imidazole and Histidine molecular structures.
(http://2015.igem.org/Team:Freiburg/Project/Protein_Purification)

The absorbance registered on the chromatogram (Figure 26) corresponds to molecules connecting to the Nickel beads, firstly a big amount of protein loading into the column and then smaller picks of Imidazole binding with nickel beads.

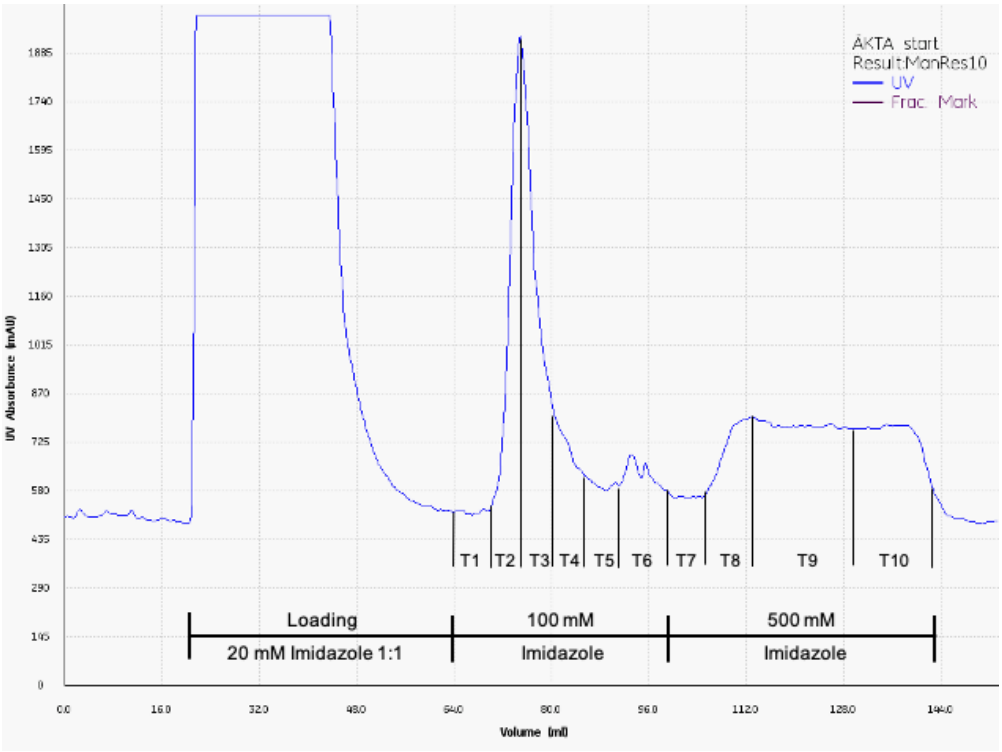

Figure 26: Chromatogram from the IFNα-2b purification using IMAC affinity chromatography with a 5 mL HisTrap HP histidine-tagged protein purification column. In the loading phase the sample was supplemented with Imidazole 20 mM, fractions T1 to T6 represent the protein elution with PBS supplemented with 100 mM Imidazole, and fractions T7 to T10 represent the final elution with PBS supplemented with 500 mM Imidazole.

Analyzing the data presented in Figure 26, it is possible to see that fractions T2 and T3 are probably the ones with a higher amount of protein, since they correspond to the biggest peak of absorbance. Some isolate peaks correspondent to the fractions T4, T5 and T6, are probable to have smaller amounts of protein as well. Fraction T8 can also present IFNα-2b.

In order to confirm that, a SDS-PAGE gel electrophoresis was made with samples of all the fractions obtained and for the initial and final protein solutions, as shown in Figure 27.

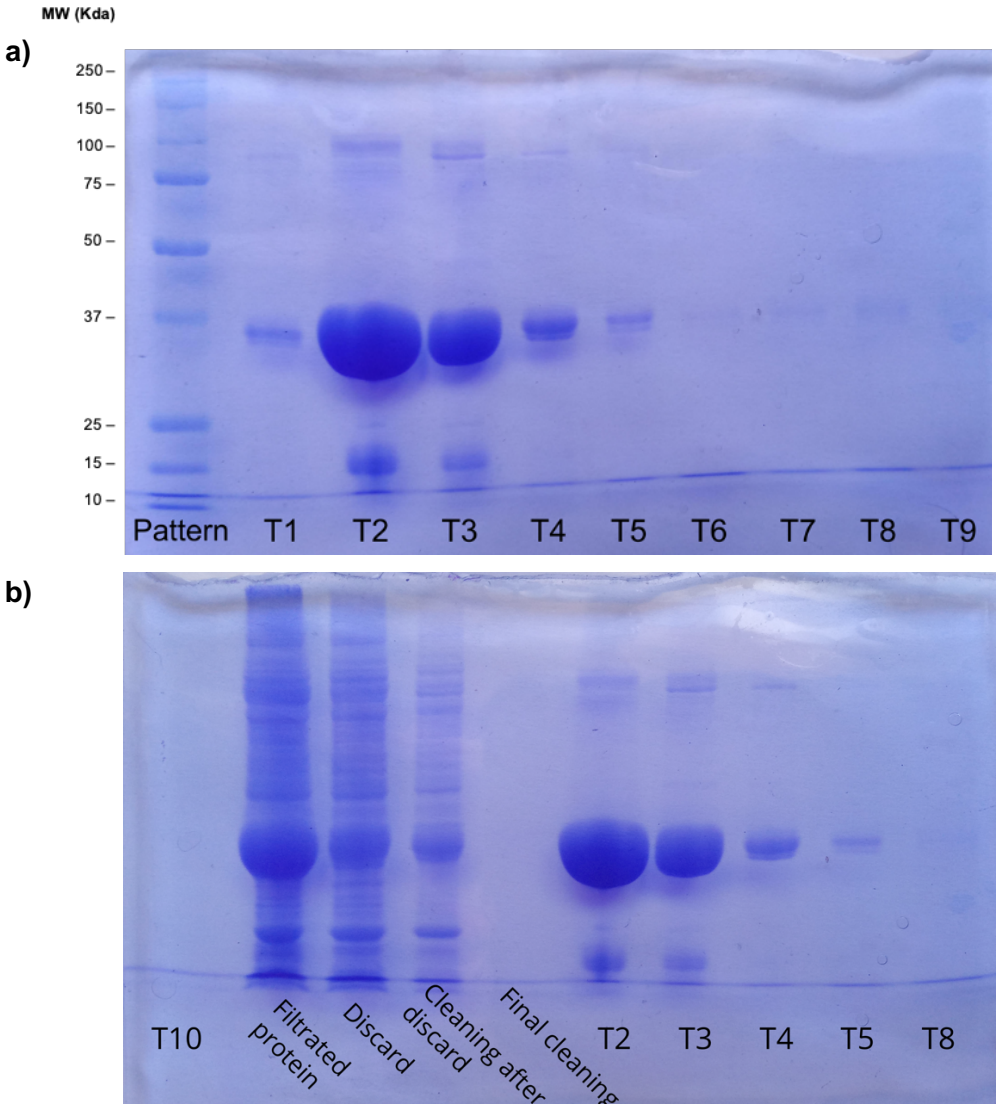

Figure 27: SDS-PAGE gel containing samples of the liquid fractions resultant from the IFNα-2b production and purification, after the IMAC affinity chromatography. **a)** Pattern – protein ladder; T1, T2, T3, T4, T5, T6 – 100 mM imidazole; T7, T8, T9 – 500 mM imidazole. **b)** T10 – 500 mM imidazole; Filtrated protein - protein sample after filtration; Discard – discard during protein loading; Cleaning after discard – flow through with PBS; Final cleaning – last automatic cleaning by the chromatography equipment; T2, T3, T4, T5 – 100 mM imidazole; T8 – 500 mM imidazole.

Comparing the samples with a patterned protein ladder was possible to identify the fractions that contain a higher amount of IFNα-2b as well as other contaminations.

The sequence of IFNα-2b present in the plasmid is known for being a protein of 31.8 KDa. Comparing with the protein ladder was possible to see where the band representative of IFNα-2b should appear, noticing that fractions T2 and T3 are the ones with a more evident band in the region between the 37 and 25 KDa. It is also important

to note, that other bands appear in these fractions, indicating that those samples have other proteins and contaminants rather than only IFNα-2b. However, T4 and T5 also presented a representative band of the recombinant protein but with much fewer contaminations. It is crucial to notice that even though these fractions presented a smaller amount of protein, they were the purest samples and, consequently, should be ones used for the evaluation of the protein activity and for loading the nanoparticles.
After comparing the chromatogram with the SDS-PAGE gels, it is clear that the majority of the protein was eluted when PBS supplemented with 100 mM of Imidazole passed through the column. This and the absence of any other bands in the region between the 25 and 37 KDa, confirm that the His-tag tail introduced in the protein structure, efficiently interacts with the nickel beads present in the chromatography column, when the filtrated protein was loaded into the column, and also that Imidazole efficiently competes with the histidine tag.
After analyzing the gels, only fractions T4, T5 and T2 and T3 (since they present a greater amount of protein and can be purified one more time) proceeded for the dialysis against water, in order to remove PBS and Imidazole. Finally, the dialysis product was freeze-dried and stored at -20º C, resulting in approximately 8 mg of protein.

This process was repeated several times to obtain a large amount of protein for the loading and cytotoxicity experiments, being the presented results representative of the majority of the protein production and purification assays that were done.

3. Protein and epirubicin loading

In order to characterize the ability of the nanosystem to load the therapeutic agents, two parameters are measured. The loading capacity (LC), which represents the amount of protein or drug-loaded per weight unit of nanoparticles. And the loading efficiency (LE), that stands for the amount of the therapeutic agent that is successfully entrapped in the nanosystem, relatively to the initial amount provided for the loading. This both parameters are expressed in percentage.
After all the stages of nanoparticles synthesis have successfully occurred, IFNα-2b was loaded into the MSN. There were tested different ratios of protein versus nanoparticles, as well as a fast (ten seconds) and a long period (overnight) of incubation in a previous work (Vieira, 2019), whose results were reproduced in an initial phase of the present project. In his work, João Vieira concluded that the incubation period didn't influence the LC and LE levels. For the ratios initially tested (1:10 and 0.5:10 (w/w) of protein vs.

nanoparticles) the loading capacity was around 8.42% and 4.78%, which means that each µg of MSN-HA contained 0.0842 µg and 0.0478 µg of IFN α-2b, respectively. Concerning the loading efficiency, in those experimental conditions 84% and 95% of the initial amount of protein was loaded in the nanoparticles for the ratios 1:10 and 0.5:10. Since these observations suggest that the majority of the protein was loaded in the nanosystems, charging them with a ratio of 1:1 (w/w) might be advantageous, possible resulting in a higher loading capacity.

For this reason, the above-mentioned approach was accessed in the present work. Suspensions of 7 mg of MSN-NH_2 or MSN-HA were loaded with solutions containing 7 mg of protein in 2 mL eppendorf tubes. After two centrifugations cycles, the supernatants were collected, and their protein contents were accessed with the bradford method, comparing them with the respective calibration curves. The LE and LC were evaluated and the obtained results, shown in Figure 28, suggest that this new methodology strongly increases nanosystems loading capacity.

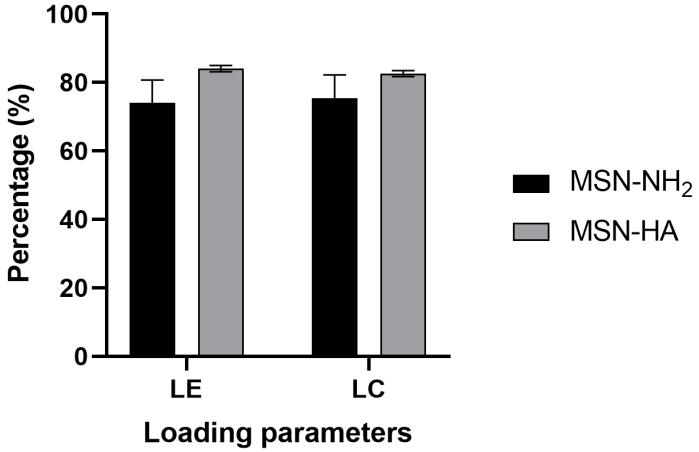

Figure 28: Loading efficiency and loading capacity of the different nanoparticles using a ratio of 1:1 (w/w) of protein to nanoparticle amount. Data are expressed as mean ± SD obtained from triplicates of two independent experiments (n=2).

As illustrated in Figure 28, both types of nanoparticles are capable of load a higher amount of protein, when the loading was done in a ratio of 1:1 (w/w), comparing to the initial results obtained by João Vieira (Vieira, 2019). For the modified nanoparticles (MSN-NH_2) the loading capacity was around 74% and for the functionalized ones (MSN-HA) was 84%, which means that each µg of particles loads 0.74 µg and 0.84 µg of

protein, respectively. Regarding the loading efficiency, 75% and 82% of the initial amount of protein was loaded in the MSN-NH_2 and MSN-HA, respectively.

Despite the high loading values obtained, it is not possible to affirm that most of the protein is found in the pores of the particles. In fact, it depends if the size of the protein and its folding is compatible with the pore diameter and volume. Previous studies already demonstrated that proteins with very similar sizes of the pore network are capable of being encapsulated into the mesopores with an average diameter (Tu et al., 2016; Zampini et al., 2019). Also, several processes might be responsible for the protein loading, such as electrostatic interactions, hydrogen bonds or the adsorption to the nanoparticles surface. Since the protein presents a negative charge at pH above 5.8, it was expected to observe higher loading results for the modified nanoparticles (MSN-NH_2), due to their positive surface charge. In reality, both nanoparticles types present very similar results, suggesting that the electrostatic interactions (occurs between two charged atoms, ions or molecules leading to Coulomb interaction) between them and the protein might not be the only driven force for the loading to occur. On the other hand, the adsorption process of the protein to the surface of the nanoparticles can also take place due to the Van der Waals forces, that include three different types of atomic or molecular interactions (dipole - dipole, dipole -induced dipole and induced dipole - induced dipole) (Hanafy, 2013) and, most probably, are one of the main reasons of IFN α-2b loading into the particles.

The epirubicin loading in MSN-HA was also analyzed to evaluate the particles capacity to load the drug. For this purpose, 1 mL of epirubicin solution (2 mg/mL) was incubated with 5 mg of MSN-HA for 24 hours protected from light, since this drug has natural fluorescence. After the particles being washed and precipitated, the Epi concentration was measured in the supernatants. Then, LE and LC were calculated using equations 1 and 2 referred in chapter 2.

Surprisingly, the loading efficiency and loading capacity were higher than the expected, 77% and 31%, respectively (Figure 29). This analysis ensures that 77% of the initial amount of Epi was loaded into the particles and, more specifically, 0.31 μg of Epi were carried by each μg of nanoparticles. Other studies of Epirubicin loading in mesoporous silica nanoparticles present loading capacity values around 10 to 18 % (Ansari, et al, 2018; Hanafi-Bojd et al, 2017; Y. Zhang, et al, 2019).
In fact, the epirubicin hydrochloride loading process occurs mainly due to electrostatic interactions (Hanafi-Bojd et al., 2017) between the positively charged molecule and the

nanoparticles, which when in solution and functionalized with HA present a negative surface charge. Furthermore, the presence of pores in the structure of the nanoparticles contributes to an extra capillary force to load substances (Kesse et al., 2019).

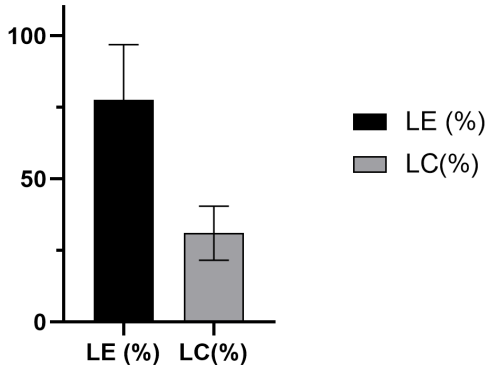

Figure 29: Loading efficiency and loading capacity of mesoporous silica nanoparticles functionalized with HA and loaded with epirubicin. Data are expressed as mean ± SD obtained from triplicates of two independent experiments (n=2).

In an attempt of loading the nanosystem with both therapeutic agents, the already loaded and freeze-dried MSN-HA with Epi were submitted to the loading of IFN α-2b. A suspension of 7 mg of MSN-HA-Epi was loaded with 7 mg of protein in Eppendorf tubes, in a final volume of 2 mL. Once again, after the wash and precipitation of the nanoparticles the LE and LC were evaluated.

The data presented in Figure 30 show the results of the loading assays, being notorious the unexpected amount of protein that was loaded by the MSN-HA-Epi. Almost 95% of the initial amount of protein was loaded into the nanoparticles and there were carried about 0.97 µg of IFN α-2b per each µg of particles.

The loading capacity of the MSN-HA-Epi for the protein was even higher than the one presented by the functionalized nanoparticles without Epi. This might suggest that since the nanoparticle is loaded with another compound, there are more molecules exposed to occur the interaction with the protein, possible leading to a greater amount of electrostatic interactions between the positively charged drug and the protein which is negatively charged. Accordingly to these results, a recent study developed by Song and his team, also verified a higher loading capacity in nanosystems already loaded with a drug than in the initial formulation (Song, Li, Wang, Zhang, & Chen, 2019).

These findings seem to be quite promising to the therapeutic activity evaluation, since the nanosystem was efficiently loaded with epirubicin and the recombinant protein IFN α-2b.

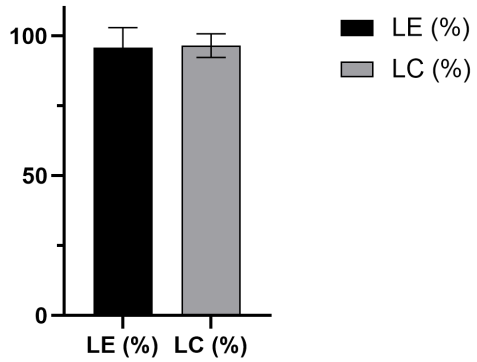

Figure 30: Loading efficiency and loading capacity of mesoporous silica nanoparticles, functionalized with HA and already carried with epirubicin, loaded with the recombinant protein IFNα-2b. Data are expressed as mean ± SD obtained from triplicates of two independent experiments (n=2).

4. Biocompatibility and therapeutic activity evaluation

4.1. Nanoparticles Biocompatibility

With the purpose of evaluating the biocompatibility of the functionalized nanoparticles, cell viability assays were performed in HepG2 cells. Cytotoxicity of MSN-HA was evaluated after 48, 72 and 144 hours of incubation, with concentrations ranging from 0 to 617.3 µg/mL, using the Alamar Blue assay.

The results presented in Figure 31 revealed that, even for the most extreme concentrations, unloaded functionalized nanoparticles do not present toxicity to HepG2 cells. After each measurement period the percentage of living cells remained above 100%.

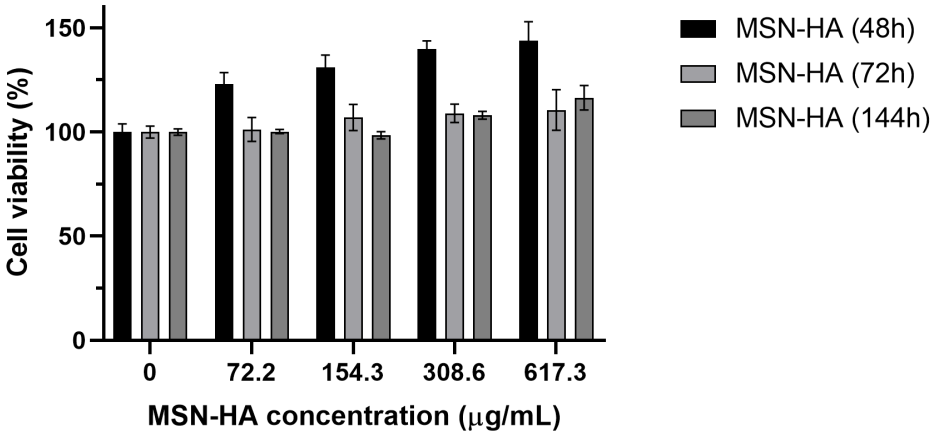

Figure 31: Viability of HepG2 cells after incubation with MSN-HA for 48, 72 and 144 hours. Data are presented as percentage of cell viability with respect to untreated control cells and are the mean ± SD obtained from triplicates (n=1).

These data ensure that the HA-functionalized nanoparticles have good biocompatibility, at least in cancer cells when unloaded, and might be safe to use as therapeutic agents delivery nanosystems. As a matter of fact, MSNs modified with APTES have already been proven as a biosafe nanosystem (Hanafi-Bojd et al., 2015; Yuan Zhang et al., 2019) and HA itself is a biodegradable polysaccharide (Wang et al., 2017; Zhao et al., 2015). So, it's not surprising that the nanosystem MSN-HA didn't present toxicity to the cells, the results obtained are within the expectations.

In addition, hybrid nanoparticles such as MSNs coated with a biopolymer, can have an advantage in the biocompatibility, showing a significant improvement in terms of toxicity, when compared with simple inorganic silica particles (Barkat et al., 2019; Hu et al., 2013). In fact, this information values the nanoformulation accomplished in this work, since the MSN are functionalized with Hyaluronic Acid, making them less susceptible to provoke any kind of cell-damaging.

4.2. Protein Activity

After producing the recombinant protein, it is crucial to make sure that it is active and has the desired effect in cancer cells, before evaluating the cytotoxicity of the loaded nanosystems. To do so, the toxicity of the produced recombinant IFNα-2b was compared with the activity of a commercial IFNα-2b (provided by the company that produced the recombinant plasmid) in HepG2 cells. Protein concentration values ranged from 0 to 25

µg/mL and were selected based on previously consulted literature (K.-J. Zhang et al., 2017).

The cell viability was assessed at 48 and 96 hours by the Alamar Blue assay (Figure 32 a)) and at 96 hours by the Sulforhodamine B (SRB) assay (Figure 32 b)).

After the 48 hours of incubation, a new dose of protein was added to cells on the same concentration range.

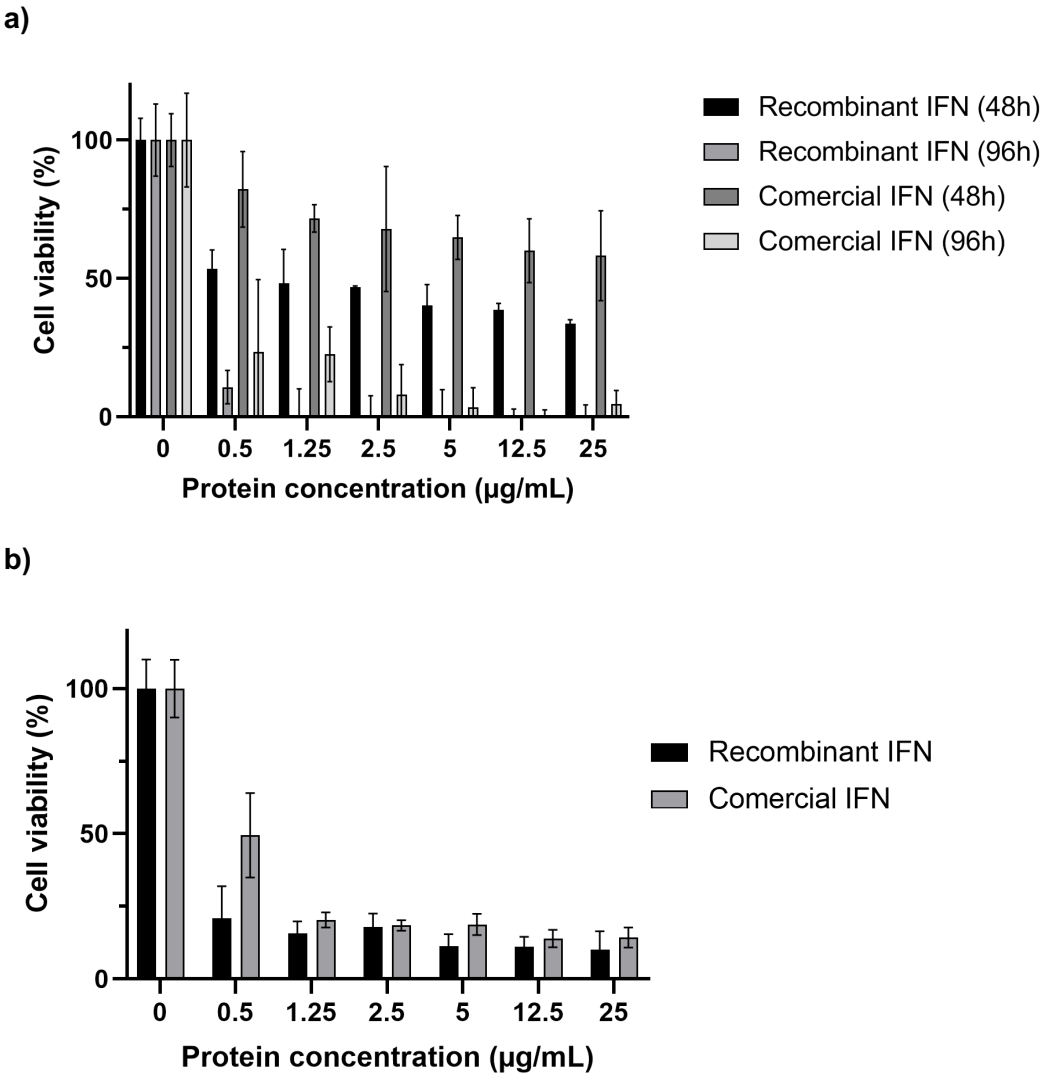

Figure 32: Viability of HepG2 cells incubated with recombinant and commercial IFNα-2b for 48 and 96 hours. Cell viability was evaluated by the Alamar Blue assay **(a)** and by the Sulforhodamine B (SRB) assay **(b).** Data are presented as percentage of cell viability with respect to untreated control cells, and the mean ± SD obtained from triplicates (n=1).

Results obtained from the Alamar Blue assay (Figure 32 a)) show a slight difference between the recombinant protein activity and the commercial one, however it might not be significant due to the high values of the standard deviation. It was also possible to see that from the lowest concentration, the cell viability sightly decreases for both proteins, reaching the maximum cell death values for the recombinant protein from 1.25 µg/mL with 0% of viable cells. However, as much as a higher protein concentration induces a higher cellular death rate, it is not necessary an extremely high concentration demonstrate the protein's activity. The results presented in Figure 32 a) show that is for concentrations lower than 0.5/1.25 µg/mL, at the 48 hours, that was verified a greater decline in cell viability. After that, it kept decreasing but without being so accentuated.

The SRB assay (Figure 32 b)) highlights similar points to the ones previously described. For the lowest protein concentration (0.5 µg/mL), it was possible to observe a difference of almost 30% of cell death between the incubation with our recombinant protein, which was once again slightly more cytotoxic, and the commercial one, however the standard deviation remained above 10%. For the other concentrations, the differences between both types of proteins are not so evident, and the maximum values of loss of cell viability are reached for the concentration of 25 µg/mL. Following the 96 hours of incubation, there were only 10% of viable cells incubated with our recombinant IFNα-2b and 14% of viable cells incubated with the commercial protein, slightly higher than the values obtained with the Alamar Blue assay.

Differences found between the two assays might be due to the Alamar Blue measures the metabolic active cells and the SRB quantifies the cell mass. Hereupon, there might be cells that are already dead and no longer have metabolic activity but still present cellular mass. In this way, SRB assay continues to detect some cellular proteins, justifying the slightly higher values of cell viability.
Remarkably, the slightly better activity of our recombinant protein in decreasing the cell viability, highlights the higher purity levels of the produced protein in comparison with the commercial one.
These assays, besides demonstrate the activity of our recombinant IFNα-2b, also indicate that it is not necessary a high dosage of protein to obtain the desired loss of viability cell effect.

4.3. Loaded MSN-HA therapeutic potential

In order to evaluate the nanosystem drug and protein release effectiveness *in vitro,* there were performed cell viability assays in HepG2 cells. During 48 and 96 hours, the cytotoxicity of the free therapeutic agents and the functionalized nanoparticles singly and simultaneously loaded with them was evaluated, using the Alamar Blue assay (48 and 96 hours) and the Sulforhodamine B (SRB) assay (96 hours). The results are present in Figures 33 and 34, respectively.

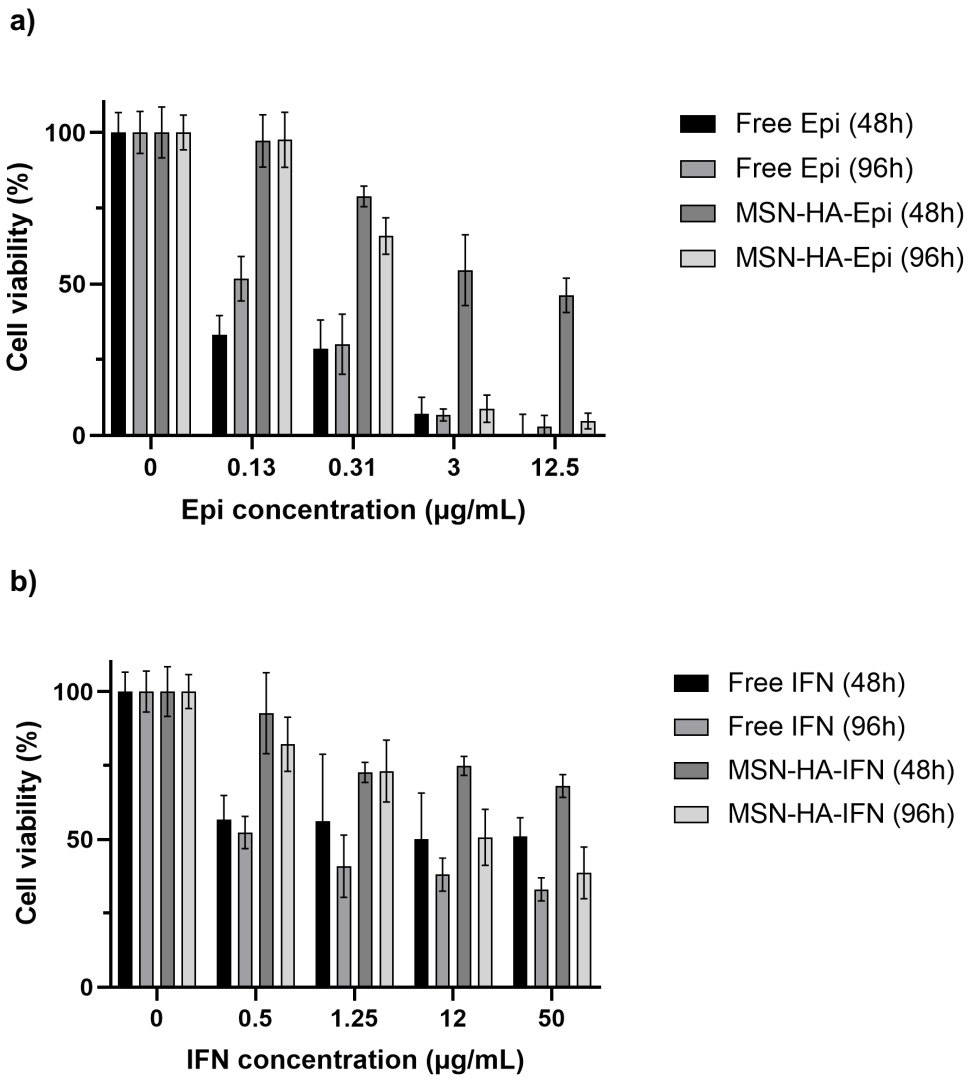

c)

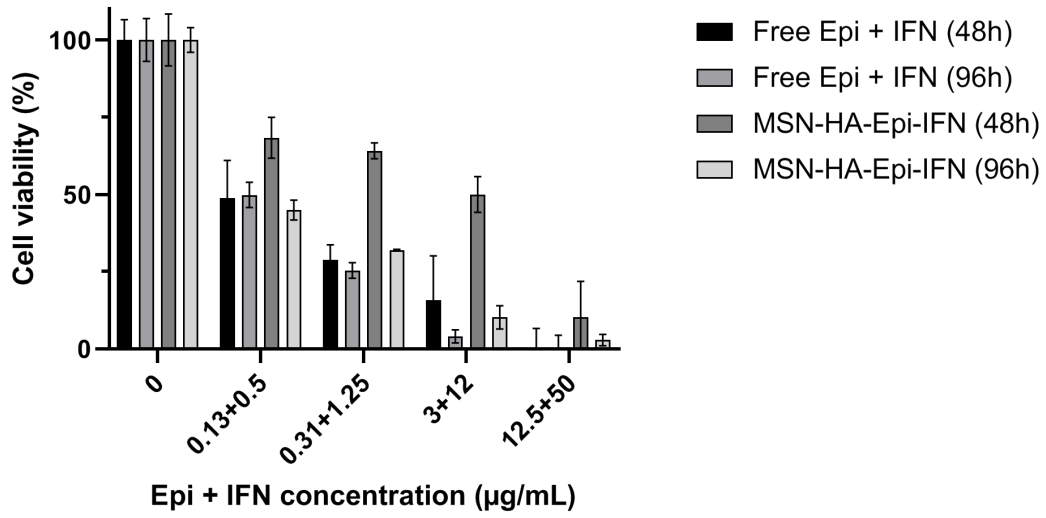

Figure 33: Viability of HepG2 cells incubated with: **a)** free Epi or MSN-HA-Epi; **b)** free recombinant IFNα-2b or MSN-HA-IFN; and **c)** free Epi and recombinant IFNα-2b or MSN-HA-Epi-IFN, for 48 and 96 hours, and evaluated with the Alamar Blue assay. Data are presented as percentage of cell viability with respect to untreated control cells, and are the mean ± SD obtained from triplicates of two independent experiments (n=2).

As it is possible to notice in Figure 33 a) there was a clear cytotoxic effect of the free Epi which is accentuated with the drug concentration increase, from 0.13 to 12.5 µg/mL. For the loaded nanoparticles with Epi, the cell viability also decreases as a result of the concentration raise, proving a dose-dependent effect. However, the greatest decrease in cell viability only occurred at 96 hours for the highest concentrations, probably due to the drug release kinetic from the MSN-HA. At the end of 96 hours, the Epi loaded nanosystem reached its maximum effectiveness where it was capable of killing almost all the cancer cells, similar to the free drug-induced death.
The results obtained with the SRB assay (Figure 34 a)) allowed reaching the same overall conclusions, the cytotoxicity profiles of the free drug and the loaded particles were very similar, even though this assay only covers the total incubation period (96 hours).

With regard to the free recombinant protein and the IFN-loaded nanoparticles, from the Alamar Blue assay (Figure 33 b)) it was also possible to see a clear dose-dependent effect, for both free protein and MSN-HA-IFN, in concentrations ranging from 0.5 to 50 µg/mL. In this case, the protein seems to be gradually released from the particles, but it would be interesting to prolong the assay to ascertain if the cell viability kept decreasing

overtime or not. Nevertheless, after 96 hours the free protein and IFN-loaded particles induced a maximum of 67% and 62% of cell death respectively, corresponding to the highest concentration.

With the SRB assay (Figure 34 b)) it was possible to obtain very close results, presenting cell death values rounding the 75% and 77% for the free IFN and MSN-HA-IFN at 50 µg/mL at the end of the 96 hours of incubation.

However, both alamar blue and SRB assays (Figures 33 b) and 34 b)) for free IFN show a low cytotoxic effect when compared with Figure 32. The results inconsistency requires further analysis and repetition of the viability assays, to characterize with more accuracy the protein activity.

The conjugation of both free therapeutic agents and the particles loaded with the drug and protein had shown even more interesting results about their effect on cell viability (Figure 33 c) and Figure 34 c)). In both assays, the combination of free Epi and IFN presented higher toxicity levels than the individual free therapeutic agents and once again a dose-dependent effect.

The results from the Alamar Blue assay (Figure 33 c)) showed that for the loaded particles, at a higher concentration was possible to notice a significative percentage of loss of cell viability and at 96 hours the cytotoxicity is much more notorious for every concentration. This may be a result of the slow drug release from the nanosystems. In spite of that, at the end of the assays period, it was obtained almost total cell death for both types of combined treatments, as much as for the Alamar Blue as for the SRB assay, for the highest concentration (12.5 µg/mL of Epi and 50 µg/mL of IFN).

a)

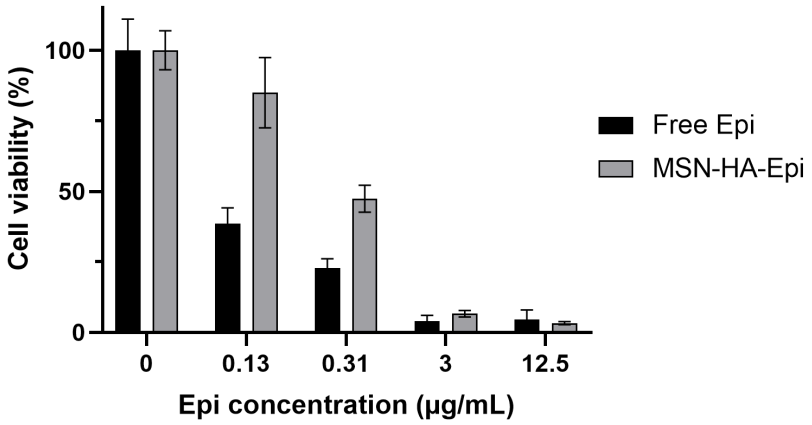

b)

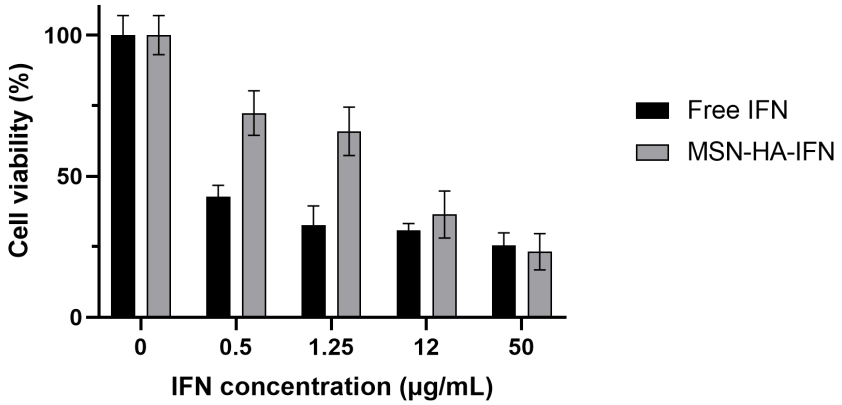

c)

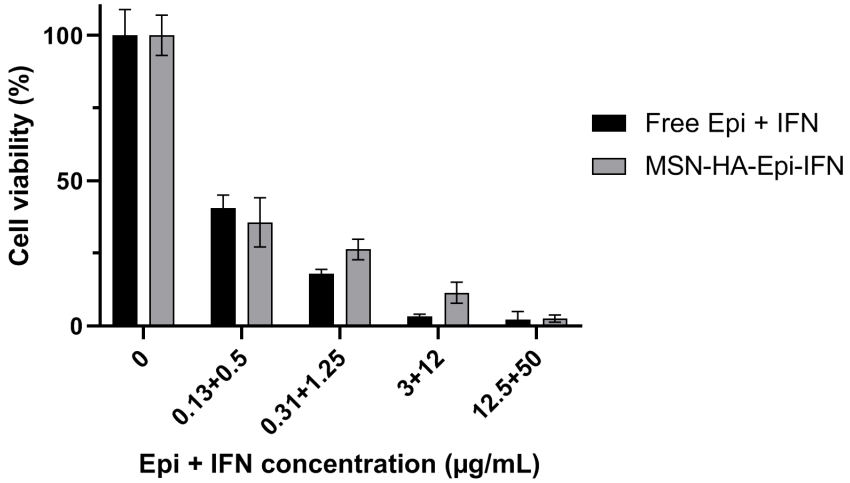

Figure 34: Viability of HepG2 cells incubated with: **a)** free Epi or MSN-HA-Epi; **b)** free recombinant IFNα-2b or MSN-HA-IFN; and **c)** free Epi and recombinant IFNα-2b or MSN-HA-Epi-IFN, for 96 hours, and evaluated with the Sulforhodamine B (SRB) assay. Data are presented as percentage of cell viability with respect to untreated control cells, and the mean ± SD obtained from triplicates of two independent experiments (n=2).

The most striking observation to emerge from the data comparison was that for the lowest concentrations the effect of the loaded nanoparticles with both therapeutic agents was greater than the effect of the particles loaded with the drug plus the effect of particles loaded with the protein (Figures 35: a) and b)), having been observed a synergistic effect. With the Alamar Blue assay, after the 96 hours, (Figure 35 a)) it was possible to see that the MSN-HA-Epi-IFN induced 56% of cell death, which is more 35% of non-viable cells than the sum of the effects obtained with MSN-HA-Epi and MSN-HA-IFN that only caused 21% of growth-inhibitory effect (3% + 18%). Through the SRB (Figure 35 b)), similar results can be seen, MSN-HA-Epi-IFN induces 65% of cellular death, which was more 22% than the 43% registered with the sum of the effects observed with MSN-HA-Epi and MSN-HA-IFN (15% and 28%, respectively).

This might be evidence of the much-desired synergistic effect in HepG2 cells, since the treatment with the co-loaded nanoparticles with Epi and IFNα-2b substantially increased the cytotoxicity when compared with the individual approaches. The synergistic effect typically occurs when the combined activity of two therapeutic agents is greater than the sum of each one's individual effect (Wambaugh et al., 2020).

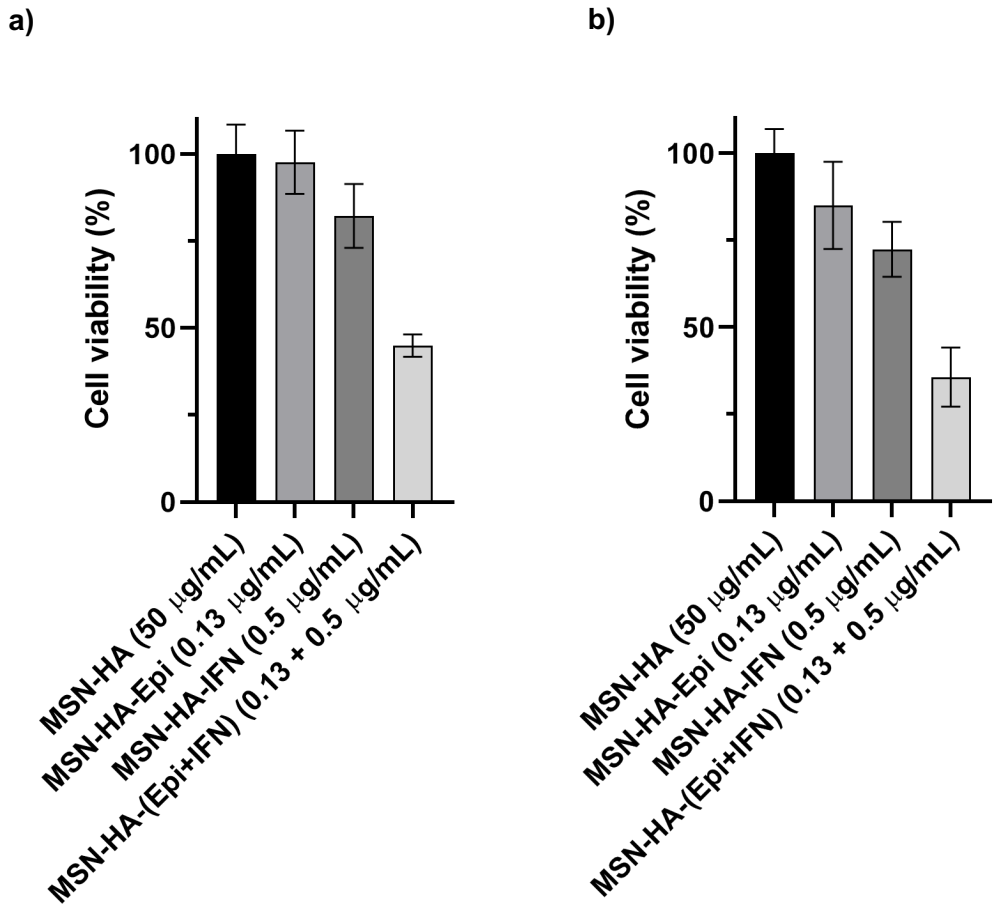

Figure 35: Viability of HepG2 cells incubated with the lowest concentrations of both therapeutic agents, summary information obtained from figures 33 and 34. **a)** Data correspondent to the Alamar Blue assay and **b)** data from the SRB assay.

Chapter 4
Conclusions

Therapeutic agents transport and delivery by nanosystems is a very promising approach for cancer treatment. Over the years, nanosystems have evolved to become more biocompatible and to have specific affinity to certain types of cells or tissues. This targeted delivery, can reduce the systemic secondary effects that come from traditional chemotherapy, ensuring that the therapeutic agents only take action in tumour site.

Combined treatments using nanosystems as a transport system, have also been a more recently explored strategy, in an attempt to find an enhanced toxic effect to cancer cells. Therefore, the main purpose of this study was to develop an efficient silica-based nanosystem capable of transporting and delivering a drug and a recombinant protein simultaneously and specifically to cancer cells.

In recent years, mesoporous silica nanoparticles (MSN) have become one of the most successful inorganic nanosystems for drug deliver, mostly due to their tunable pore diameter, high surface area, stable mesostructure, easy functionalizable surfaces, and biocompatibility. Hence, this type of nanoparticles was chosen to be synthesized and functionalized with hyaluronic acid, which allowed them to specifically bind to receptors mostly expressed in cancer cells (CD44), inducing the MSN cellular internalization.

Throughout the present work, MSN were successfully synthesized, and their modification with APTES to be then capable of being functionalized with HA took place. All these steps in the formulation process were proved by shifts in the particles surface charge from negative (MSN-OH, -31mV), to positive (MSN-NH_2, 30 mV) to negative again (MSN-HA, -29 mV). Their hydrodynamic diameter was also accessed, although with some possible particles' aggregation demonstrated by the high values obtain, the functionalized MSN ended up with an average hydrodynamic diameter of 467 nm.

The production and purification of the soluble recombinant human protein IFNα-2b were optimized and resulted in a great and pure protein stock, and new glycerol stocks of transformed cells were also prepared and stored to further use.

Concerning the nanoparticles loading, three conditions were evaluated, the loading of functionalized nanoparticles with the recombinant protein (MSN-HA-IFN), with epirubicin (MSN-HA-Epi), and with both therapeutic agents (MSN-HA-Epi-IFN). The results were very optimistic, the loading efficiency for the MSN-HA-IFN was approximately 82% using

a w/w ratio of protein to nanoparticle of 1:1, for the MSN-HA-Epi was about 31% with a drug to particle w/w ratio of 2:5, and finally for the particles already loaded with epirubicin the loading efficiency of MSN-HA-Epi-IFN with the protein was almost 97%, once again with a w/w ratio of 1:1. Very promising outcomes may arise in terms of cytotoxicity while administrating these nanoparticles to tumour cell lines, since they present high loading capacity and efficiency values when compared with previous studies.

The biocompatibility of the unloaded nanoparticles was evaluated in HepG2 cell line, proving to be safe even for the highest concentrations tested for 144 hours, with the percentage of living cells remaining always above 100%.

In order to see if the produced recombinant protein achieved the correct conformation and was able to exert its antitumour effect, its toxicity in HepG2 cells was compared to the cytotoxicity of a commercial version of IFNα-2b. The obtained results showed that our recombinant IFNα-2b always promoted slightly higher levels of toxicity that the commercial protein, reaching 90% of cell death for the highest concentration tested. These findings proved that the recombinant protein was efficiently expressed and is totally functional for the purpose of inducing cell death as expected.

Finally, the efficiency of the nanosystems loaded with both therapeutic agents on promoting cancer cells death was once again accessed in HepG2 cell line. At the end of the 96 hours of the assay, the incubation with the highest loaded particles concentration resulted in more than 97% of cell death. Nevertheless, for the lowest concentrations, MSN-HA-Epi-IFN were responsible for an average of 60% of cell death, which represents almost more 30% than the sum of the cytotoxicity induced by the MSN-HA-Epi and MSN-HA-IFN. With this evidence was possible to demonstrate the synergistic antitumor effect of the co-loaded nanosystem.

In conclusion, the formulation of a targeted nanosystem was successfully achieved as well as its loading with two therapeutic agents which lead to cellular death of cancer cells, probably by inducing the activation of apoptotic pathways, that should be further analyzed. With this work, it was also possible to develop a synergistic combined therapy capable of improving treatment efficiency and potentially reducing the side effects associated with the traditional chemotherapy treatments.

Although the main goal of this work has been accomplished there are some experiments that can still be done to complete this project. In the first place, TEM and SEM analysis can be done to have a more precise idea of the nanoparticles size, structure and shape without considering the hydration layer around them. In addition to the loading experiments, drug and protein release assays should be performed at least for two weeks, to have a better comprehension of the nanosystem behaviour in releasing the

therapeutic agents in a shorter and longer period. The specificity of the nanosystems to the CD44 receptor present in tumour cells as well as the mechanisms involved in their cellular internalization should also be accessed, in order to correlate their interaction with the target cells with their therapeutic activity. The *in vitro* cytotoxicity should be evaluated in more hepatocellular carcinoma cell lines, like Hep3B and HuH-7, and the mechanisms involved in the cell death process should also be analyzed.

After these final studies, it is expected to define the nanosystem synthesized in this work as a specific and efficient combined anticancer approach for HCC treatment.

Chapter 5

References

Albanese, A., Tang, P. S., & Chan, W. C. W. (2012). The Effect of Nanoparticle Size, Shape, and Surface Chemistry on Biological Systems. *Annual Review of Biomedical Engineering*, *14*(1), 1–16. https://doi.org/10.1146/annurev-bioeng-071811-150124

Ally, A., Balasundaram, M., Carlsen, R., Chuah, E., Clarke, A., Dhalla, N., … Laird, P. W. (2017). Comprehensive and Integrative Genomic Characterization of Hepatocellular Carcinoma. *Cell*, *169*(7), 1327-1341.e23. https://doi.org/10.1016/j.cell.2017.05.046

Alvarez-Toral, A., Fernández, B., Malherbe, J., Claverie, F., Pecheyran, C., & Pereiro, R. (2017). Synthesis of amino-functionalized silica nanoparticles for preparation of new laboratory standards. *Spectrochimica Acta - Part B Atomic Spectroscopy*, *138*, 1–7. https://doi.org/10.1016/j.sab.2017.10.002

Ansari, L., Jaafari, M. R., Bastami, T. R., & Malaekeh-Nikouei, B. (2018). Improved anticancer efficacy of epirubicin by magnetic mesoporous silica nanoparticles: in vitro and in vivo studies. *Artificial Cells, Nanomedicine and Biotechnology*, *46*(sup2), 594–606. https://doi.org/10.1080/21691401.2018.1464461

Arakawa, Y., Shimada, M., Utsunomiya, T., Imura, S., Morine, Y., & Ikemoto, T. (2012). Effects of pegylated interferon α2b on metastasis of hepatocellular carcinoma. *Journal of Surgical Research*, *172*(1), 95–101. https://doi.org/10.1016/j.jss.2010.07.023

Asmana Ningrum, R. (2014). Human Interferon Alpha-2b: A Therapeutic Protein for Cancer Treatment. *Scientifica*, *2014*, 1–8. https://doi.org/10.1155/2014/970315

Avila, M. A., Berasain, C., Sangro, B., & Prieto, J. (2006). New therapies for hepatocellular carcinoma. *Oncogene*, *25*(27), 3866–3884. https://doi.org/10.1038/sj.onc.1209550

Banerjee, S. S., & Chen, D. H. (2010). Grafting of 2-hydroxypropyl-β-cyclodextrin on gum Arabic-modified iron oxide nanoparticles as a magnetic carrier for targeted delivery of hydrophobic anticancer drug. *International Journal of Applied Ceramic Technology*, *7*(1), 111–118. https://doi.org/10.1111/j.1744-7402.2008.02332.x

Barba, A. A., Bochicchio, S., Dalmoro, A., Caccavo, D., Cascone, S., & Lamberti, G. (2019). Polymeric and lipid-based systems for controlled drug release: An engineering point of view. In *Nanomaterials for Drug Delivery and Therapy* (pp. 267–304). https://doi.org/10.1016/B978-0-12-816505-8.00013-8

Bardal, S. K., Waechter, J. E., Martin, D. S., Bardal, S. K., Waechter, J. E., & Martin, D. S. (2011). Neoplasia. In *Applied Pharmacology* (pp. 305–324). https://doi.org/10.1016/B978-1-4377-0310-8.00020-8

Barkat, A., Beg, S., Panda, S. K., S Alharbi, K., Rahman, M., & Ahmed, F. J. (2019). Functionalized mesoporous silica nanoparticles in anticancer therapeutics. *Seminars in Cancer Biology*, (August), 0–1. https://doi.org/10.1016/j.semcancer.2019.08.022

Batista, C. A. S., Larson, R. G., & Kotov, N. A. (2015). Nonadditivity of nanoparticle interactions. *Science*, *350*(6257). https://doi.org/10.1126/science.1242477

Beck, J. S., Vartuli, J. C., Roth, W. J., Leonowicz, M. E., Kresge, C. T., Schmitt, K. D., … Schlenker, J. L. (1992). A New Family of Mesoporous Molecular Sieves Prepared with Liquid Crystal Templates. *Journal of the American Chemical Society*, *114*(27), 10834–10843. https://doi.org/10.1021/ja00053a020

Bekisz, J., Baron, S., Balinsky, C., Morrow, A., & Zoon, K. C. (2010). Antiproliferative properties of type I and type II interferon. *Pharmaceuticals*, *3*(4), 994–1015. https://doi.org/10.3390/ph3040994

Bhakta, G., Sharma, R. K., Gupta, N., Cool, S., Nurcombe, V., & Maitra, A. (2011). Multifunctional silica nanoparticles with potentials of imaging and gene delivery. *Nanomedicine: Nanotechnology, Biology, and Medicine*, *7*(4), 472–479. https://doi.org/10.1016/j.nano.2010.12.008

Bis, R. L., Stauffer, T. M., Singh, S. M., Lavoie, T. B., & Mallela, K. M. G. (2014). High yield soluble bacterial expression and streamlined purification of recombinant human interferon α-2a.

Protein Expression and Purification, *99*, 138–146. https://doi.org/10.1016/j.pep.2014.04.010
Blank, V. C., Peña, C., & Roguin, L. P. (2007). A cyclic chimeric interferon-α2b peptide induces apoptosis in tumor cells. *Cancer Biology and Therapy*, *6*(11), 1787–1793. https://doi.org/10.4161/cbt.6.11.4859
Bogush, G. H., & Zukoski IV, C. F. (1991). Studies of the kinetics of the precipitation of uniform silica particles through the hydrolysis and condensation of silicon alkoxides. *Journal of Colloid And Interface Science*, *142*(1), 1–18. https://doi.org/10.1016/0021-9797(91)90029-8
Bonci, E. A., Irimie, A., Buiga, R., Lisencu, I. C., Maja, L. I., & Piciu, D. (2017). Follicle-stimulating hormone receptors: A new immunohistochemical marker in cancers? *Journal of B.U.ON.*, *22*(5), 1352–1359.
Bray, F., Ferlay, J., Soerjomataram, I., Siegel, R. L., Torre, L. A., & Jemal, A. (2018). Global cancer statistics 2018: GLOBOCAN estimates of incidence and mortality worldwide for 36 cancers in 185 countries. *CA: A Cancer Journal for Clinicians*, *68*(6), 394–424. https://doi.org/10.3322/caac.21492
Calderaro, J., Couchy, G., Imbeaud, S., Amaddeo, G., Letouzé, E., Blanc, J. F., … Zucman-Rossi, J. (2017). Histological subtypes of hepatocellular carcinoma are related to gene mutations and molecular tumour classification. *Journal of Hepatology*, *67*(4), 727–738. https://doi.org/10.1016/j.jhep.2017.05.014
Cam, R. (2003). *pET System Tutorial*. 88–92.
Cánepa, C., Imperiale, J. C., Berini, C. A., Lewicki, M., Sosnik, A., & Biglione, M. M. (2017). Development of a Drug Delivery System Based on Chitosan Nanoparticles for Oral Administration of Interferon-α. *Biomacromolecules*, *18*(10), 3302–3309. https://doi.org/10.1021/acs.biomac.7b00959
Chang, L. C., Wu, S. C., Tsai, J. W., Yu, T. J., & Tsai, T. R. (2009). Optimization of epirubicin nanoparticles using experimental design for enhanced intravesical drug delivery. *International Journal of Pharmaceutics*, *376*(1–2), 195–203. https://doi.org/10.1016/j.ijpharm.2009.04.045
Chen, F., Hableel, G., Zhao, E. R., & Jokerst, J. V. (2018). Multifunctional Nanomedicine with Silica: Role of Silica in Nanoparticles for Theranostic, Imaging, and Drug Monitoring. *Physiology & Behavior*, *176*(1), 139–148. https://doi.org/10.1016/j.physbeh.2017.03.040
Chen, J., Wang, Y., Ma, B., Guan, L., Tian, Z., Lin, K., & Zhu, Y. (2020). Biodegradable hollow mesoporous organosilica-based nanosystems with dual stimuli-responsive drug delivery for efficient tumor inhibition by synergistic chemo- and photothermal therapy. *Applied Materials Today*, *19*. https://doi.org/10.1016/j.apmt.2020.100655
Chen, Z., Li, Z., Lin, Y., Yin, M., Ren, J., & Qu, X. (2013). Bioresponsive hyaluronic acid-capped mesoporous silica nanoparticles for targeted drug delivery. *Chemistry - A European Journal*, *19*(5), 1778–1783. https://doi.org/10.1002/chem.201202038
Cheng, C. T., Castro, G., Liu, C. H., & Lau, P. (2019). Advanced nanotechnology: An arsenal to enhance immunotherapy in fighting cancer. *Clinica Chimica Acta*, *492*(October 2018), 12–19. https://doi.org/10.1016/j.cca.2019.01.027
Chew, S. A., Moscato, S., George, S., Azimi, B., & Danti, S. (2019). Liver Cancer : Current and Future Trends Using Biomaterials. *Cancers*, *11*(2026).
Chung, T. H., Wu, S. H., Yao, M., Lu, C. W., Lin, Y. S., Hung, Y., … Huang, D. M. (2007). The effect of surface charge on the uptake and biological function of mesoporous silica nanoparticles in 3T3-L1 cells and human mesenchymal stem cells. *Biomaterials*, *28*(19), 2959–2966. https://doi.org/10.1016/j.biomaterials.2007.03.006
Conlon, K. C., Miljkovic, M. D., & Waldmann, T. A. (2019). Cytokines in the Treatment of Cancer. *Journal of Interferon and Cytokine Research*, *39*(1), 6–21. https://doi.org/10.1089/jir.2018.0019
Cordeiro, R. A., Santo, D., Farinha, D., Serra, A., Faneca, H., & Coelho, J. F. J. (2017). High transfection efficiency promoted by tailor-made cationic tri-block copolymer-based nanoparticles. *Acta Biomaterialia*, *47*, 113–123. https://doi.org/10.1016/j.actbio.2016.10.015
Craig, A. J., von Felden, J., Garcia-Lezana, T., Sarcognato, S., & Villanueva, A. (2019). Tumour evolution in hepatocellular carcinoma. *Nature Reviews. Gastroenterology & Hepatology*. https://doi.org/10.1038/s41575-019-0229-4
Cui, L. Y., Li, Y. H., Zhang, W., Zhang, J. P., & Duan, Q. (2014). Hyaluronic acid functionalized porous silica nanoparticles for drug delivery and release. *Advanced Materials Research*, *936*, 322–326. https://doi.org/10.4028/www.scientific.net/AMR.936.322

Damdinsuren, B., Nagano, H., Wada, H., Kondo, M., Ota, H., Nakamura, M., … Monden, M. (2007). Stronger growth-inhibitory effect of interferon (IFN)-β compared to IFN-α is mediated by IFN signaling pathway in hepatocellular carcinoma cells. *International Journal of Oncology*, *30*(1), 201–208. https://doi.org/10.3892/ijo.30.1.201

Damdinsuren, B., Nagano, H., Wada, H., Noda, T., Natsag, J., Marubashi, S., … Monden, M. (2007). Interferon alpha receptors are important for antiproliferative effect of interferon-α against human hepatocellular carcinoma cells. *Hepatology Research*, *37*(1), 77–83. https://doi.org/10.1111/j.1872-034X.2007.00007.x

de Luján Alvarez, M., Cerliani, J. P., Monti, J., Carnovale, C., Ronco, M. T., Pisani, G., … Carrillo, M. C. (2002). The in vivo apoptotic effect of interferon alfa-2b on rat preneoplastic liver involves bax protein. *Hepatology*, *35*(4), 824–833. https://doi.org/10.1053/jhep.2002.32099

Dhar, D., Antonucci, L., Nakagawa, H., Kim, J. Y., Glitzner, E., Caruso, S., … Karin, M. (2018). Liver Cancer Initiation Requires p53 Inhibition by CD44-Enhanced Growth Factor Signaling. *Cancer Cell*, *33*(6), 1061-1077.e6. https://doi.org/10.1016/j.ccell.2018.05.003

Di-Wen, S., Pan, G. Z., Hao, L., Zhang, J., Xue, Q. Z., Wang, P., & Yuan, Q. Z. (2016). Improved antitumor activity of epirubicin-loaded CXCR4-targeted polymeric nanoparticles in liver cancers. *International Journal of Pharmaceutics*, *500*(1–2), 54–61. https://doi.org/10.1016/j.ijpharm.2015.12.066

Dipak, S. P., Kosloski, M. P., & Balu-Iyer, S. V. (2010). DELIVERY OF THERAPEUTIC PROTEINS. *J Pharm Sci.*, *99*(6), 2557–2575. https://doi.org/10.1002/jps.22054.DELIVERY

Du, X., & He, J. (2011). Spherical silica micro/nanomaterials with hierarchical structures: Synthesis and applications. *Nanoscale*, *3*(10), 3984–4002. https://doi.org/10.1039/c1nr10660k

El-Serag, H. B., & Rudolph, K. L. (2007). Hepatocellular Carcinoma: Epidemiology and Molecular Carcinogenesis. *Gastroenterology*, *132*(7), 2557–2576. https://doi.org/10.1053/j.gastro.2007.04.061

Endo, K., & Terada, T. (2000). Protein expression of CD44 (standard and variant isoforms) in hepatocellular carcinoma: Relationships with tumor grade, clinicopathologic parameters, p53 expression, and patient survival. *Journal of Hepatology*, *32*(1), 78–84. https://doi.org/10.1016/S0168-8278(00)80192-0

Fang, J., Wang, Q., Yang, G., Xiao, X., Li, L., & Yu, T. (2019). Albumin-MnO 2 gated hollow mesoporous silica nanosystem for modulating tumor hypoxia and synergetic therapy of cervical carcinoma. *Colloids and Surfaces B: Biointerfaces*, *179*(February), 250–259. https://doi.org/10.1016/j.colsurfb.2019.03.070

Farinha, D., Pedroso De Lima, M. C., & Faneca, H. (2014). Specific and efficient gene delivery mediated by an asialofetuin-associated nanosystem. *International Journal of Pharmaceutics*, *473*(1–2), 366–374. https://doi.org/10.1016/j.ijpharm.2014.07.019

Farjadian, F., Roointan, A., Mohammadi-Samani, S., & Hosseini, M. (2019). Mesoporous silica nanoparticles: Synthesis, pharmaceutical applications, biodistribution, and biosafety assessment. *Chemical Engineering Journal*, *359*(June 2018), 684–705. https://doi.org/10.1016/j.cej.2018.11.156

Forner, A., Reig, M., & Bruix, J. (2018). Hepatocellular carcinoma. *The Lancet*, *391*(10127), 1301–1314. https://doi.org/10.1016/S0140-6736(18)30010-2

Frey, H., Schroeder, N., Manon-Jensen, T., Iozzo, R. V., & Schaefer, L. (2013). Biological interplay between proteoglycans and their innate immune receptors in inflammation. *FEBS Journal*, *280*(10), 2165–2179. https://doi.org/10.1111/febs.12145

Galarneau, A., Cambon, H., Di Renzo, F., Ryoo, R., Choi, M., & Fajula, F. (2003). Microporosity and connections between pores in SBA-15 mesostructured silicas as a function of the temperature of synthesis. *New Journal of Chemistry*, *27*(1), 73–79. https://doi.org/10.1039/b207378c

Galarneau, A., Renzo, F. Di, Fajula, F., Mollo, L., Fubini, B., & Ottaviani, M. F. (1998). Kinetics of formation of micelle-templated silica mesophases monitored by electron paramagnetic resonance. *Journal of Colloid and Interface Science*, *201*(2), 105–117. https://doi.org/10.1006/jcis.1998.5413

Ganta, S., Singh, A., Coleman, T. P., Williams, D., & Amiji, M. (2014). *Pharmaceutical Nanotechnology: Overcoming Drug Delivery Challenges in Contemporary Medicine*. https://doi.org/10.1007/978-1-4614-2140-5_10

Gao, B., Hong, F., & Radaeva, S. (2004). Host Factors and Failure of Interferon-α Treatment in Hepatitis C Virus. *Hepatology*, *39*(4), 880–890. https://doi.org/10.1002/hep.20139

Gao, B., Wang, H., Lafdil, F., & Feng, D. (2012). STAT proteins - key regulators of anti-viral

responses, inflammation, and tumorigenesis in the liver. *J Hepatol*, *57*(2), 430–441. https://doi.org/10.1038/jid.2014.371

Gbolahan, O. B., Schacht, M. A., Beckley, E. W., LaRoche, T. P., O'Neil, B. H., & Pyko, M. (2017). Locoregional and systemic therapy for hepatocellular carcinoma. *Journal of Gastrointestinal Oncology*, *8*(2), 215–228. https://doi.org/10.21037/jgo.2017.03.13

Ge, S., Geng, W., He, X., Zhao, J., Zhou, B., Duan, L., … Zhang, Q. (2018). Effect of framework structure, pore size and surface modification on the adsorption performance of methylene blue and Cu2+ in mesoporous silica. *Colloids and Surfaces A: Physicochemical and Engineering Aspects*, *539*(December 2017), 154–162. https://doi.org/10.1016/j.colsurfa.2017.12.016

Ghaffari, M., Dehghan, G., Baradaran, B., Zarebkohan, A., Mansoori, B., Soleymani, J., … Hamblin, M. R. (2020). Co-delivery of curcumin and Bcl-2 siRNA by PAMAM dendrimers for enhancement of the therapeutic efficacy in HeLa cancer cells. *Colloids and Surfaces B: Biointerfaces*, *188*(July 2019). https://doi.org/10.1016/j.colsurfb.2019.110762

Glick, B. R., Pasternak, J. J., & Patten, C. L. (2008). *Molecular Biotechnology - Principles and Applications of Recombinant DNA* (4th ed.).

Green, D. S., Husain, S. R., Johnson, C. L., Sato, Y., Han, J., Joshi, B., … Zoon, K. C. (2019). Combination immunotherapy with IL-4 Pseudomonas exotoxin and IFN-α and IFN-γ mediate antitumor effects in vitro and in a mouse model of human ovarian cancer. *Immunotherapy*, *11*(6), 483–496. https://doi.org/10.2217/imt-2018-0158

Gu, J., Huang, K., Zhu, X., Li, Y., Wei, J., Zhao, W., … Shi, J. (2013). Sub-150 nm mesoporous silica nanoparticles with tunable pore sizes and well-ordered mesostructure for protein encapsulation. *Journal of Colloid And Interface Science*, *407*, 236–242. https://doi.org/10.1016/j.jcis.2013.06.028

Hadipour Moghaddam, S. P., Saikia, J., Yazdimamaghani, M., & Ghandehari, H. (2017). Redox-Responsive Polysulfide-Based Biodegradable Organosilica Nanoparticles for Delivery of Bioactive Agents. *ACS Applied Materials and Interfaces*, *9*(25), 21133–21146. https://doi.org/10.1021/acsami.7b04351

Hadipour Moghaddam, S. P., Yazdimamaghani, M., & Ghandehari, H. (2018). Glutathione-sensitive hollow mesoporous silica nanoparticles for controlled drug delivery. *Journal of Controlled Release*, *282*(January), 62–75. https://doi.org/10.1016/j.jconrel.2018.04.032

Hanafi-Bojd, M. Y., Ansari, L., Mosaffa, F., & Malaekeh-Nikouei, B. (2017). The effect of mesoporous silica nanoparticles loaded with epirubicin on drug-resistant cancer cells. *Nanomedicine Journal*, *4*(3), 135–141. https://doi.org/10.22038/nmj.2017.8954

Hanafi-Bojd, M. Y., Jaafari, M. R., Ramezanian, N., Xue, M., Amin, M., Shahtahmassebi, N., & Malaekeh-Nikouei, B. (2015). Surface functionalized mesoporous silica nanoparticles as an effective carrier for epirubicin delivery to cancer cells. *European Journal of Pharmaceutics and Biopharmaceutics*, *89*, 248–258. https://doi.org/10.1016/j.ejpb.2014.12.009

Hanafy, N. A. (2013). *Development and production of multifunctional bio- nano-engineered drug delivery systems loaded by tgf ß1 inhibitors for delivering into hepatocellular carcinoma cells.*

Herheliuk, T., Perepelytsina, O., Ugnivenko, A., Ostapchenko, L., & Sydorenko, M. (2019). Response of breast cancer cells to IFNα-2b in 2D and 3D cell cultures. *Turkish Journal of Biology*, *43*(1), 13–20. https://doi.org/10.3906/biy-1808-36

Hermanson, G. T. (2008). *Bioconjugate Techniques* (2nd Editio).

Hisaka, T., Yano, H., Ogasawara, S., Momosaki, S., Nishida, N., Takemoto, Y., … Kojiro, M. (2004). Interferon-αCon1 suppresses proliferation of liver cancer cell lines in vitro and in vivo. *Journal of Hepatology*, *41*(5), 782–789. https://doi.org/10.1016/j.jhep.2004.07.012

Hu, X., Hao, X., Wu, Y., Zhang, J., Zhang, X., Wang, P. C., Liang, X. J. (2013). Multifunctional hybrid silica nanoparticles for controlled doxorubicin loading and release with thermal and pH dual response. *Journal of Materials Chemistry B*, *1*(8), 1109–1118. https://doi.org/10.1039/c2tb00223j

Huang, D. M., Hung, Y., Ko, B. S., Hsu, S. C., Chen, W. H., Chien, C. L., Chen, Y. C. (2005). Highly efficient cellular labeling of mesoporous nanoparticles in human mesenchymal stem cells: Implication for stem cell tracking. *FASEB Journal*, *19*(14), 2014–2016. https://doi.org/10.1096/fj.05-4288fje

Ingersoll, S. B., Patel, S., Caballero, L., Ahmad, S., Edwards, D., Holloway, R. W., & Edwards, J. R. (2009). Synergistic cytotoxicity of interferonα-2b and interleukin-2 in combination with PBMC against ovarian cancer: Development of an experimental model for cellular therapy. *Gynecologic Oncology*, *112*(1), 192–198. https://doi.org/10.1016/j.ygyno.2008.09.028

Instruments, M. (2011). Dynamic Light Scattering - Common terms defined. In *Malvern Guides* (pp. 1–6).

Itano, N., & Koji, K. (2002). *Mammalian Hyaluronan Synthases*. *1*, 195–199. https://doi.org/10.1080/15216540290114478

Jafari, S., Derakhshankhah, H., Alaei, L., Fattahi, A., Varnamkhasti, B. S., & Saboury, A. A. (2019). Mesoporous silica nanoparticles for therapeutic/diagnostic applications. *Biomedicine and Pharmacotherapy*, *109*(October 2018), 1100–1111. https://doi.org/10.1016/j.biopha.2018.10.167

Jammaer, J., Aerts, A., D'Haen, J., Seo, J. W., & Martens, J. A. (2009). Convenient synthesis of ordered mesoporous silica at room temperature and quasi-neutral pH. *Journal of Materials Chemistry*, *19*(44), 8290–8293. https://doi.org/10.1039/b915273c

Jeevanandam, J., Chan, Y. S., & Danquah, M. K. (2016). Nano-formulations of drugs: Recent developments, impact and challenges. *Biochimie*, *128–129*, 99–112. https://doi.org/10.1016/j.biochi.2016.07.008

Jin, R., Liu, Z., Bai, Y., Zhou, Y., & Chen, X. (2018). Multiple-Responsive Mesoporous Silica Nanoparticles for Highly Accurate Drugs Delivery to Tumor Cells. *ACS Omega*, *3*(4), 4306–4315. https://doi.org/10.1021/acsomega.8b00427

Jonasch, E., & Haluska, F. G. (2001). Interferon in Oncological Practice: Review of Interferon Biology, Clinical Applications, and Toxicities. *The Oncologist*, *6*(1), 34–55. https://doi.org/10.1634/theoncologist.6-1-34

Kalie, E., Jaitin, D. A., Abramovich, R., & Schreiber, G. (2007). An interferon α2 mutant optimized by phage display for IFNAR1 binding confers specifically enhanced antitumor activities. *Journal of Biological Chemistry*, *282*(15), 11602–11611. https://doi.org/10.1074/jbc.M610115200

Karpuz, M., Silindir-Gunay, M., Kursunel, M. A., Esendagli, G., Dogan, A., & Ozer, A. Y. (2020). Design and in vitro evaluation of folate-targeted, co-drug encapsulated theranostic liposomes for non-small cell lung cancer. *Journal of Drug Delivery Science and Technology*, *57*(April), 101707. https://doi.org/10.1016/j.jddst.2020.101707

Kesse, S., Boakye-Yiadom, K. O., Ochete, B. O., Opoku-Damoah, Y., Akhtar, F., Filli, M. S., Wang, B. (2019). Mesoporous silica nanomaterials: Versatile nanocarriers for cancer theranostics and drug and gene delivery. *Pharmaceutics*, *11*(2), 1–26. https://doi.org/10.3390/pharmaceutics11020077

Khemlina, G., Ikeda, S., & Kurzrock, R. (2017). The biology of Hepatocellular carcinoma: Implications for genomic and immune therapies. *Molecular Cancer*, *16*(1), 1–10. https://doi.org/10.1186/s12943-017-0712-x

Kim, Y. J., Jung, J., Joo, J. H., Kim, S. Y., Kim, J. H., Lim, Y. S., … Yoon, S. M. (2019). Combined transarterial chemoembolization and radiotherapy as a first-line treatment for hepatocellular carcinoma with macroscopic vascular invasion: Necessity to subclassify Barcelona Clinic Liver Cancer stage C. *Radiotherapy and Oncology*, *141*, 95–100. https://doi.org/10.1016/j.radonc.2019.08.009

Kimchi-Sarfaty, C., Schiller, T., Hamasaki-Katagiri, N., Khan, M. A., Yanover, C., & Sauna, Z. E. (2013). Building better drugs: Developing and regulating engineered therapeutic proteins. *Trends in Pharmacological Sciences*, *34*(10), 534–548. https://doi.org/10.1016/j.tips.2013.08.005

Kleitz, F., Liu, D., Anilkumar, G. M., Park, I. S., Solovyov, L. A., Shmakov, A. N., & Ryoo, R. (2003). Large Cage Face-Centered-Cubic Fm3m Mesoporous Silica: Synthesis and Structure. *Journal of Physical Chemistry B*, *107*(51), 14296–14300. https://doi.org/10.1021/jp036136b

Kondo, M., Nagano, H., Wada, H., Damdinsuren, B., Yamamoto, H., Hiraoka, N., Monden, M. (2005). Combination of IFN-α and 5-fluorouracil induces apoptosis through IFN-α/β receptor in human hepatocellular carcinoma cells. *Clinical Cancer Research*, *11*(3), 1277–1286.

Kotredes, K. P., & Gamero, A. M. (2013). Interferons as inducers of apoptosis in malignant cells. *Journal of Interferon and Cytokine Research*, *33*(4), 162–170. https://doi.org/10.1089/jir.2012.0110

Kouvidi, K., Berdiaki, A., Nikitovic, D., Katonis, P., Afratis, N., Hascall, V. C., Tzanakakis, G. N. (2011). Role of Receptor for Hyaluronic Acid-mediated Motility (RHAMM) in Low Molecular Weight Hyaluronan (LMWHA)- mediated fibrosarcoma cell adhesion. *Journal of Biological Chemistry*, *286*(44), 38509–38520. https://doi.org/10.1074/jbc.M111.275875

Kumar, A., & Dixit, C. K. (2017). Methods for characterization of nanoparticles. In *Advances in Nanomedicine for the Delivery of Therapeutic Nucleic Acids* (pp. 44–58).

https://doi.org/10.1016/B978-0-08-100557-6.00003-1
Kumar, D., Schumacher, K., Du Fresne von Hohenesche, C., Grün, M., & Unger, K. K. (2001). MCM-41, MCM-48 and related mesoporous adsorbents: their synthesis and characterisation. *Colloids and Surfaces A: Physicochemical and Engineering Aspects*, *187–188*, 109–116. https://doi.org/10.1016/S0927-7757(01)00638-0
Kuo, J. W., Swarm, D. A., & Prestwich, G. D. (1991). Chemical Modification of Hyaluronic Acid by Carbodiimides. *Bioconjugate Chemistry*, *2*(4), 232–241. https://doi.org/10.1021/bc00010a007
Kusano, H., Akiba, J., Ogasawara, S., Sanada, S., Yasumoto, M., Nakayama, M., … Yano, H. (2013). Pegylated interferon-α2a inhibits proliferation of human liver cancer cells in vitro and in vivo. *PLoS ONE*, *8*(12), 1–10. https://doi.org/10.1371/journal.pone.0083195
Kusano, H., Ogasawara, S., Akiba, J., Nakayama, M., Ueda, K., & Yano, H. (2013). Antiproliferative effects of sorafenib and pegylated IFN-α2b on human liver cancer cells in vitro and in vivo. *International Journal of Oncology*, *42*(6), 1897–1903. https://doi.org/10.3892/ijo.2013.1904
Leader, B., Baca, Q. J., & Golan, D. E. (2008). Protein therapeutics: A summary and pharmacological classification. *Nature Reviews Drug Discovery*, *7*(1), 21–39. https://doi.org/10.1038/nrd2399
Li, J., Qiao, Y., & Wu, Z. (2017). Nanosystem trends in drug delivery using quality-by-design concept. *Journal of Controlled Release*, *256*(April), 9–18. https://doi.org/10.1016/j.jconrel.2017.04.019
Li, T., Shi, S., Goel, S., Shen, X., Xie, X., Chen, Z., … Liu, Y. (2019). Recent advancements in mesoporous silica nanoparticles towards therapeutic applications for cancer. *Acta Biomaterialia*, *89*, 1–13. https://doi.org/10.1016/j.actbio.2019.02.031
Li, Xiaoming, Wang, L., Fan, Y., Feng, Q., & Cui, F. Z. (2012). Biocompatibility and toxicity of nanoparticles and nanotubes. *Journal of Nanomaterials*, *2012*. https://doi.org/10.1155/2012/548389
Li, Xu, Chen, Y., Wang, M., Ma, Y., Xia, W., & Gu, H. (2013). A mesoporous silica nanoparticle - PEI - Fusogenic peptide system for siRNA delivery in cancer therapy. *Biomaterials*, *34*(4), 1391–1401. https://doi.org/10.1016/j.biomaterials.2012.10.072
Lim, J., Lee, K., Choi, J., & Hwang, Y. (2012). Intracellular protein delivery by hollow mesoporous silica capsules with a large surface hole. *Nanotechnology*, *23*. https://doi.org/10.1088/0957-4484/23/8/085101
Limeres, M. J., Moretton, M. A., Bernabeu, E., Chiappetta, D. A., & Cuestas, M. L. (2019). Thinking small, doing big: Current success and future trends in drug delivery systems for improving cancer therapy with special focus on liver cancer. *Materials Science and Engineering C*, *95*(September 2018), 328–341. https://doi.org/10.1016/j.msec.2018.11.001
Lin, G., Zhou, H., Lian, J., Chen, H., Xu, H., & Zhou, X. (2019). Preparation of pH-responsive avermectin/feather keratin-hyaluronic acid with anti-UV and sustained-release properties. *Colloids and Surfaces B: Biointerfaces*, *175*(December 2018), 291–299. https://doi.org/10.1016/j.colsurfb.2018.11.074
Liu, F., Huang, P., Huang, D., Liu, S., Cao, Q., Dong, X., Zhou, W. (2019). Smart “on-off” responsive drug delivery nanosystems for potential imaging diagnosis and targeted tumor therapy. *Chemical Engineering Journal*, *365*(February), 358–368. https://doi.org/10.1016/j.cej.2019.02.037
Liu, Y., Wei, C., Lin, A., Pan, J., Chen, X., Zhu, X., Luo, Z. (2020). Responsive functionalized MoSe2 nanosystem for highly efficient synergistic therapy of breast cancer. *Colloids and Surfaces B: Biointerfaces*, *189*(August 2019). https://doi.org/10.1016/j.colsurfb.2020.110820
Longmire, M., Choyke, P. L., & Kobayashi, H. (2008). Clearance properties of nano-sized particles and molecules as imaging agents: Considerations and caveats. *Nanomedicine*, *3*(5), 703–717. https://doi.org/10.2217/17435889.3.5.703
Lopez-Campos, F., Candini, D., Carrasco, E., & Berenguer Francés, M. A. (2019). Nanoparticles applied to cancer immunoregulation. *Reports of Practical Oncology and Radiotherapy*, *24*(1), 47–55. https://doi.org/10.1016/j.rpor.2018.10.001
Ma, H., Yang, W., Zhang, L., Liu, S., Zhao, M., Zhou, G., Hu, J. (2019). Interferon-alpha promotes immunosuppression through IFNAR1/STAT1 signalling in head and neck squamous cell carcinoma. *British Journal of Cancer*, *120*(3), 317–330. https://doi.org/10.1038/s41416-018-0352-y
Madduru, D., Ijaq, J., Dhar, S., Sarkar, S., Poondla, N., Das, P. S., Suravajhala, P. (2019).

Systems Challenges of Hepatic Carcinomas: A Review. *Journal of Clinical and Experimental Hepatology*, *9*(2), 233–244. https://doi.org/10.1016/j.jceh.2018.05.002
Magdeldin, S., & Moser, A. (2012). Affinity Chromatography: Principles and Applications. In *Affinity Chromatography*. https://doi.org/10.5772/39087
Mahjub, R., Jatana, S., Lee, S. E., Qin, Z., Pauli, G., Soleimani, M., … Li, S. D. (2018). Recent advances in applying nanotechnologies for cancer immunotherapy. *Journal of Controlled Release*, *288*(July), 239–263. https://doi.org/10.1016/j.jconrel.2018.09.010
Manning, M. C., Chou, D. K., Murphy, B. M., Payne, R. W., & Katayama, D. S. (2010). Stability of protein pharmaceuticals: An update. *Pharmaceutical Research*, *27*(4), 544–575. https://doi.org/10.1007/s11095-009-0045-6
Matsoukas, T., & Gulari, E. (1988). Dynamics of growth of silica particles from ammonia-catalyzed hydrolysis of tetra-ethyl-orthosilicate. *Journal of Colloid And Interface Science*, *124*(1), 252–261. https://doi.org/10.1016/0021-9797(88)90346-3
Matsoukas, Themis, & Gulari, E. (1989). Monomer-addition growth with a slow initiation step: A growth model for silica particles from alkoxides. *Journal of Colloid And Interface Science*, *132*(1), 13–21. https://doi.org/10.1016/0021-9797(89)90210-5
Mays, A. N., Osheroff, N., Xiao, Y., Wiemels, J. L., Felix, C. A., Byl, J. A. W., … Grimwade, D. (2010). Evidence for direct involvement of epirubicin in the formation of chromosomal translocations in t(15;17) therapy-related acute promyelocytic leukemia. *Blood*, *115*(2), 326–330. https://doi.org/10.1182/blood-2009-07-235051
Mekaru, H., Lu, J., & Fuyuhiko, T. (2017). Development of mesoporous silica-based nanoparticles with controlled release capability for cancer therapy. *Physiology & Behavior*, *176*(1), 139–148. https://doi.org/10.1016/j.physbeh.2017.03.040
Meng, J., Guo, F., Xu, H., Liang, W., Wang, C., & Yang, X. Da. (2016). Combination Therapy using Co-encapsulated Resveratrol and Paclitaxel in Liposomes for Drug Resistance Reversal in Breast Cancer Cells in vivo. *Scientific Reports*, *6*(February), 1–11. https://doi.org/10.1038/srep22390
Min, Y., Roche, K. C., Tian, S., Eblan, M. J., Karen, P., Caster, J. M., … Vincent, B. G. (2017). Antigen-capturing nanoparticles improve the abscopal effect and cancer immunotherapy. *Nature Nanotechnolog*, *12*(9), 877–882. https://doi.org/10.1038/nnano.2017.113.Antigen-capturing
Moghaddam, S. V., Abedi, F., Alizadeh, E., Baradaran, B., Annabi, N., Akbarzadeh, A., & Davaran, S. (2020). Lysine-embedded cellulose-based nanosystem for efficient dual-delivery of chemotherapeutics in combination cancer therapy. *Carbohydrate Polymers*, *250*(March), 116861. https://doi.org/10.1016/j.carbpol.2020.116861
Mokhtari, R. B., Homayouni, T. S., Baluch, N., Morgatskaya, E., Kumar, S., Das, B., & Yeger, H. (2017). Combination therapy in combating cancer. *Oncotarget*, *8*(23), 38022–38043. Retrieved from www.impactjournals.com/oncotarget
Mondaca, S., Yarmohammadi, H., & Kemeny, N. E. (2019). Regional Chemotherapy for Biliary Tract Tumors and Hepatocellular Carcinoma. *Surgical Oncology Clinics of North America*, *28*(4), 717–729. https://doi.org/10.1016/j.soc.2019.06.008
Monslow, J., Govindaraju, P., & Puré, E. (2015). Hyaluronan - a functional and structural sweet spot in the tissue microenvironment. *Frontiers in Immunology*, *6*(MAY), 4–10. https://doi.org/10.3389/fimmu.2015.00231
Nairi, V., Magnolia, S., Piludu, M., Nieddu, M., Caria, C. A., Sogos, V., … Salis, A. (2018). Mesoporous silica nanoparticles functionalized with hyaluronic acid. Effect of the biopolymer chain length on cell internalization. *Colloids and Surfaces B: Biointerfaces*, *168*, 50–59. https://doi.org/10.1016/j.colsurfb.2018.02.019
Nalaskowski, M. M., Bertsch, U., Fanick, W., Stockebrand, M. C., Schmale, H., & Mayr, G. W. (2003). Rat inositol 1,4,5-trisphosphate 3-kinase C is enzymatically specialized for basal cellular inositol trisphosphate phosphorylation and shuttles actively between nucleus and cytoplasm. *Journal of Biological Chemistry*, *278*(22), 19765–19776. https://doi.org/10.1074/jbc.M211059200
Narayan, R., Nayak, U. Y., Raichur, A. M., & Garg, S. (2018). Mesoporous silica nanoparticles: A comprehensive review on synthesis and recent advances. *Pharmaceutics*, *10*(3), 1–49. https://doi.org/10.3390/pharmaceutics10030118
Nicolas W. Cortes-Penfield, Barbara W. Trautner, R. J. (2017). Design considerations for nanotherapeutics in oncology. *Physiology & Behavior*, *176*(5), 139–148. https://doi.org/10.1016/j.physbeh.2017.03.040
Patra, J. K., Das, G., Fraceto, L. F., Campos, E. V. R., Rodriguez-Torres, M. D. P., Acosta-Torres,

L. S., … Shin, H. S. (2018). Nano based drug delivery systems: Recent developments and future prospects. *Journal of Nanobiotechnology*, *16*(1), 1–33. https://doi.org/10.1186/s12951-018-0392-8

Perry, J. L., Reuter, K. G., Luft, J. C., Pecot, C. V., Zamboni, W., & DeSimone, J. M. (2017). Mediating Passive Tumor Accumulation through Particle Size, Tumor Type, and Location. *Nano Letters*, *17*(5), 2879–2886. https://doi.org/10.1021/acs.nanolett.7b00021

Petrey, A. C., & de la Motte, C. A. (2014). Hyaluronan, a crucial regulator of inflammation. *Frontiers in Immunology*, *5*(MAR), 1–13. https://doi.org/10.3389/fimmu.2014.00101

Petros, R. A., & Desimone, J. M. (2010). Strategies in the design of nanoparticles for therapeutic applications. *Nature Reviews Drug Discovery*, *9*(8), 615–627. https://doi.org/10.1038/nrd2591

Poonia, N., Lather, V., & Pandita, D. (2018). Mesoporous silica nanoparticles: a smart nanosystem for management of breast cancer. *Drug Discovery Today*, *23*(2), 315–332. https://doi.org/10.1016/j.drudis.2017.10.022

Prevo, R., Banerji, S., Ferguson, D. J. P., Clasper, S., & Jackson, D. G. (2001). Mouse LYVE-1 Is an Endocytic Receptor for Hyaluronan in Lymphatic Endothelium. *Journal of Biological Chemistry*, *276*(22), 19420–19430. https://doi.org/10.1074/jbc.M011004200

Qing, G., Ma, L. C., Khorchid, A., Swapna, G. V. T., Mal, T. K., Takayama, M. M., … Inouye, M. (2004). Cold-shock induced high-yield protein production in Escherichia coli. *Nature Biotechnology*, *22*(7), 877–882. https://doi.org/10.1038/nbt984

Quesada, P., Malanga, M., Di Meglio, S., De Lorenzo, S., Fabbrocini, A., Garbi, C., … Pepe, S. (2003). Recombinant IFN-α2b treatment activates poly (ADPR) polymerase-1 (PARP-1) in KB cancer cells. *European Journal of Cancer*, *39*(14), 2103–2109. https://doi.org/10.1016/S0959-8049(03)00433-7

Rawal, S., & Patel, M. M. (2019). Threatening cancer with nanoparticle aided combination oncotherapy. *Journal of Controlled Release*, *301*(March), 76–109. https://doi.org/10.1016/j.jconrel.2019.03.015

Rayner, D. M., & Cutts, S. M. (2014). Anthracyclines. In *Side Effects of Drugs Annual* (Vol. 36, pp. 683–694). https://doi.org/10.1016/B978-0-444-63407-8.00045-9

Reiter, M., Eckhardt, I., Haferkamp, A., & Fulda, S. (2016). Smac mimetic sensitizes renal cell carcinoma cells to interferon-α-induced apoptosis. *Cancer Letters*, *375*(1), 1–8. https://doi.org/10.1016/j.canlet.2016.02.019

Rosebeck, S., & Leaman, D. W. (2008). Mitochondrial localization and pro-apoptotic effects of the interferon-inducible protein ISG12a. *Apoptosis*, *13*(4), 562–572. https://doi.org/10.1007/s10495-008-0190-0

Rosenholm, J. M., Mamaeva, V., Sahlgren, C., & Lindén, M. (2012). Nanoparticles in targeted cancer therapy: Mesoporous silica nanoparticles entering preclinical development stage. *Nanomedicine*, *7*(1), 111–120. https://doi.org/10.2217/nnm.11.166

Sábio, R. M., Meneguin, A. B., Ribeiro, T. C., Silva, R. R., & Chorilli, M. (2019). New insights towards mesoporous silica nanoparticles as a technological platform for chemotherapeutic drugs delivery. *International Journal of Pharmaceutics*, *564*(February), 379–409. https://doi.org/10.1016/j.ijpharm.2019.04.067

Sahay, G., Alakhova, D. Y., & Kabanov, A. V. (2010). Endocytosis of nanomedicines. *Journal of Controlled Release*, *145*(3), 182–195. https://doi.org/10.1016/j.jconrel.2010.01.036

Saito, G., Swanson, J. A., & Lee, K. D. (2003). Drug delivery strategy utilizing conjugation via reversible disulfide linkages: Role and site of cellular reducing activities. *Advanced Drug Delivery Reviews*, *55*(2), 199–215. https://doi.org/10.1016/S0169-409X(02)00179-5

Samarin, Z. E., Abolghasemi, S., Dehnavi, E., Akbarzadeh, A., Hadian, A., Khodabandeh, M., & Aghaeepoor, M. (2018). Response surface optimization of the expression conditions for synthetic human interferon α-2B gene in Escherichia coli. *Indian Journal of Pharmaceutical Sciences*, *80*(3), 470–479. https://doi.org/10.4172/pharmaceutical-sciences.1000380

Sambrook, J., & Russel, D. W. (2001). *Molecular cloning: a laboratory manual* (3rd ed.).

Santo, D., Cordeiro, R. A., Sousa, A., Serra, A., Coelho, J. F. J., & Faneca, H. (2017). Combination of Poly[(2-dimethylamino)ethyl methacrylate] and Poly(β-amino ester) Results in a Strong and Synergistic Transfection Activity. *Biomacromolecules*, *18*(10), 3331–3342. https://doi.org/10.1021/acs.biomac.7b00983

Seehawer, M., Heinzmann, F., D'Artista, L., Harbig, J., Roux, P. F., Hoenicke, L., … Zender, L. (2018). Necroptosis microenvironment directs lineage commitment in liver cancer. *Nature*, *562*(7725), 69–75. https://doi.org/10.1038/s41586-018-0519-y

Serna, N., Sánchez-García, L., Unzueta, U., Díaz, R., Vázquez, E., Mangues, R., & Villaverde,

A. (2018). Protein-Based Therapeutic Killing for Cancer Therapies. *Trends in Biotechnology*, *36*(3), 318–335. https://doi.org/10.1016/j.tibtech.2017.11.007
Shahbazi, M. A., Herranz, B., & Santos, H. A. (2012). Nanostructured porous Si-based nanoparticles for targeted drug delivery. *Biomatter*, *2*(4), 296–312. https://doi.org/10.4161/biom.22347
Shi, H., Liu, S., Cheng, J., Yuan, S., Yang, Y., Fang, T., … Liu, Y. (2019). Charge-Selective Delivery of Proteins Using Mesoporous Silica Nanoparticles Fused with Lipid Bilayers. *ACS Applied Materials and Interfaces*, *11*(4), 3645–3653. https://doi.org/10.1021/acsami.8b15390
Shimomura, S., & Nishiguchi, S. (2012). Anticarcinogenic impact of interferon therapy on the progression of hepatocellular carcinoma in patients with chronic viral infection. *Hepatology Research*, *42*(1), 22–32. https://doi.org/10.1111/j.1872-034X.2011.00889.x
Šimůnek, T., Štěrba, M., Popelová, O., Adamcová, M., Hrdina, R., & Gerši, V. (2009). Anthracycline-induced cardiotoxicity: Overview of studies examining the roles of oxidative stress and free cellular iron. *Pharmacological Reports*, *61*(1), 154–171. https://doi.org/10.1016/S1734-1140(09)70018-0
Slowing, I., Trewyn, B. G., & Lin, V. S. Y. (2006). Effect of surface functionalization of MCM-41-type mesoporous silica nanoparticles on the endocytosis by human cancer cells. *Journal of the American Chemical Society*, *128*(46), 14792–14793. https://doi.org/10.1021/ja0645943
Song, F., Li, Y., Wang, S., Zhang, L., & Chen, Q. L. (2019). Multifunctional dual-mesoporous silica nanoparticles loaded with a protein and dual antitumor drugs as a targeted delivery system. *New Journal of Chemistry*, *43*(44), 17284–17297. https://doi.org/10.1039/c9nj03001h
Stern, R., Asari, A. A., & Sugahara, K. N. (2006). Hyaluronan fragments: An information-rich system. *European Journal of Cell Biology*, *85*(8), 699–715. https://doi.org/10.1016/j.ejcb.2006.05.009
Stöber, W., & Fink, A. (1968). Controlled Growth of Monodisperse Silica Spheres in the Micron Size Range. *JOURNAL OF COLLOID AND INTERFACE SCIENCE*, *26*(1), 62–69. https://doi.org/10.1589/jpts.29.112
Sun, T., Zhang, Y. S., Pang, B., Hyun, D. C., Yang, M., & Xia, Y. (2014). Engineered nanoparticles for drug delivery in cancer therapy. *Angewandte Chemie - International Edition*, *53*(46), 12320–12364. https://doi.org/10.1002/anie.201403036
Tagliavia, M., & Nicosi, A. (2012). Regeneration and Recycling of Supports for Biological Macromolecules Purification. In *Current Frontiers and Perspectives in Cell Biology*. https://doi.org/10.5772/32286
Tao, Z., Toms, B. B., Goodisman, J., & Asefa, T. (2009). Mesoporosity and functional group dependent endocytosis and cytotoxicity of silica nanomaterials. *Chemical Research in Toxicology*, *22*(11), 1869–1880. https://doi.org/10.1021/tx900276u
Thyrell, L., Hjortsberg, L., Arulampalam, V., Panaretakis, T., Uhles, S., Dagnell, M., … Pokrovskaja, K. (2004). Interferon α-induced apoptosis in tumor cells is mediated through the phosphoinositide 3-kinase/mammalian target of rapamycin signaling pathway. *Journal of Biological Chemistry*, *279*(23), 24152–24162. https://doi.org/10.1074/jbc.M312219200
Tian, Z., Xu, Y., & Zhu, Y. (2017). Aldehyde-functionalized dendritic mesoporous silica nanoparticles as potential nanocarriers for pH-responsive protein drug delivery. *Materials Science and Engineering C*, *71*, 452–459. https://doi.org/10.1016/j.msec.2016.10.039
Tolia, N. H., & Joshua-Tor, L. (2006). Strategies for protein coexpression in Escherichia coli. *Nature Methods*, *3*(1), 55–64. https://doi.org/10.1038/nmeth0106-55
Toole, B. P., & Slomiany, M. G. (2008). Hyaluronan: A constitutive regulator of chemoresistance and malignancy in cancer cells. *Seminars in Cancer Biology*, *18*(4), 244–250. https://doi.org/10.1016/j.semcancer.2008.03.009
Tu, J., Boyle, A. L., Friedrich, H., Bomans, P. H. H., Bussmann, J., Sommerdijk, N. A. J. M., … Kros, A. (2016). Mesoporous Silica Nanoparticles with Large Pores for the Encapsulation and Release of Proteins. *ACS Applied Materials and Interfaces*, *8*(47), 32211–32219. https://doi.org/10.1021/acsami.6b11324
Ukmar, T., & Planinšek, O. (2010). Ordered mesoporous silicates as matrices for controlled release of drugs. *Acta Pharmaceutica*, *60*(4), 373–385. https://doi.org/10.2478/v1007-010-0037-4
Unzueta, U., Céspedes, M. V., Vázquez, E., Ferrer-Miralles, N., Mangues, R., & Villaverde, A. (2015). Towards protein-based viral mimetics for cancer therapies. *Trends in Biotechnology*, *33*(5), 253–258. https://doi.org/10.1016/j.tibtech.2015.02.007
Vasvani, S., Kulkarni, P., & Rawtani, D. (2019). Hyaluronic acid : A review on its biology , aspects

of drug delivery , route of administrations and a special emphasis on its approved marketed products and recent clinical studies. *International Journal of Biological Macromolecules*. https://doi.org/10.1016/j.ijbiomac.2019.11.066

Vieira, J. P. (2019). Utilization of silica nanoparticles for transport and delivery of a recombinant protein for cancer treatment. Master's thesis, Universidade de Coimbra, Coimbra Portugal.

Villiers, M. M. de, Aramwit, P., & Kwon, G. S. (2019). Nanotechnology in Drug Delivery. In *Journal of Chemical Information and Modeling* (Vol. 53). https://doi.org/10.1017/CBO9781107415324.004

Wambaugh, M. A., Denham, S. T., Ayala, M., Brammer, B., Stonhill, M. A., & Brown, J. C. S. (2020). Synergistic and antagonistic drug interactions in the treatment of systemic fungal infections. *ELife*, *9*, 1–26. https://doi.org/10.7554/eLife.54160

Wan, L., Jiao, J., Cui, Y., Guo, J., Han, N., Di, D., Wang, S. (2016). Hyaluronic acid modified mesoporous carbon nanoparticles for targeted drug delivery to CD44-overexpressing cancer cells. *Nanotechnology*, *27*(13). https://doi.org/10.1088/0957-4484/27/13/135102

Wang, J., Shen, Y., Bai, L., Lv, D., Zhang, A., Miao, F., Zhang, J. (2014). Mesoporous silica shell alleviates cytotoxicity and inflammation induced by colloidal silica particles. *Colloids and Surfaces B: Biointerfaces*, *116*, 334–342. https://doi.org/10.1016/j.colsurfb.2013.12.036

Wang, S., & Li, H. (2006). Structure directed reversible adsorption of organic dye on mesoporous silica in aqueous solution. *Microporous and Mesoporous Materials*, *97*(1–3), 21–26. https://doi.org/10.1016/j.micromeso.2006.08.005

Wang, Y., Cui, Y., Zhao, Y., He, B., Shi, X., Di, D., … Wang, S. (2017). Fluorescent carbon dot-gated multifunctional mesoporous silica nanocarriers for redox/enzyme dual-responsive targeted and controlled drug delivery and real-time bioimaging. *European Journal of Pharmaceutics and Biopharmaceutics*, *117*, 105–115. https://doi.org/10.1016/j.ejpb.2017.03.019

Watermann, A., & Brieger, J. (2017). Mesoporous silica nanoparticles as drug delivery vehicles in cancer. *Nanomaterials*, *7*(7). https://doi.org/10.3390/nano7070189

Xu, C., Hu, W., Zhang, N., Qi, Y., Nie, J. J., Zhao, N., … Xu, F. J. (2020). Genetically multimodal therapy mediated by one polysaccharides-based supramolecular nanosystem. *Biomaterials*, *248*(April). https://doi.org/10.1016/j.biomaterials.2020.120031

Yang, H. (2016). Targeted nanosystems: Advances in targeted dendrimers for cancer therapy. *Nanomedicine: Nanotechnology, Biology, and Medicine*, *12*(2), 309–316. https://doi.org/10.1016/j.nano.2015.11.012

Yang, J. D., Hainaut, P., Gores, G. J., Amadou, A., Plymoth, A., & Roberts, L. R. (2019). A global view of hepatocellular carcinoma: trends, risk, prevention and management. *Nature Reviews Gastroenterology and Hepatology*, *16*(10), 589–604. https://doi.org/10.1038/s41575-019-0186-y

Yano, H., Ogasawara, S., Momosaki, S., Akiba, J., Kojiro, S., Fukahori, S., … Kojiro, M. (2006). Growth inhibitory effects of pegylated IFN α-2b on human liver cancer cells in vitro and in vivo. *Liver International*, *26*(8), 964–975. https://doi.org/10.1111/j.1478-3231.2006.01321.x

Yano, H., Yanai, Y., Momosaki, S., Ogasawara, S., Akiba, J., Kojiro, S., … Kojiro, M. (2006). Growth inhibitory effects of interferon-α subtypes vary according to human liver cancer cell lines. *Journal of Gastroenterology and Hepatology (Australia)*, *21*(11), 1720–1725. https://doi.org/10.1111/j.1440-1746.2006.04357.x

Yao, V. J., D'Angelo, S., Butler, K. S., Theron, C., Smith, T. L., Marchiò, S., … Pasqualini, R. (2016). Ligand-targeted theranostic nanomedicines against cancer. *Journal of Controlled Release*, *240*, 267–286. https://doi.org/10.1016/j.jconrel.2016.01.002

Ye, F., Zhao, Y., El-Sayed, R., Muhammed, M., & Hassan, M. (2018). Advances in nanotechnology for cancer biomarkers. *Nano Today*, *18*, 103–123. https://doi.org/10.1016/j.nantod.2017.12.008

Yi, Z., Dumée, L. F., Garvey, C. J., Feng, C., She, F., Rookes, J. E., … Kong, L. (2015). A New Insight into Growth Mechanism and Kinetics of Mesoporous Silica Nanoparticles by in Situ Small Angle X-ray Scattering. *Langmuir*, *31*(30), 8478–8487. https://doi.org/10.1021/acs.langmuir.5b01637

Zampini, G., Matino, D., Quaglia, G., Tarpani, L., Gargaro, M., Cecchetti, F., … Latterini, L. (2019). Experimental evidences on the role of silica nanoparticles surface morphology on the loading, release and activity of three proteins. *Microporous and Mesoporous Materials*, *287*(June), 220–227. https://doi.org/10.1016/j.micromeso.2019.06.005

Zhang, B., Liu, Q., Liu, M., Shi, P., Zhu, L., Zhang, L., & Li, R. (2019). Biodegradable hybrid mesoporous silica nanoparticles for gene/chemo-synergetic therapy of breast cancer.

Journal of Biomaterials Applications, *33*(10), 1382–1393. https://doi.org/10.1177/0885328219835490

Zhang, K.-J., Yin, X.-F., Yang, Y.-Q., Li, H.-L., Xu, Y.-N., Chen, L.-Y., … Fuchs, S. Y. (2017). A potent in vivo anti-tumor efficacy of novel recombinant type I interferon. *Clin Cancer Res.*, *23*(8), 2038–2049. https://doi.org/10.1097/CCM.0b013e31823da96d.Hydrogen

Zhang, K., Meng, X., Yang, Z., Dong, H., & Zhang, X. (2020). Enhanced cancer therapy by hypoxia-responsive copper metal-organic frameworks nanosystem. *Biomaterials*, *258*(February), 120278. https://doi.org/10.1016/j.biomaterials.2020.120278

Zhang, Ying, Li, X., Zhang, Y., Wang, L., Xu, J., Du, J., & Guan, Y. (2019). Pegylated interferon-α inhibits the proliferation of hepatocellular carcinoma cells by downregulating miR-155. *Annals of Hepatology*, *18*(3), 494–500. https://doi.org/10.1016/j.aohep.2018.11.007

Zhang, Yuan, Xing, Y., Xian, M., Shuang, S., & Dong, C. (2019). Folate-targeting and bovine serum albumin-gated mesoporous silica nanoparticles as a redox-responsive carrier for epirubicin release. *New Journal of Chemistry*, *43*(6), 2694–2701. https://doi.org/10.1039/C8NJ05476B

Zhang, Yuanyuan, Ang, C. Y., Li, M., Tan, S. Y., Qu, Q., & Luo, Z. (2015). Polymer Coated Hollow Mesoporous Nanoparticles for Triple-Responsive Delivery Silica Drug. *ACS Applied Materials & Interfaces Polymer*, *7*(32), 18179–18187.

Zhao, Q., Liu, J., Zhu, W., Sun, C., Di, D., Zhang, Y., … Wang, S. (2015). Dual-stimuli responsive hyaluronic acid-conjugated mesoporous silica for targeted delivery to CD44-overexpressing cancer cells. *Acta Biomaterialia*, *23*, 147–156. https://doi.org/10.1016/j.actbio.2015.05.010

Zhou, Y., Quan, G., Wu, Q., Zhang, X., Niu, B., Wu, B., … Wu, C. (2018). Mesoporous silica nanoparticles for drug and gene delivery. *Acta Pharmaceutica Sinica B*, *8*(2), 165–177. https://doi.org/10.1016/j.apsb.2018.01.007

Zhuravlev, L. T. (2000). The surface chemistry of amorphous silica. Zhuravlev model. *Colloids and Surfaces A: Physicochemical and Engineering Aspects*, *173*(1–3), 1–38. https://doi.org/10.1016/S0927-7757(00)00556-2